LOS ALAMOS SCIENTIFIC LABORATORY
of the
University of California
LOS ALAMOS • NEW MEXICO

Status Report of the LASL Controlled Thermonuclear Research Program for 12 Month Period Ending October 31, 1966

UNITED STATES
ATOMIC ENERGY COMMISSION
CONTRACT W-7405-ENG. 36

All LA...MS reports are informal documents, usually prepared for a special purpose. This LA...MS report has been prepared, as the title indicates, to present the status of the LASL program for controlled thermonuclear research. It has not been reviewed or verified for accuracy in the interest of prompt distribution. All LA...MS reports express the views of the authors as of the time they were written and do not necessarily reflect the opinions of the Los Alamos Scientific Laboratory or the final opinion of the authors on the subject.

Printed in USA. Price $4.00. Available from the Clearinghouse for Federal Scientific and Technical Information, National Bureau of Standards, United States Department of Commerce, Springfield, Virginia

LA-3628-MS
UC-20, CONTROLLED
THERMONUCLEAR PROCESSES
TID-4500

LOS ALAMOS SCIENTIFIC LABORATORY
of the
University of California
LOS ALAMOS • NEW MEXICO

Report compiled: November 1966
Report distributed: December 14, 1966

Status Report of the LASL Controlled Thermonuclear Research Program for 12 Month Period Ending October 31, 1966

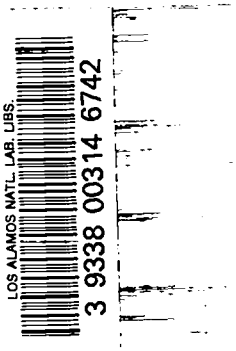

INTRODUCTION

(J.L. Tuck)

After operating at a fairly constant level for many years, the LASL Sherwood research effort has started to expand. It is hoped approximately to double over the next four years, i.e., to about 120 people. Changes in the last year should round out the effort; two new groups have been formed: mathematical physics (P-18) led by W. Riesenfeld and basic plasma physics (P-13) led by H. Dreicer. The high-temperature, high-β philosophy, with which the LASL studies have been mainly concerned, has been productive. In the main, the expansion has been motivated by the need to exploit and extend the achievement of a strongly thermonuclear plasma in the Scylla IV θ-pinch having an $n\tau$ (density x time) exceeding 10^{11} ion cm^{-3} sec at an ion temperature > 3 keV; and also by the opening out of interesting possibilities in a still higher density regime, e.g., hot z-pinches, and by ideas peculiarly related to the pulsed reactor concept, e.g., higher power plasma guns and cross field plasma injection.

The Scyllac proposal, if adopted, will probably take up more than half the LASL Sherwood effort. It will (1) extend Scylla IV from 1 m length to 15 m. This may be expected to increase the lifetime of the plasma, if determined by straightforward end loss as at present, to the point where anomalous (Bohm) diffusion, if it is occurring, might be detected and measured. It will also allow tests of magnetic field bumpiness and special configurations needed for (2) the toroidal θ-pinch of 15-m circumference, necessary for gross equilibrium of the plasma column with respect to the torus walls. The torus will be constructed subsequent to the straight tube. Both will use the same building, as well as the same power supply which is the main expense.

The proposal is the first to have undergone the rigorous new review procedure devised for all future large-scale, AEC Sherwood experiments. The proposal has received the unanimous approval of a specially created committee drawn from the four AEC laboratories and outside authorities. Before that, it was strongly recommended for construction by the Herb Committee and finally by the U.S. Sherwood Standing Committee. The installation will cost $\sim \$8.5$ million and take about three years to come into operation. This does not include the cost of the straight or toroidal tube and the dynamic stabilization, which may come later. The domains of τ, n, T_i, and β involved in these projects are entirely beyond present experience. Thus far, the Scylla IV plasma is much better behaved than would have been predicted from low-power (more particularly low-E_θ), low-temperature θ-pinches (studies of Kvartskava, for example); consequently, the behavior of a hot, high-β plasma in toroidal geometry may be better than that observed in the current low-β, low-temperature devices. The dynamic stabilization may not even be needed. If needed, it may work, although it may possibly not. In any case, an adaptable and potent facility will be available for pulsed experiments.

For reasons which are not entirely clear, the simple z-pinches studied in the early days of controlled thermonuclear research never yielded the high temperatures like those currently obtained in high-E_θ theta-pinch of the Scylla type. The simplest hypothesis is that the growth rate of the strong hydromagnetic instability of the z-pinch was such that the true compressions never approached the geometrical thin sheath values. Whatever it was, it may be instructive to observe z-pinches at the high temperatures, under high conductivity and non-small ion Larmor radius conditions, such as are now attainable in Scylla IV and similar θ-pinches. It may be possible to do this by using such a θ-pinch plasma as the starting point for a z-pinch. This is the philosophy of

the Columba experiment (P-14). It is fully appreciated, however, that reality will probably be complicated, e.g., by trapping of magnetic fields in the tenuous gas outside the θ-pinch, which could prevent the substitution of B_θ for B_z in the transition from θ-pinch to z-pinch.

No attempt will be made here to catalogue the contents of this annual report. But two items selected for reasons of personal interest are: (1) a new hydromagnetic gun geometry in which the sheath starts out with strong hydromagnetic stability as an inverse pinch, and which seems to gain some advantage from internal magnetic energy storage (P-17), and (2) a dream of plasma diagnosticians has been to measure the ion and electron velocity distribution functions inside a hot plasma; there are indications that by the most refined optical technique (triple etalons) the already known coherent scattering from a laser beam can be observed to the requisite precision (P-15).

SCYLLA IV

(R.F. Gribble, E.M. Little, N. Lowry, L.H. McDowell, W.E. Quinn)

Use of Quartz Discharge Tubes

Experimental Arrangement

A quartz discharge tube with an inside diameter of 8.5 cm was installed in the 1-m length compression coil of Scylla IV. In order to accommodate quartz tubes of "standard" size, the inside diameter of the compression coil was bored out from 10 to 10.2 cm. Other θ-pinch experimenters have found it essential to wrap quartz tubes to prevent uv absorption in the air space between the tube o.d. and the coil i.d. Without a wrap, tube breakage occurs; this has been attributed to uv shock generation in the air space.

The exterior surface of the quartz tube was wrapped tightly with two opposed spirals of a 5-cm wide glass tape (3M No. 27). In addition, a double wrap of glass fiber tape was applied to hold the glass tape tightly to the tube and to contain the fragments in case of breakage. The wrap prescription is essentially that used by the Culham group and more recently on Scylla III.

The compression coil has three radial viewing slits at zero, 20.3 cm, and 35.6 cm from the coil midplane, transverse to the coil axis and spaced along half of the coil length. Corresponding slits were in the tube wrap. The quartz tube has been operated successfully in the low-pressure regime (P_{D_2} = 10 to 25 mtorr) without breakage.

Three streak cameras were used to photograph the plasma "side-on" through the coil slits. The Mach-Zehnder interferometer was also installed with giant pulse illumination.

Neutron Emission

In the low-pressure regime without B_o, the average neutron emission in the quartz discharge tube was found to be approximately two orders of magnitude less than in normal operation with a high-alumina tube. A possible cause of this anomaly may be the rippled inside surface of the quartz discharge tube, consisting of reworked quartz. This rippled surface could possibly be breaking up the initial sheath formed in the early dynamical phase of the discharge, which is particularly important in the low-pressure regime. The application of only 0.5 kG of reversed magnetic bias field brings the neutron yield back to its normal level. It is conceivable that this field assists in the formation of a uniform cylindrical sheath in the initial phase of the discharge. Drawn quartz tubes with a more uniform bore are being procured to check this hypothesis. The data presently obtained in quartz tubes are probably not representative of typical hot plasmas previously produced in high-alumina discharge tubes.

Plastic scintillation neutron detectors at various positions along the compression coil show that in the low-pressure regime the time distribution of the neutron emission in the central region of the compression coil is approximately symmetrical about the maximum of the magnetic field. At 25-cm from the coil midplane the neutron emission tends to peak before the time of peak magnetic field. These results are particularly characteristic of the low-pressure regime with reversed bias fields of 0.5 to 2 kG.

Motion and Stability of the Plasma Column

Axial interferograms taken simultaneously with the "side-on" streak photographs show the effects of the plasma motion. Simultaneous interferograms and streak photographs taken with an initial filling pressure of 15 mtorr are given in Fig. 1. The interferograms were taken

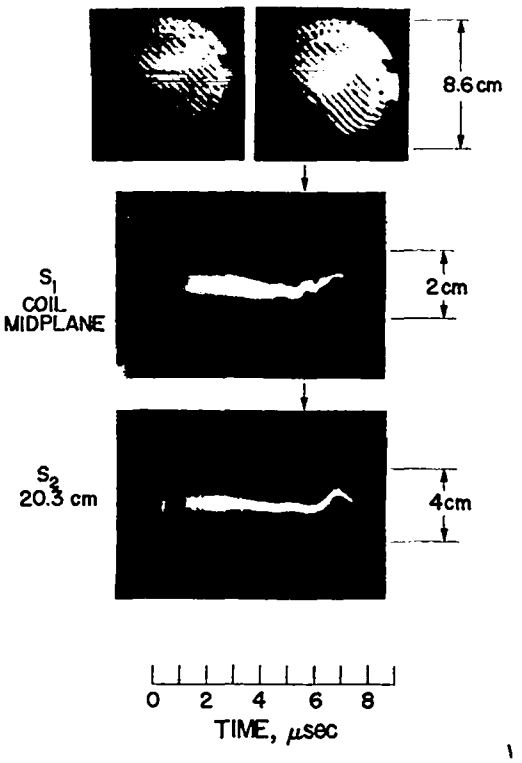

Fig. 1. Scylla IV interferograms and streak photographs with quartz discharge tube.

at the times indicated by the arrows on the streak photographs. The interferograms show noncylindrical, asymmetrical plasma cross sections consistent with the "wobbling" and "bifurcating" motions observed in the streak photographs. These interferograms are in contrast with those obtained under the same operating conditions in high-alumina tubes. In the latter case, the interferograms showed a cylindrical, symmetrical plasma cross section throughout the magnetic half cycle.

With the quartz discharge tube, the interferograms indicate very dense plasmas with densities considerably greater than 5×10^{16} cm^{-3}. These densities and the observed low neutron emissions imply that a dense, cold plasma is being produced. The observed instabilities are also consistent with previous experiments in which instabilities were observed in very dense, cold plasmas.

Changeover of Collector Plate to Cable Cartridges

A major electrical breakdown occurred between the Scylla IV collector plates in the latter part of March 1966. The failure resulted from stress cracking in the polyethylene hat insulators around a through-bolt. The existence of the stress cracks was discovered previously. It was decided at that time, however, to operate the machine until a fault occurred. In addition to repairing the collector-plate system, a modification of the collector plate - header system is being made to eliminate high-voltage breakdowns in the header system and to gain

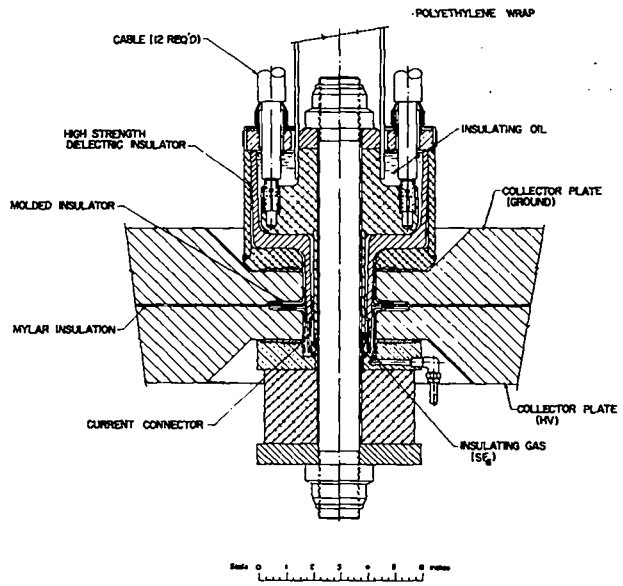

Fig. 2. Cable cartridge used in Scylla IV.

experience with the Scyllac-type cable connection. The original header system, which transformed the coaxial cables from the capacitor banks into the parallel plate collector system, was located around the perimeter of the collector plates with the cables closely packed and seven rows deep. The modified design distributes the cable feeds over the entire area of the collector plates. This design uses the cable cartridges which have been designed for the Scyllac device. The use of these cartridges in Scylla IV will also serve to test their reliability in a large system.

A schematic cross section of a single cable cartridge assembly in the Scylla IV collector plates is shown in Fig. 2. Each such cartridge accepts 12 RG 17/14 coaxial cables and provides a single coaxial feed for them into the parallel-plate collector. Electrical insulating oil insulates the cable "strip-backs" in the cartridges; a vacuum impregnated epoxy-glass fiber insulator and SF_6 gas insulate the through-bolts and lower portions of the cartridges. These cartridges are distributed approximately uniformly over the collector-plate area. The original through-bolts, which hold the collector plates together, also hold the cartridges together.

Scylla IV has been reassembled with a sufficient number of cable cartridges to connect the primary, preionization, and bias capacitor banks. Additional holes have been bored in the collector-plate system such that additional cable cartridges can be added at a later date to accommodate the cables from the power-crowbar capacitor bank.

The collector-plate modifications for accepting the cable cartridges involved enlarging the through-bolt holes from 5 to 6.8 cm and "buffing" a finish for the cartridge seat. These modifications have been completed and the collector plates reassembled with new Mylar insulation and new electrical insulating hats. The latter were molded by CMB Division at LASL from Dupont Surlyn A. This material has twice the dielectric strength of polyethylene and is highly resistant to corona.

Considerable difficulty was encountered in the procurement of the high-strength dielectric insulator (Fig. 2) for the cable cartridge assembly. The commercial insulators were molded from diallyl phthalate with a glass fiber fill. These insulators cracked when they were subjected to the compressive stress (6000 psi) developed by the through-bolt torque that holds the collector plates together. After various modifications failed to produce a satisfactory insulator, a mold was fabricated and an epoxy-glass fiber insulator was vacuum-impregnated. Mechanical and electrical tests showed the products to be completely satisfactory. This insulator, which contains approximately 60% glass fiber, was impregnated with Epon-828, having 10% polysulfide (LP-3) to reduce the brittleness, and diethanolamine was used as the curing agent. The molded part was cured for 16 h at 75°C. The fabrication and installation of 146 cable cartridges and all cables has now been completed. A view of the new Scylla IV collector system is shown in Fig. 3; for ease of viewing,the vacuum system and coil clamp were left off for this photograph.

Fig. 3. New Scylla IV collector system.

Experiments with Sectored Compression Coils

Anticipated Experiments Related to Scyllac

There are two basic kinds of experiments planned for Scylla IV over the next three years that are important in testing Scyllac concepts. The first is to test certain engineering features, such as the use of the cable-cartridge technique for spreading the cable currents uniformly over the collector plate (described above) and the application of solid dielectric switches to crowbar the compression current in a passive manner. The second is to test, to the extent possible on a short (1-m) linear plasma, some of the stabilization concepts involved in making the eventual torus, namely, measuring ballooning growth rates on a "static" bumpy cylindrical plasma and testing the feasibility of the particular dynamic stabilization method which involves auxiliary longitudinal currents and B_θ. Some studies will be made of drift in a curved coil (and tube) and of the use of static (bumpy) stabilization fields to overcome it. A report (LA-3596-MS) has been prepared describing these experiments.

Sectored-Coil and Static Stabilization Capacitor Bank

A new capacitor bank is being installed for driving the bumpy or "static" stabilizer fields. This stabilization bank is located at the front

end of Scylla IV and consists of two large overhead racks of 108 50-kV capacitors, having an energy storage of 270 kJ. This is about half the energy storage of the Scylla IV primary bank, and the capacitors and switches are of the same type.

The sectored compression coil for static, bumpy-field excitation and for the dynamic stabilization tests is on hand. The collector system to connect the stabilization bank to the static stabilization conductors is designed, and fabrication is under way.

A general cutaway view of the "static" stabilization conductors, whose feeds are embedded in the three slots of the sectored compression coil as well as at the two ends, is shown in Fig. 4. Mirror ($\ell = 0$) coils in the slots and at the ends are driven by one parallel-plate transmission line, and the four longitudinal bars of each quadrupole ($\ell = 2$) section are driven from a second parallel-plate line in each

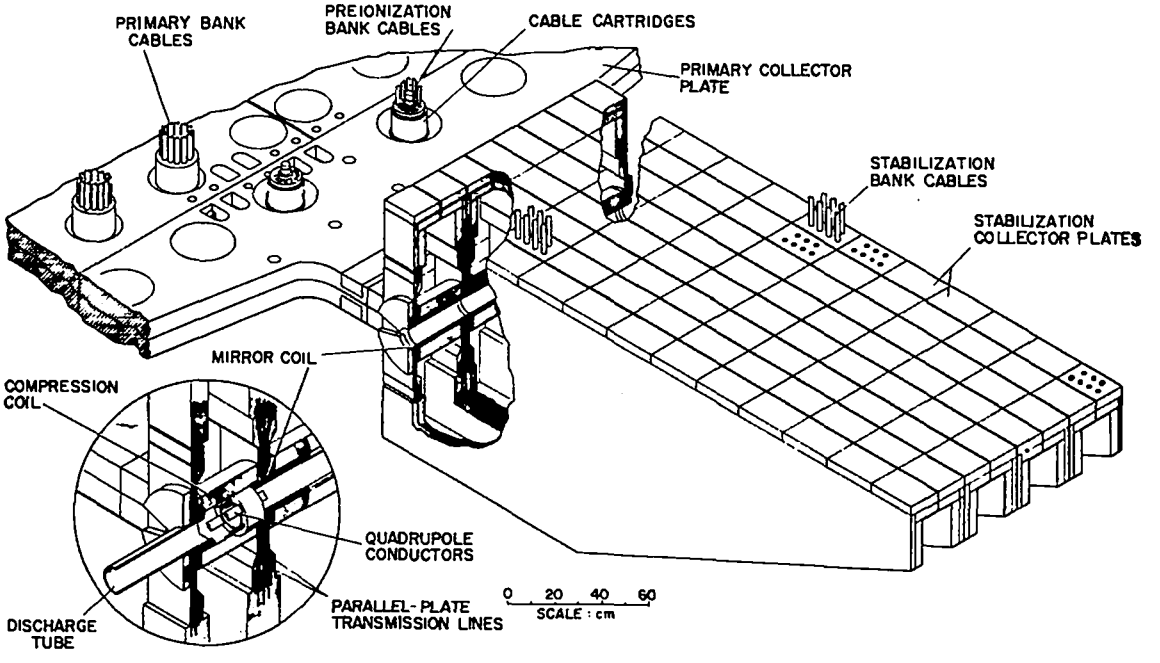

Fig. 4. "Static" stabilization conductor arrangement for producing a bumpy plasma column in Scylla IV.

slot and at the left-hand end. These transmission lines in turn connect to the heavy aluminum stabilization collector plates which are connected by vertical cables to the stabilization capacitor bank above.

Dynamic Stabilization Parameter Test

A basic question which has arisen in regard to the method of dynamic stabilization with longitudinal rf currents is whether the fast B_θ fields can penetrate the tenuous plasma ("halo") between the dense θ-pinch column and the discharge-tube wall. At halo densities of the order of 10^{12} - 10^{14} cm^{-3} this must occur by counterstreaming instabilities which make a high microresistivity in the halo owing to longitudinal electron drift velocities of the order of the electron thermal velocity. If because of this B_θ penetrates to the edge of the dense plasma core where the number of current-carrying electrons is much greater, but the total longitudinal current is approximately the same (set by external inductance), the electron drift velocity may then drop below the thermal limit in the current-carrying layer so that the plasma stabilizes. The combination of phenomena implies that the stabilizing B_θ field must not exceed a value B_c whose precise magnitude is uncertain, but is in the neighborhood of the value actually required to stabilize Scyllac. In addition, the amount of heating of halo plasma is uncertain, as also is the relative fraction of "runaway" relativistic electrons which may occur and load the wall.

The primary objective will be to try to observe these phenomena, seeing if B_θ can be made to penetrate under realistic Scyllac conditions, and, if it does, to determine the side effects. A limitation of the short Scylla IV system is that end electrodes must be used to connect to the plasma core and that cold gas is uncomfortably nearby at the ends of the discharge tube.

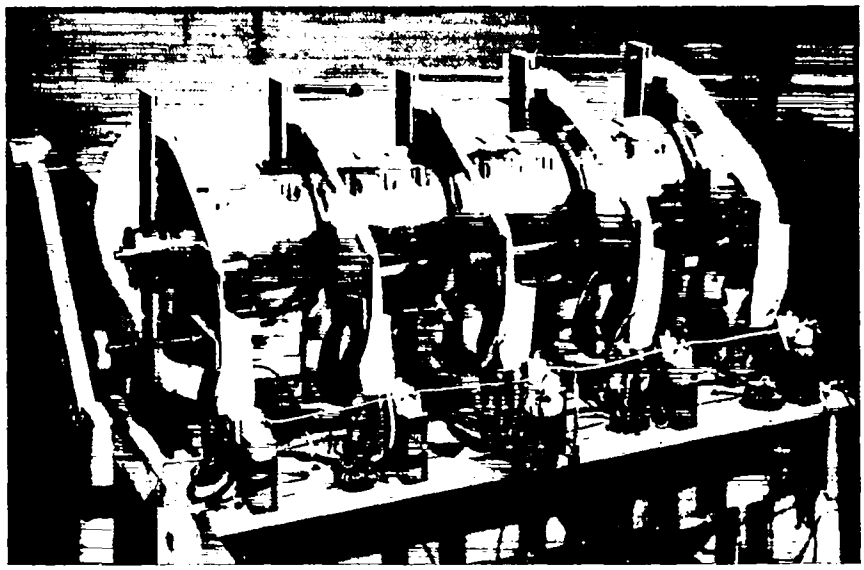

Fig. 5. Test arrangement for checking parameters of dynamic stabilization circuit.

A realistic test requires a longitudinal electric field E_z near the wall of about 3 kV/cm, a maximum longitudinal current I_z of about 150 kA with a frequency of about 1 mc. In these tests for side effects, a high-Q circuit, which will allow ~ 100 cycles of ringing, is not essential. Therefore, use can be made of 120-kV, 0.8-μF capacitors of ordinary Q value, which are on hand.

The method used to generate the high value of E_z is similar to that proposed for the Scyllac torus. An outer coaxial conductor (of which the plasma is the center conductor) is driven in four 26-cm sections connected in parallel, inducing their voltages in series along the inside of the discharge tube.

To test some engineering aspects of the experimental arrangement, a mockup was constructed using the present sectioned Scylla IV coil and 0.5-μF, 25-kV capacitors, each charged to 15 kV and switched with three element trigatron gaps. A plasma was simulated with a 1-in. o.d. copper pipe. A photograph of the arrangement is shown in Fig. 5. The plasma return current conductor consists of a split copper pipe insulated from and placed just inside the θ-pinch coil i.d. The measured "plasma" current was 20 kA at a

frequency of 650 kHz, and the ground current was less than 5 kA. An inductance per sector calculated from the period and the capacitance per sector, assuming zero ground current, is 130 nH, indicating a total peak voltage across the "plasma" of 45 kV. This compares favorably with a measured value of 60 kV obtained by inserting a 100-Ω noninductive resistor in series with the "plasma" and measuring the resulting current. Allowing for the increased inductance of the 120-kV capacitor to be used in the actual experiment and parallel plate transmission lines insulated for 120-kV, the mockup indicates that the electrical requirements for the experiment will be met.

Curved-Sector Experiments

It is planned to design a sectored, curved compression coil which can be driven by the Scylla IV primary bank. This will be used to check the toroidal plasma drift, if it is not hindered by line tying out the ends. In addition, the stabilization bank can be used to drive transverse fields to attempt to stop the drift and "M and S" bumpy plasma configurations.

Two approaches in design and procurement have been initiated for 5-m major diam discharge tubes. One approach is to fabricate the tubes from high-alumina ceramic and the other is to obtain them in either clear fused quartz or Rotosil fused silica.

Following discussions with Coors Porcelain Co. and with CMB Division, a segmented alumina ceramic design was worked out. Each segment, with a length of 17.4 cm, is ground to the appropriate curvature on both the inside (7.5 cm) and outside (8.4 cm) diameters. In addition, step joints are ground on each end of the segments with rather close tolerances. The segments will be jointed together with epoxy in such a way that it is not exposed to the discharge. This design has been fabricated from 99% alumina. Of these segments, 28 have been received and only three rejected because of failure to meet specifications.

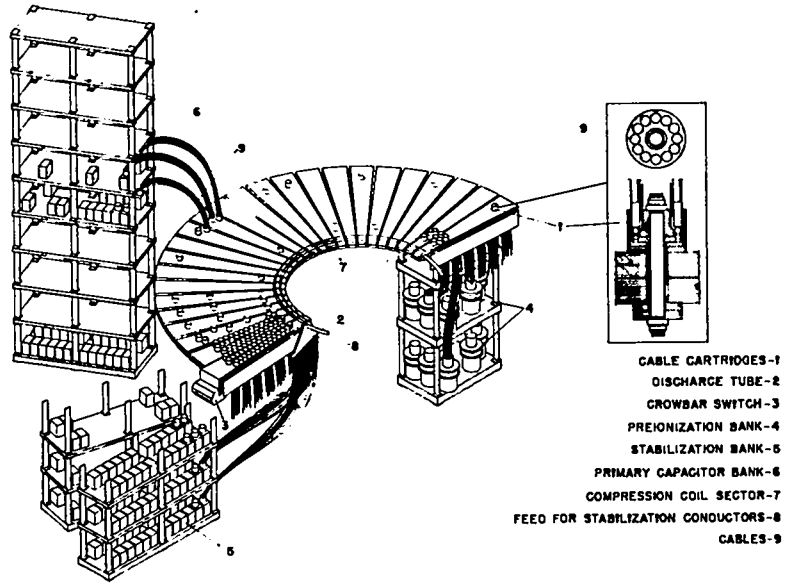

Fig. 6. Schematic view of the proposed toroidal Scyllac device.

Two shipments of curved quartz tubes have been received. One, from Karel Hackl, consists of tubes of poor quality, failing to meet specifications. The other tubes from Westdeutsche Quartzschmelze appear to be quite good and meet dimensional tolerances.

SCYLLAC PROPOSAL

(D. Baker, E. Kemp, R. Morse, W. Quinn, G. Sawyer, F. Ribe, W. Riesenfeld)

Scyllac Proposal

The Proposed Experiments

The proposal for constructing Scyllac, a 5-m diam toroidal θ-pinch with plasma properties like those of Scylla IV, is embodied in LA-3289-MS and LA-3487-MS, as well as the Schedule 44 Construction Project Data Sheet for the Scyllac Facility (Project No. 68-5-a). A schematic view of the eventual torus of 5-m major diam is shown in Fig. 6. The proposal includes discussions of the possibility of both low-β (of the order of a few tenths

percent) and $\beta = 1$ equilibrium configurations. The latter, however, provide the main theoretical framework. A sectioned compression coil would drive the θ-pinch, with separately-excited, azimuthally varying stabilization windings providing an "M and S"-like equilibrium. Theoretical estimates of the growth rates of gross "ballooning" instabilities at $\beta = 1$ indicate that they can be stabilized in principle by the application of longitudinal (azimuthal) currents in the form of a rapidly alternating "screw" pinch, or by other means of dynamic stabilization, not involving longitudinal currents.

Early in the discussions of the review panel (see below), the question came up of building a preliminary, long linear θ-pinch having a length ($\sim$ 15 m) about equal to that of the proposed torus. This was proposed as a first step in the Scyllac program to see if theoretical end-loss scaling with length applies and, if so, to investigate what the sidewise diffusion under the extended containment times might be. It would also allow ballooning growth rates of a long bumpy cylinder to be investigated and problems of applying dynamic stabilization fields to be studied. (The last two problems are directly applicable to torus stabilization.) The LASL Scyllac staff investigated the suitability of the proposed building and capacitor bank for such a linear design and the problem of then converting to a torus. As a result of this and the panel's urging, it has been decided to undertake the long linear experiment as the first phase of the Scyllac program. A preliminary report on the proposed linear experiments (LA-3553-MS) was given to the panel on May 26. It has recently been produced in final form and circulated to the CTR Standing Committee. A plan view of a straight θ-pinch, using the same capacitor banks as envisioned for the torus, is shown in Fig. 7.

Review of the Scyllac Proposal

In order to review this proposal an Ad-Hoc working panel was first convened in Washington, D. C., on April 23, 1966. Its membership consisted of H. Griem, (Chairman), H. Grad, D. Grove, C. Hartman, R. Kilb,

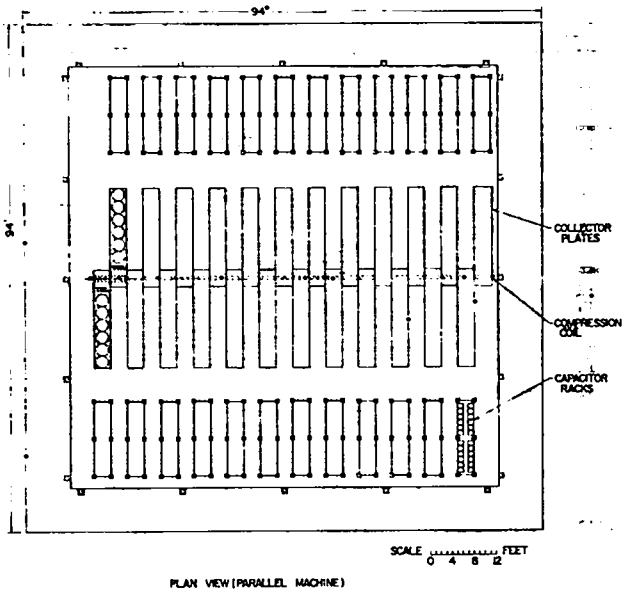

Fig. 7. Plan view of linear Scyllac device.

N. Lazar, and F. Ribe, with participation by S. Dean of AEC Washington. A meeting of the panel was held at that time, followed by a meeting in Los Alamos on May 26 and 27, 1966. Within 10 days the components of a first draft of the panel report were provided, its various parts being written by the panel members from an outline proposed by Griem and elaborated at the Los Alamos meeting. The first draft was then circulated on June 13, 1966. Following extensive written comments by all panel members, the second draft was circulated on July 8, 1966. This was followed by further written and telephoned comment, as well as personal discussion by some of the panel members at the meeting on toroidal confinement in Princeton, July 11-15, 1966. The third draft was circulated on July 25, 1966. This was finally produced as a unanimous report (University of Maryland Report ORO-AT-(40-1)-3393-1) recommending construction of Scyllac with a preliminary 15-m linear experiment. Reservations were expressed about the workability of the proposed dynamic stabilization method in the presence of tenuous plasma outside the dense θ-pinch core.

On Aug. 5 and 6, 1966, the CTR Standing Committee (composed of the Project Directors, together with S. J. Buchsbaum, L. M. Branscomb,

W. A. Fowler, and H. W. Lewis) met at Los Alamos to hear a presentation, including material on Scylla and Scyllac, and for preliminary consideration of the Ad-Hoc Panel report. During and following this meeting there was considerable further discussion of the uncertainties involved in the proposed dynamic stabilization scheme, and this was communicated to the Standing Committee in writing on Aug. 6 and 26, 1966. The Standing Committee met again in Livermore, California, on Sep. 8, 1966, and gave final consideration to the Ad-Hoc Panel report and to the Scyllac proposal. The motion drafted and unanimously approved by the committee is quoted below.

"The Committee has studied the Scyllac proposal, as submitted by LASL in LA-3487-MS and modified in LA-3553-MS to absorb constructive suggestions made in the Griem Ad Hoc Panel Report. The Committee is impressed by the importance of the unique LASL effort in the study of high-β plasmas, and strongly supports the extension of that work into the domain envisaged in these proposals. The construction of the long straight θ-pinch described in LA-3553-MS should proceed expeditiously, to provide a test bed for the study of high-β stability under conditions of reduced end-loss. In addition, it is expected that our understanding of dynamic stabilization schemes can be greatly extended by experiments in the linear device. The subsequent transition to a toroidal device will then serve to test this understanding in a MHD-unstable configuration without end losses, and can also serve to determine the β-dependence of the instabilities.

"It is expected that, simultaneously, a theoretical and small-scale experimental effort will continue to be expended on questions relevant to dynamic stabilization, in order to refine further the details of the toroidal transition. In summary, the Committee finds, in agreement with the Griem Panel, that the program is expected to contribute enormously to our information about the confinement and stability of high-β plasmas. We unanimously urge that it be pursued vigorously, through its incorporation in the FY-68 budget."

SCYLLAC ENGINEERING

(Scyllac Engineering Team)

An engineering feasibility study of Scyllac was made and incorporated into the proposal for Scyllac (LA-3487-MS). Four new engineers and a draftsman were hired for the project; in addition, three engineers and three draftsmen from the LASL Eng Department were assigned to assist the Sherwood staff in designing Scyllac.

There will be three phases in the design of Scyllac: component development, prototype design and evaluation, and final system design.

Component Development

2-μF, 60-kV Capacitor (G.P. Boicourt, E.L. Kemp)

Scyllac requires ~5000 2-μF, 60-kV capacitors with the same low inductance and physical dimensions as the 2-μF, 50-kV capacitors now used in Scylla IV. A specification was prepared and sent to appropriate capacitor manufacturers whose representatives were invited to Los Alamos to hear a thorough presentation of the Scyllac requirements. Two capacitors were purchased from each of five companies and evaluated for Scyllac operation. Only one company has been successful in meeting the rigid performance specification but the other four are making new units for evaluation. All companies were visited by LASL engineers to discuss their individual design problems and also to consider the future requirement for a high-Q, high-voltage capacitor.

Reliable, High-Voltage, Low-Inductance Cable (G. P. Boicourt, E. L. Kemp)

The performance of the low-inductance cable on Scylla IV showed that it is imperative to develop reliable, high-voltage, low-inductance cable for Scyllac. Three of the major cable manufacturers were visited to discuss cable design problems. Then specifications were written to evaluate various suggested designs and samples procured from each

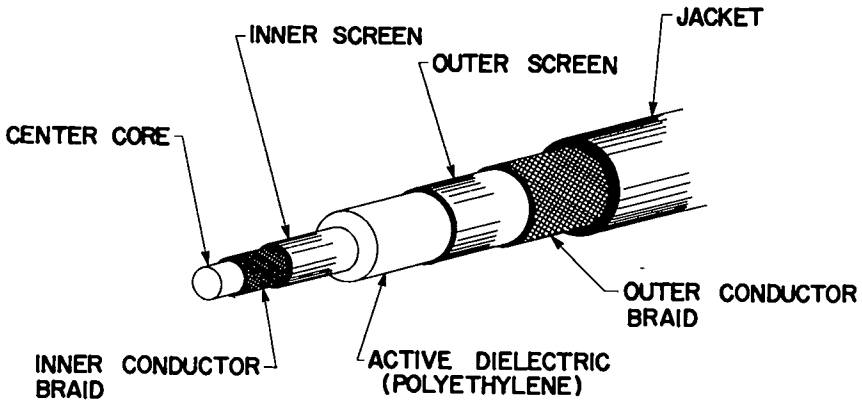

Fig. 8. General configuration of new cable proposed for Scyllac.

company. Figure 8 shows the general configuration of the new cable. The only unique feature is the two conducting screens which prevent high stress points when a braid wire breaks.

A cable evaluation test system was set up to test all new designs. The first cable tested was a control sample which had been used in Scylla IV and was known to be unsatisfactory for the required application. This was confirmed by the test. A Weibull statistical model, which provides a high confidence level with a relatively small sample, was used to analyze the test data. A total of seven different designs were evaluated from the three companies. Every cable design was much better than the control sample. After discussion with the companies, a composite design specification was written and new cable ordered for evaluation.

Switch Development (G.P. Boicourt, C. Hammer)

Scyllac will require over 4500 individual 60-kV "start" spark gaps. The 4-element atmospheric spark gap now used on Scylla IV is being redesigned for 60-kV operation. The crowbar switch is the most difficult component in Scyllac. Three different designs are being evaluated for this application. A solid dielectric switch developed at the Culham Laboratory is shown in Fig. 9. This switch uses an exploding trigger wire to

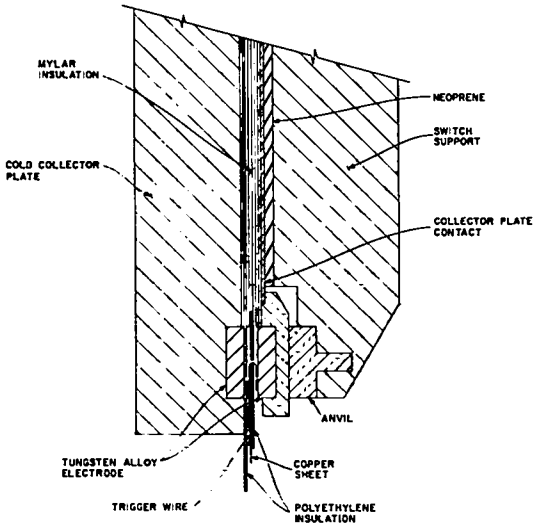

Fig. 9. Solid dielectric crowbar switch.

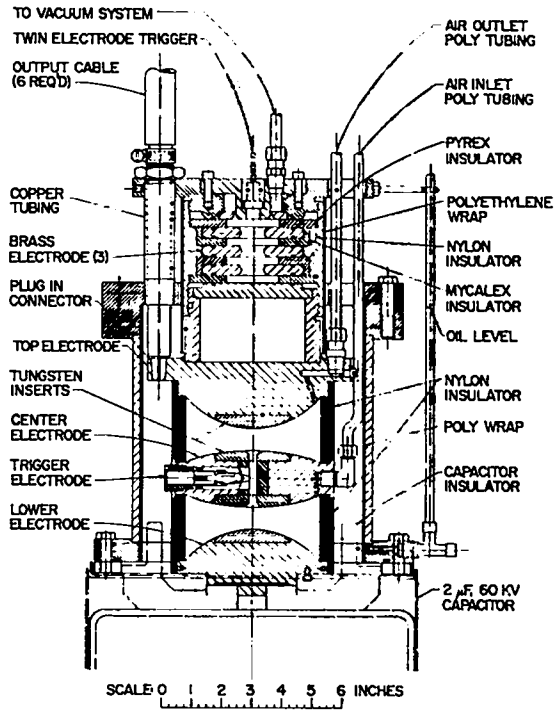

Fig. 11. Vacuum spark gap

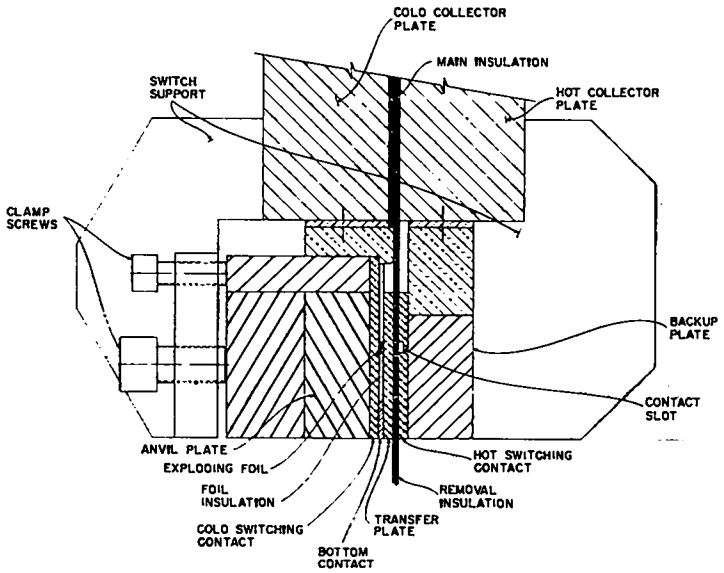

Fig. 10. Metallic contact dielectric switch.

rupture the insulation and carry the current in the resulting arc; it closes with low jitter and will conduct over 1 MA satisfactorily. One switch of this type has been made and will be tested.

A metallic contact, dielectric switch developed by J. Marshall at LASL is represented in Fig. 10. This switch has the advantage of having only a few μΩ resistance when it is closed, but the closing time is about 10 μsec. Use of the Marshall switch to relieve the Culham switch after 10 μsec is being considered as a possible means of extending the L/R time of the crowbar circuit. The main disadvantage of both switches is the time and effort required to replace the dielectric parts after each shot.

A vacuum spark gap that is integral with the 4-element gap is shown in Fig. 11. This type of vacuum gap was developed by J. W. Mather at LASL. The top electrode of the 4-element gap is common with the vacuum gap thus minimizing the cost. It can be fired routinely without maintenance. The disadvantage is the large number required and the necessity for a reliable vacuum system for the gaps. One of these gaps has been made and is being evaluated.

Prototype Design and Evaluation (R.S. Dike, K.W. Hanks, E.L. Kemp, W.L. Willis, A.S. Rawcliffe, J.D. Harbour, E. Holmes, J. McMullen)

The purpose of the prototype is to evaluate all newly developed components and circuits that will be used in the final Scyllac machine. The prototype system will be a linear design consisting of about 5% of the full-scale machine. An experimental area has been assigned to the prototype and the building modified to accommodate the system hardware. The charging and triggering systems have been designed and most of the components ordered. The capacitor racks have been designed and ordered. The triggering circuit has been mocked up and is being tested.

Complete Scyllac System (Scyllac Engineering Team)

The linear version of Scyllac will be built first. The main requirements for the system have been identified, and preliminary system design is under way. The control system requirements have been studied and a conceptual design completed.

SCYLLA III

(V. Finlayson, F. Jahoda, G. Sawyer, K. Thomas, M. Thomas)

Scylla III Measurements

Use of Quartz Tubes

Quartz discharge tubes are now used routinely in Scylla III. Although not as durable as ceramic tubes, they survive indefinitely unless there is a failure of the crowbar, and they frequently even survive that. Quartz tubes outgas and "warm up" to give neutron yields in fewer discharges than in ceramic tubes. Based on the limited data under identical low-pressure regime operating conditions, neutron yields appear identical in quartz and ceramic: $8.6 \pm 3.2 \times 10^8$ for ceramic and $8.3 \pm 1.6 \times 10^8$ for quartz.

Electron Temperature Measurements in Quartz Tubes

The electron temperature of the Scylla III plasma in the low-density regime without bias field was measured by means of a dual-channel, x-ray detector. With main bank voltages of 73 and 68.6 keV, the electron temperatures were 265 ± 50 and 425 ± 30 eV, respectively.

Differential Magnetic Loop Probe Measurements

A magnetic probe technique (first suggested by T. Green) has been developed for measuring flux excluded by the plasma. When these measurements are combined with the density profile measurements, a measurement of β is obtained. The probe system is shown in Fig. 12. A small magnetic probe ($nA \sim 1$ cm^2) senses dB/dt just outside the discharge tube wall. Since the B field only varies 5% with radius, the measured dB/dt represents the B field everywhere outside the plasma. A one-turn loop around the discharge tube senses $d\phi/dt$ inside the discharge tube and is, therefore, sensitive

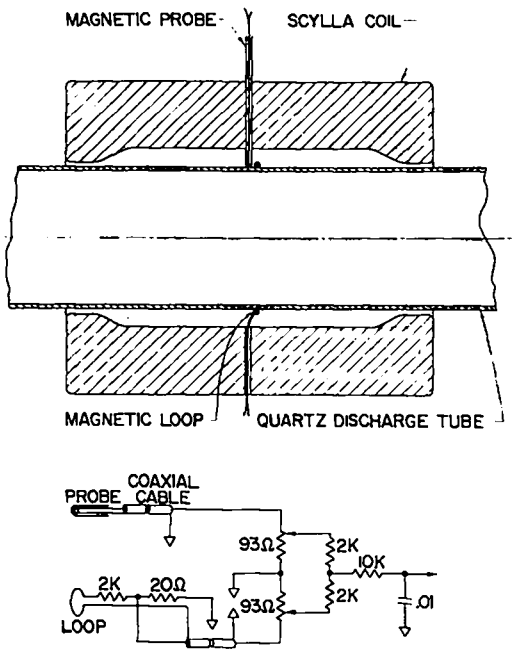

Fig. 12. Magnetic loop probe for Scylla III.

to flux excluded by the plasma. The loop signal is about 30 kV, so a well insulated voltage divider is required to reduce its signal to manageable size. The signals from loop and probe are nulled without plasma using the differencing circuit shown in Fig. 12. A residual unbalance of only 0.1% has been achieved.

When plasma is present, the measured difference signal, divided by the probe signal, gives a quantitative measure of the flux excluded by the plasma. Plasma difference signals are a few percent of the individual probe and loop signals. Figure 13 shows typical magnetic difference signals with and without plasma in the high-density regime, and Fig. 14 gives reduced data for the low-density regimes plotted as effective area of flux excluded by the plasma vs time. The most striking feature is the rapid decay of excluded flux during the peak magnetic field time, giving another indication of substantial end-loss.

Density Profile Measurements

An experiment was performed to measure the plasma β in Scylla III using the technique reported by the Culham Laboratory. The continuum radiation from different chords through the plasma is measured by imaging the plasma radiation with a lens on a stack of optical fibers (Fig. 15). Each fiber connects to a separate photomultiplier. The outputs of the photomultipliers are monitored simultaneously, and nine channels are available. An interference filter is used to select a wavelength region

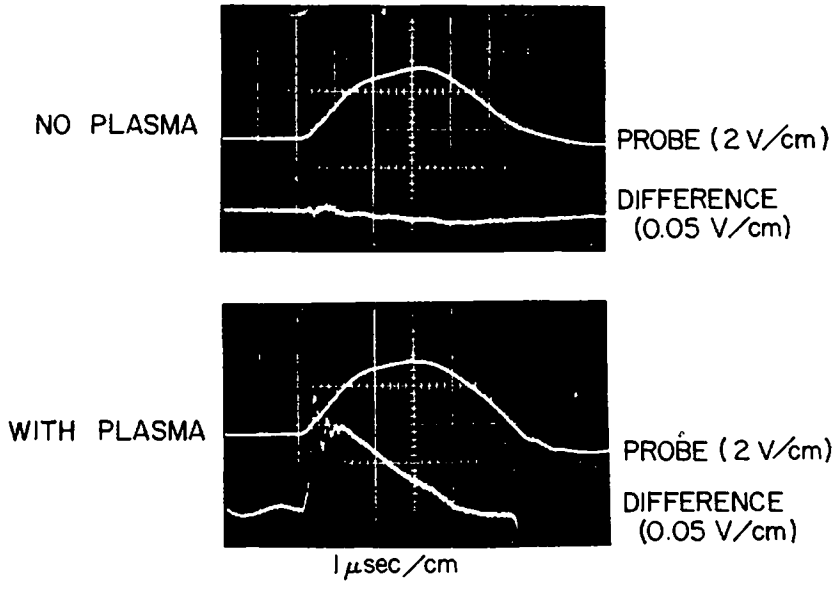

Fig. 13. Magnetic probe signals with and without plasma.

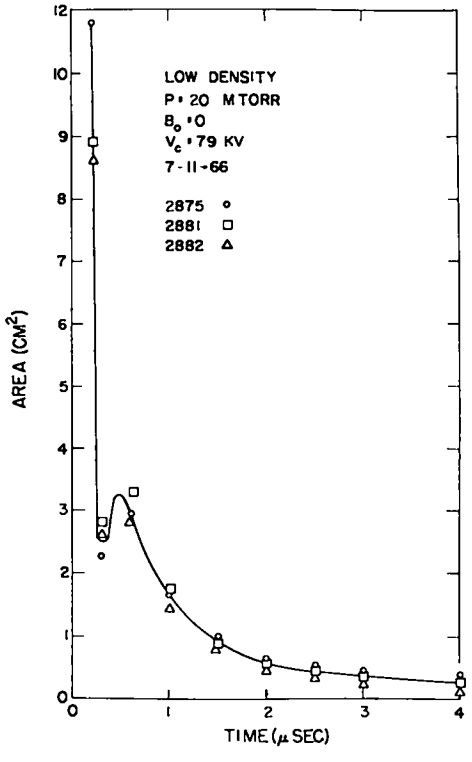

Fig. 14. Effective area of flux excluded by plasma vs time.

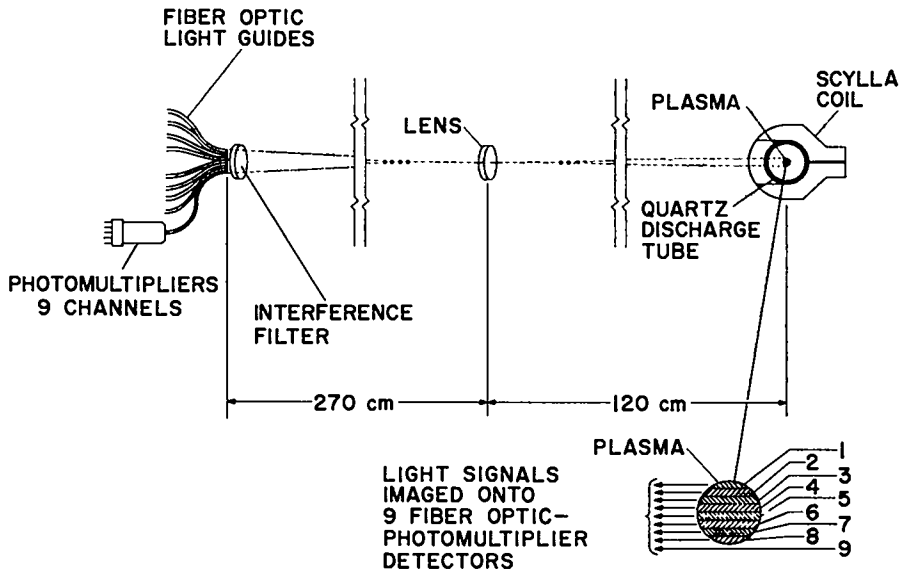

Fig. 15. Optical fiber system for measuring continuum radiation.

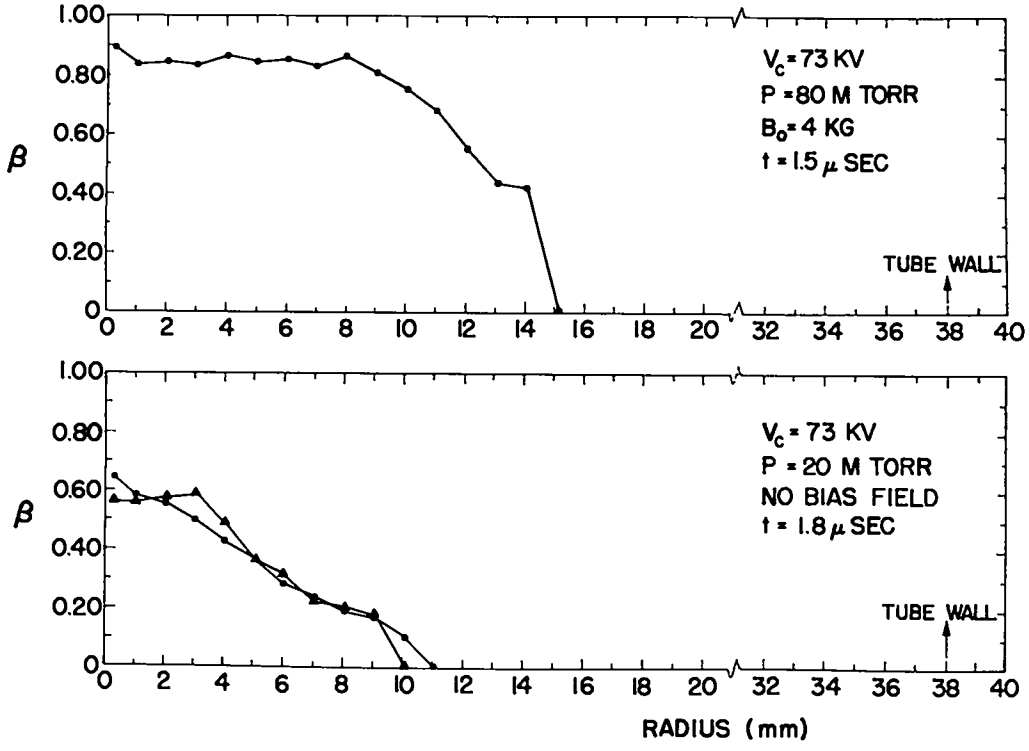

Fig. 16. Radial density distribution in low- and high-density regimes.

free of line spectra. In order to find a suitable region, the spectrum of the plasma (viewed side-on) was recorded photographically with the McPherson 1-m spectrograph. Most lines were identified as low ionization states of O and Si (II through IV). The spectra of all other elements were too weak to be detected except for some very intense lines of C III and C V. Several lines were examined photoelectrically. The radiation from them was found to occur mostly during the preionization period and after the main compression had occurred. An appropriate wavelength region free of lines (4978 ± 7.5Å) was selected with an interference filter. Wall light proved to be a serious problem but it was overcome to a large extent, since the intensity of this light appears to be constant in all channels.

The data from the nine channels were unfolded by an Abel inversion to give the radial density distribution. Results are presented in Fig. 16 for both the low- and high-density regimes. The square root of the relative light intensity is proportional to number density, and the absolute β scale is fixed by the magnetic probe experiments described below.

Side-On Density Measurements

An experiment was done to measure absolute integrated electron density along a vertical line (transverse to the plane of the feed-point) through the geometrical coil center with a He-Ne gas laser interferometer operating at 3.39 μ (Fig. 17). The presence of plasma in the external path between the laser source and the rotating corner reflector modulates the laser output, each fringe giving the integrated density. A regular progression of fringes is obtained when the feed-back mirror is effectively moved (by means of two traversals of a roof reflector on a rotating wheel) at a rate giving ~ 4 cycles/μsec of intensity modulation, with the plasma effects superposed as time distortions on this progression. Although the plasma effect is not now quite so qualitatively apparent, a comparison of the period of fringes on such a trace with a background trace obtained

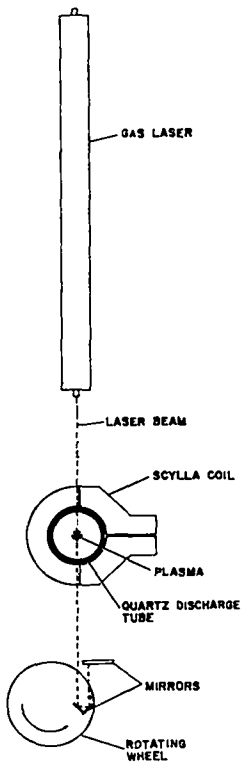

Fig. 17. Apparatus for side-on density measurement.

in the absence of gas filling leads to quantitative integrated density plots, such as that illustrated in Fig. 18. The data reduction is exacting and tedious. It is feasible to analyze many such traces only by using a large magnification comparator, digitalizing coordinates directly onto punched IBM cards, and obtaining the final results by an IBM machine program. In Fig. 18 the effect of the preionizer is first seen, followed by a sudden rise of density as the main compression bank is fired (and crowbarred).

Summary of the Scylla III Measurements

The three coordinated measurements on Scylla III described above yield (a) β, the ratio of plasma pressure to external magnetic

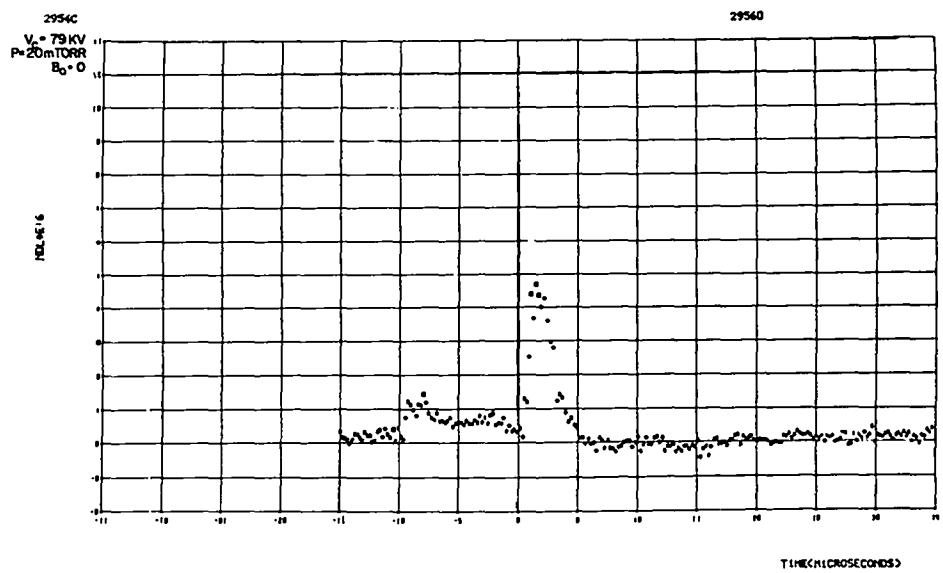

Fig. 18. Integrated density signal vs time.

field pressure, (b) n, the plasma density as a function of radius, and (c) T_i, the ion temperature. The three measurements are (1) the differential magnetic loop-probe measurement which determines flux excluded by the plasma, (2) side-on measurement of light intensity emitted by the plasma which yields the relative density profile, and (3) the side-on gas laser interferometer measurement which gives the absolute density integrated through the plasma diameter.

The assumed pressure balance equation

$$\frac{B_o^2}{8\pi} = \frac{B(r)^2}{8\pi} + n(r)k(T_e + T_i)$$

is solved for B(r) and integrated over plasma area, giving

$$\phi = 2\pi \int B(r)\, rdr = 2\pi \int \sqrt{B_o^2 - 8\pi n(r)k(T_e + T_i)}\ \ rdr.$$

Upon dividing through by B_o it follows that

$$\phi / B_o = \int \sqrt{1 - \beta(r)}\ \ rdr.$$

The magnetic probe loop experiment gives the flux excluded by the plasma on the left of the equation, whereas the light intensity profile gives the right side except for a normalization factor. The equation is then solved for the normalization factor and thus yields β as a function of radius (Fig. 16).

The gas laser interferometer gives $\int ndx$ across the tube, but since the shape of the density profile (or of β) is known from the light intensity profile, true plasma density, n, can be obtained as a function of radius.

Finally, using the definition

$$\beta = \frac{8\pi n\, k(T_e + T_i)}{B_o^2} \quad ,$$

and additional measurements of B_o from magnetic probing and of T_e from x-ray absorption, all quantities in the relation are determined except T_i and this can be derived.

Results averaged over many Scylla discharges are given in Table I. Measurements have been made in both low- and high-pressure regimes of Scylla III, but the gas laser interferometer results are relatively poor for the high-pressure case because the measurements were made before some refinements had been made in the technique. The doubtful values are in parentheses.

Table I

Scylla III Operating Conditions

	Low-Pressure Regime		High-Pressure Regime
V_{cap}, kV	73	79	73
Pressure, mtorr	20	20	100
B_o, kG	62.7	67.2	62.7
β on axis	0.57 ± 0.15	0.70 ± 0.15	0.85 ± 0.15
n on axis, cm^{-3}	2.6×10^{16}	3.0×10^{16}	(3.5×10^{16})
N, cm^{-1}	4.3×10^{16}	4.9×10^{16}	(1.2×10^{17})
T_e, eV	265	425	(400)
T_i, keV	1.9	2.2	(1.7)

As seen in Table I, the value of β for the high-pressure regime is nearly unity on the axis whereas that for the low-pressure regime is only about 0.7. This behavior is predicted by theory (R. L. Morse, this report, p.105) , which treats the adiabatic relaxation of an initially thin plasma sheath to a thickness of the order of an ion collisionless skin depth,

$\lambda_i = c/\omega_{pi}$. The theory predicts that for a particle line density $N = \int_0^r n(r)\, rdr$ less than about 5×10^{16} cm^{-1}, the relaxed sheath will be too thick to have the appearance of a distinct boundary region and the penetration of the B_z field into the center of the plasma will cause β to be significantly less than unity.

COHERENT SCATTERING EXPERIMENT ON SCYLLA III

(M. Daehler, F. Ribe, G. Sawyer, E. Zimmermann)

Introduction

Plans and motivation for this experiment were mentioned in a previous progress report (LA-3320-MS) and procurement of the giant-pulse ruby laser and Fabry-Perot monochromator were discussed in LA-3434-MS. Since then the ruby laser has undergone more development; the monochromator has been put into operation, and preliminary data have been obtained on Scylla III.

Mode-Control of the Ruby Laser

Considerable difficulty was experienced with the laser (Korad Model K-1Q) which used a sapphire resonant-reflector end plate and a cryptocyanine cell for mode selection. The original Pockels cell and electronics were replaced by a new unit involving pulse-on operation with a $\lambda/2$, fluid-immersed Pockels cell. The flash-lamp triggering system was also replaced. With these modifications the laser has operated quite dependably at power levels of between 50 and 100 MW. Considerable effort was required, however, to obtain an output consisting of a single line of about 0.02 Å width.

The laser originally tended to emit two or three narrow lines separated by 0.43 Å. Fabry-Perot etalons with 0.4- and 3-mm plate separation were used to study the structure of the laser emission. It was at first assumed that the mode spacing was due to Fabry-Perot action of the two surfaces of the sapphire plate used as a front resonant reflector in the Korad laser. But, since substitution of other sapphire plates of different thickness produced no change in the mode separation, it was concluded that some other sub-spacing in the optical cavity was dominating the mode structure. The

origin of this resonance was not identified. The mode structure could not be controlled satisfactorily either by temperature control of the ruby in the range 0°-25°C or with addition of a cryptocyanine saturable dye.

The sapphire-plate front reflector has been replaced by a sealed double sapphire-plate resonator consisting of two plates separated by an air space of optical thickness (~ 2.5 mm) equal to that of the plates. No saturable dye is used with the double resonator. The double sapphire plate has higher reflectivity and it governs the mode structure, where the single plate did not. At room temperature two or three modes separated by about 0.7 Å are observed. These modes are presumably adjacent orders of the double resonant reflector acting as a triple Fabry-Perot etalon. As the ruby is cooled, its emission wavelength shifts and the relative intensity of the observed modes changes progressively as the laser line becomes centered on successive orders of the resonant reflector. The natural line width also becomes narrower as the ruby is chilled, and at 8°-10°C the ruby line is sufficiently narrow so that only a single mode of the resonant reflector is selected. More accurately, photographic and photometric measurements show that other modes are about 0.3% of the main line.

The mode structure is illustrated in Fig. 19, as seen by the 0.4-mm spaced Fabry-Perot, with and without proper temperature settings of the mode-control system. Since the precise wavelength is determined by a particular order of the resonant reflector, the laser wavelength varies with the temperature of the reflector. A temperature change of 1°C shifts the laser wavelength 0.05 Å. It is necessary, therefore, to control the temperature of the sapphire resonant reflector to $\pm$ 0.25°C in order to achieve the desired wavelength stability. The ruby rod temperature must be controlled to about $\pm$ 1.5°C.

The Fabry-Perot Monochromator

The three matched Fabry-Perot etalons were delivered by Optical Surfaces, Ltd. Each is of 60-mm diam and has soft optical coatings of 95%

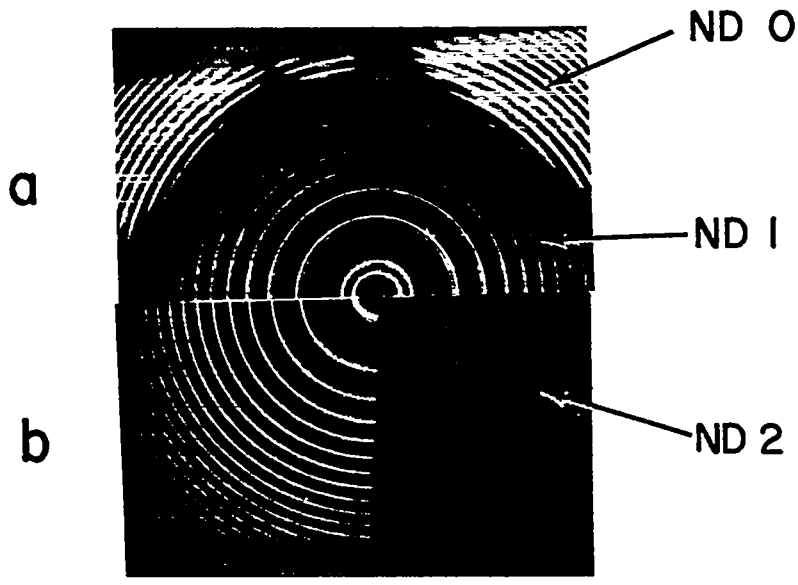

Fig. 19. Mode structure of Fabry-Perot patterns.

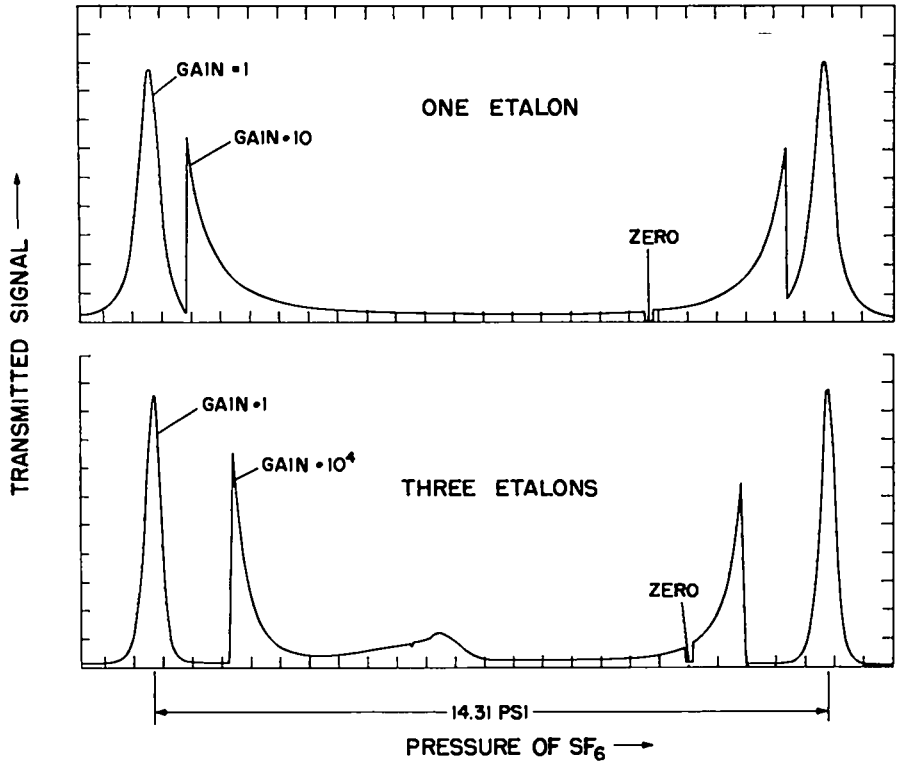

Fig. 20. Pressure scans of the Fabry-Perot patterns.

reflectivity at λ 6940Å. The etalons have identical, optical-contacted, quartz spacers of 0.44-mm thickness. By visual observation of the ring pattern and careful pressure scans with SF_6 in the sealed chambers of the monochromator the etalons are adjusted to maximum parallelism (about λ/100) and the spacings matched to about λ/200. Photoelectric pressure scans of the etalons with 1-mm apertures in the spectrometer are shown in Fig. 20. These were made with a λ 6328Å He-Ne gas laser as a light source, illuminating the same annular area of the etalons as that used in the scattering experiment. For a single etalon the contrast is 360, whereas for the three etalons in series it is 10^6.

Optical System of the Scattering Experiment

Schematic diagrams of the optical system for the scattering experiment are shown in Figs. 21 and 22. On the right-hand side of Fig. 22 is an optical bench supporting the Korad laser plus other optical elements to facilitate alignment of the entire system. A reproducibly insertable mirror allows the beam from a Spectra-Physics He-Ne laser (Model 130) to enter the scattering chamber for alignment purposes. A beam expander increases the lateral dimensions of the gas laser beam to match those of the Korad laser. The gas laser is aligned so that its beam exactly matches that of the ruby laser, both in direction and in lateral positioning. This alignment is facilitated by an auxiliary autocollimating telescope, which is suitable for aligning the axes of the poorly reflecting laser surfaces.

Before entering the scattering chamber, the laser beam is focused by a 30.5-cm f.l. lens and passed through a 1-mm aperture, to limit the angular divergence of the laser beam to 3 mrad. The 1-mm aperture is focused with unit magnification onto the scattering position, and again onto the entrance aperture of the spectrometer. The direct laser beam is stopped outside the scattering chamber by a beam dump consisting of two pieces of Corning-5113 blue glass, set at the Brewster angles for zero

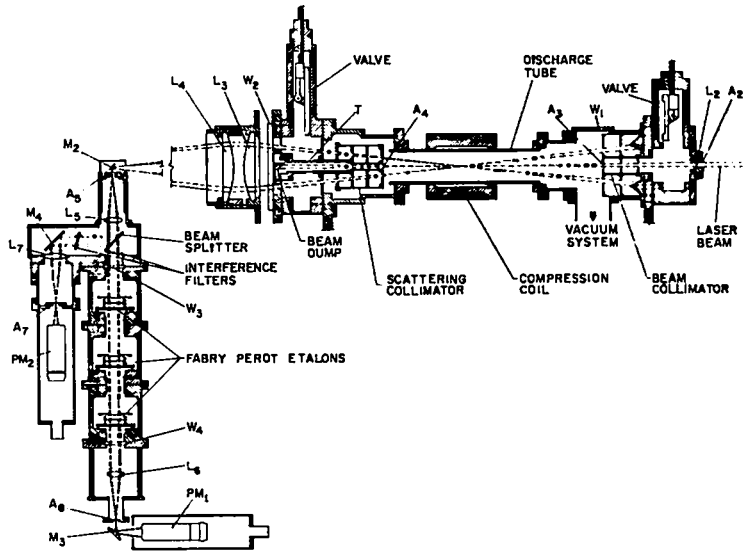

Fig. 21. Schematic diagram of optical system for scattering experiment.

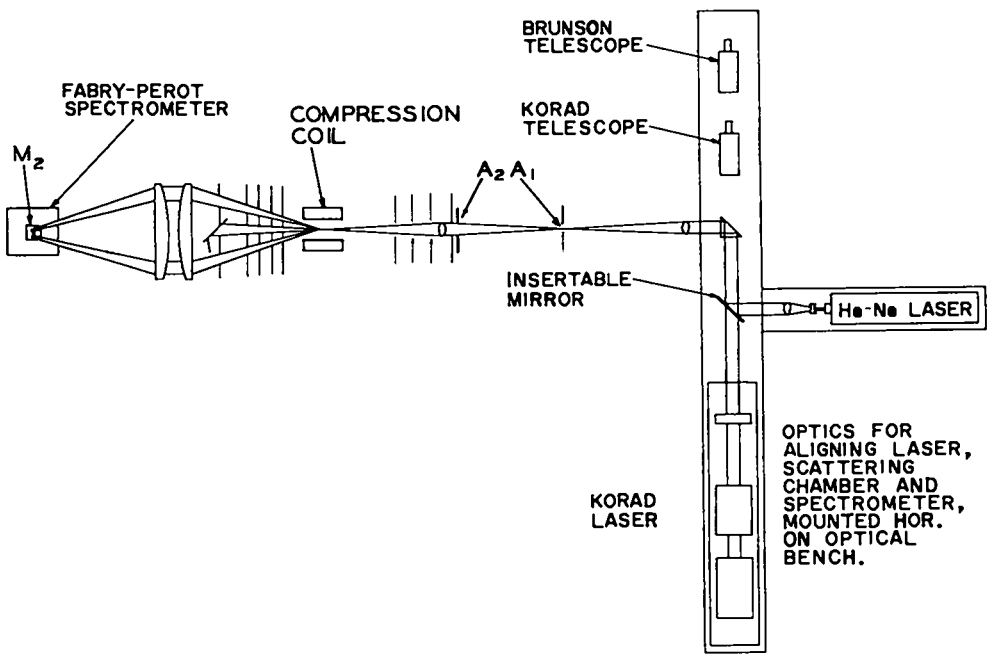

Fig. 22. Simplified view of optical system.

reflectance. The pair of plano-convex collecting lenses gather light which is scattered into angles from the axis between $5^{\circ}30'$ and $7^{\circ}0'$.

In the spectrometer (Fig. 21) the scattered light is collimated and transmitted through an interference filter and as many as three identical Fabry-Perot interferometers, and then refocused onto the exit aperture and detected by a RCA-7265Å photomultiplier. A beam splitter reflects a few percent of the beam into a lens-aperture-photomultiplier system identical with that of the spectrometer, providing a reference system to measure the intensity of scattered light after passing through the interference filter but before entering the Fabry-Perot etalons.

Scattering Measurements

As a calibration of the scattering system, the discharge tube was filled with air and SF_6 and Rayleigh-scattered signals measured as functions of filling pressure; the results are shown in Fig. 23. The ratio of SF_6 scattering to air scattering is found to be 4.7, which is to be compared with 5.9 reported in the literature.[1] It seems likely that the discrepancy is due to an excessively large value for the air scattering in the present experiment, resulting from impurities in the air.

The fact that the measured scattered signal does not go to zero with decreased pressure is due to stray light in the scattering chamber. From the data of Fig. 23, this stray light is smaller than the SF_6 scattering signal by the factor 10.4, and than the air scattering signal by the factor 3.2.

Preliminary scattering measurements have been made, using the Scylla III plasma in the low-pressure regime (20 mtorr filling pressure, $B_0 = 0$), at an average neutron yield per discharge of 6.2×10^8. Figure 24 is a graph of the net scattered signal at a mean scattering angle of

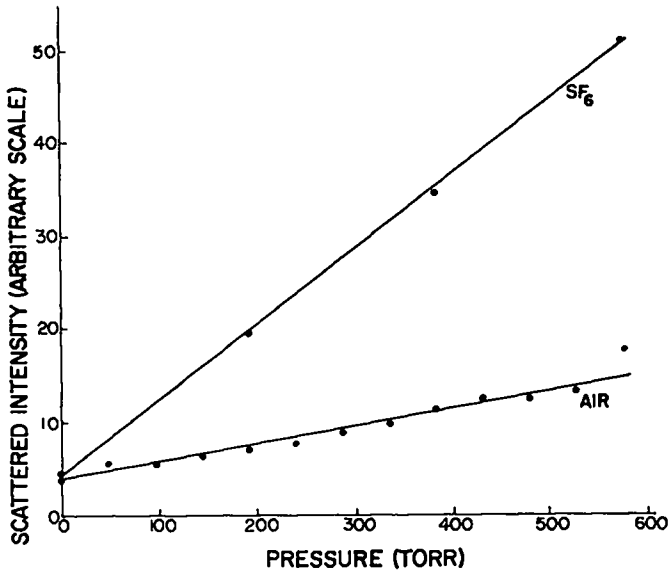

Fig. 23. Rayleigh scattering vs gas pressure.

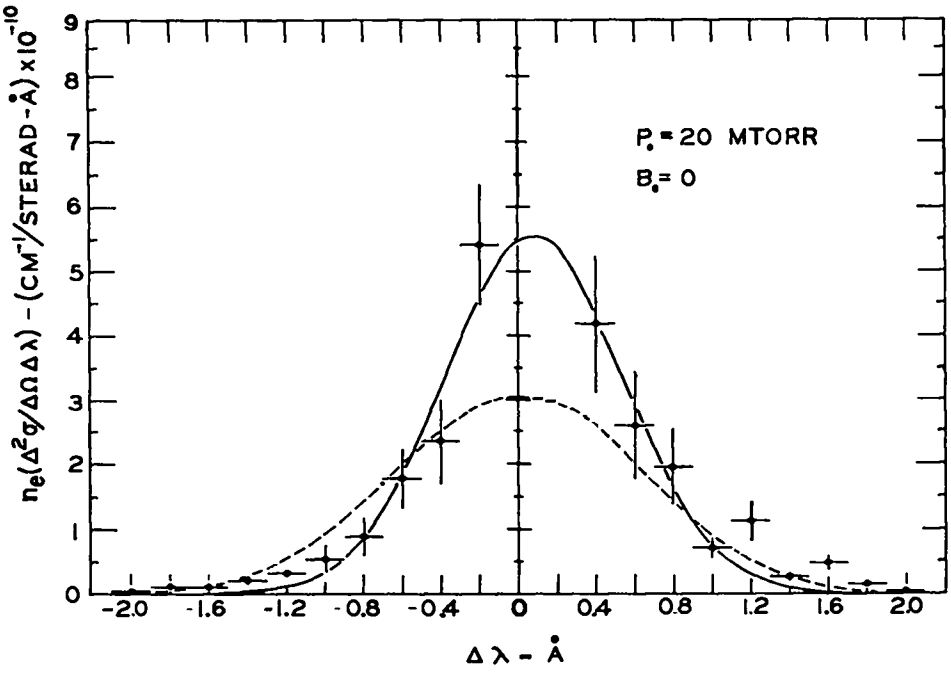

Fig. 24. Scattering signal of Scylla III plasma in low-pressure regime.

6.25° ($5.5^{\circ} < \theta < 7.0^{\circ}$). The ordinate plotted is electron density times differential cross section per unit wavelength interval, normalized to SF_6 Rayleigh scattering, for which the ratio $(SF_6)/N_2 = 5.85$ is adopted. The wavelength interval of the Fabry-Perot spectrometer was taken as 0.150 Å. The solid curve plotted is the least-squares fit of a Gaussian function to all the data points. The dashed curve is a corresponding fit of a centered Gaussian to all but the upper two points.

Reference

1. T. V. George, et al., Phys. Rev., 137, A369 (1965).

HOLOGRAPHY

(F. Jahoda, R. Jeffries, T. Langham, V. Finlayson)

Interferograms with a Continuously Operating Laser

A start has been made in the application of holography to plasma diagnosis. Of immediate interest to plasma research is the demonstration at Hughes and at TRW that holograms can be made with giant-pulse ruby lasers, and by the group at TRW (among others) that the ability to record phase is readily extended to recording interference effects if phase changes occur in the object field between consecutive exposures on a single hologram plate. Applied to plasmas of interest, this means that it should be possible to duplicate most of what has been done with the Mach-Zehnder in the past, separating the "comparison beam" in time rather than space. The advantages of this approach are:(1) there is no longer a restriction to only high quality optical flats in the path, e.g., it is possible to look through an ordinary curved (transparent) vacuum vessel; (2) if a diffuser is used in the beam before illuminating the object field, additional information is retrievable from the three-dimensional effect, i.e., the fringe shifts reflect phase changes which themselves are a function of the viewing direction by the observer; and (3) as illustrated below for the case of a gas laser hologram, a set of background fringes can be accurately and reproducibly located in space with plasma effects, which may be only superposed fractional fringes.

The first step taken was to learn how to make and play back holograms of objects in transmission or reflection and demonstrate interference phenomena for double exposures with a 5 mW, single-mode, Perkin-Elmer He-Ne gas laser. The geometry is indicated in Fig. 25. With the laser beam

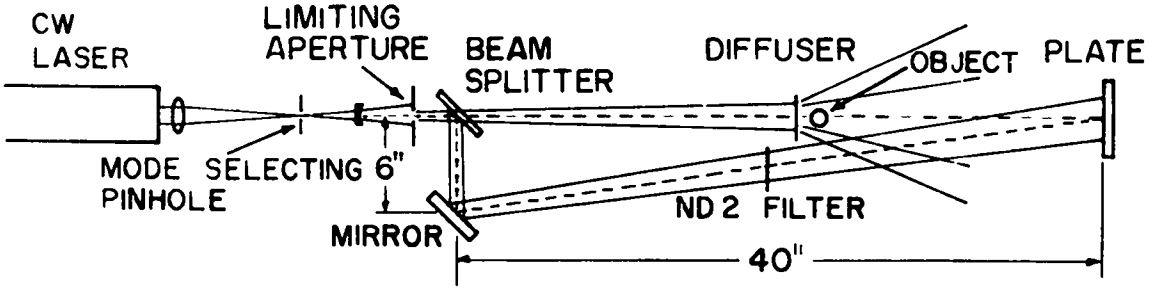

Fig. 25. Arrangement for study of holograms.

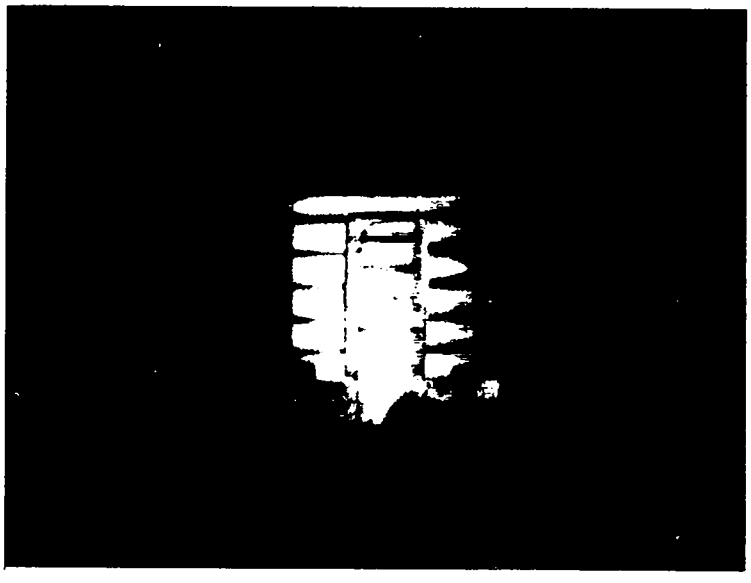

Fig. 26. Double-exposure hologram of two wedges.

expanded to the order of 50 cm^2, a 50-50 beam splitter, a diffuser in the object field at a distance of ~ 15 cm from the hologram plate (and ND-2 attenuation in the reference beam to improve equalization of intensities at the plate), exposure times of 2-10 min were required for the very high resolution but correspondingly slow 649F plates.

Figure 26 is a photograph of the reconstructed virtual image of a double-exposure hologram of two lucite wedges placed in series behind a diffuser in the object field; the two wedges have their apex lines parallel but differing in wedge angle. The wedges were filled with air for one exposure and with He for the other. For these gases at atmospheric pressure an optical path difference corresponding to one fringe results for a path length of about 3 mm. The distortion of the straight line fringes of the large wedge introduced by the small wedge can be easily seen. The wedges were made of poor quality lucite and no further optics were introduced. The spacing and location of the background fringes--other symmetries, e.g., circular fringes, could be utilized--is controlled by gross adjustments of wedge angle and position rather than by delicate optical alignment. In a plasma experiment, which will differ primarily in the use of a giant pulsed ruby laser instead of the gas laser in order to give the requisite time resolution, the large wedge would be retained to form, on double exposure, a set of background fringes whereas the smaller wedge would be replaced by plasma and no plasma, respectively, on the two exposures. The plasma will thus show up as a distortion on the background.

Pulsed-Laser Interferograms

The TRG-302 giant-pulse laser amplifier-oscillator has also been used successfully to make short exposure time holograms on SO-243 film. This film has a resolution in excess of 500 lines/mm and is about 1000 times faster than 649F at the ruby wavelength. The key parameter is a sufficiently narrow wavelength band laser emission. This was achieved by chilling the cooling water to about 10°C, and, surprisingly, operating the laser well in excess of threshold. Unlike the Korad 1-Q laser, for which mode control is

discussed on p. 34, the only front "resonant" reflector in this case is the combination of the exit face and entrance face of the oscillator and amplifier ruby rods,respectively. Invariably, the insertion of cryptocyanine into the cavity considerably complicated the mode structure. Omitting the passive dye results in two or three consecutive pulses, the main two separated by 1 μsec. This is due to the "slow" switching action of the rotating prism. Each pulse has the desirable mode structure discussed above (that is, the Fabry-Perot patterns have not been time resolved).

The double-pulse feature has been used to advantage in the holographic interferometry of an exploding wire. Figure 27 is a picture of a squib, consisting of a 0.090-in. length of fine gold wire mounted on a threaded insulator. The upper portion of Fig. 28 is an oscillograph in which the upper trace indicates the time when about 1 J of capacitively stored energy is dumped into the wire and the lower trace shows the double laser pulse. The lower portion of Fig. 28 shows the mode structure (3-mm Fabry-Perot etalon, 0.8 Å free spectral range) for this particular laser firing. Figure 29 is a photograph of the reconstructed virtual hologram image, showing a differential interferogram due to shock heating of the air between the separate laser pulses. The squib is seen in profile with the screw threads clearly outlined.

The hologram picture does not look very different from one that could be made with an ordinary interferometer. However, the important differences are as follows: (1) No optical flats were used, and the wire could have been inside an arbitrary shape transparent vessel. (2) More information than shown remains stored in the hologram, for the fringe structure changes as the viewing direction changes; to utilize this feature quantitatively, it is only necessary to add two fiducial scales separated in depth to the original scene. (3) The fringe structure reflects the refractive index changes between two moments in time, the first of which may or may not be chosen to occur before any initial disturbance starts. No attempt was made to analyze this event quantitatively, or to improve the quality of the interference hologram, since it is considered to be only a feasibility demonstration.

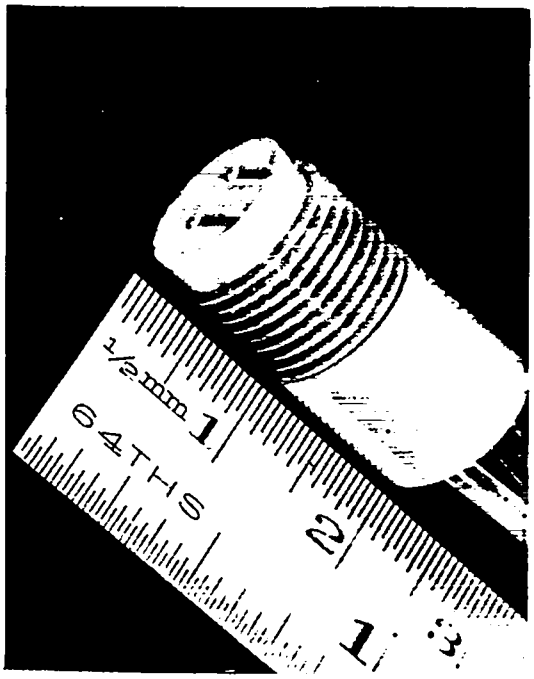

Fig. 27. Photograph of exploding-wire squib.

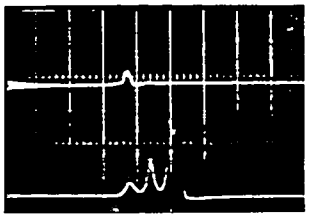

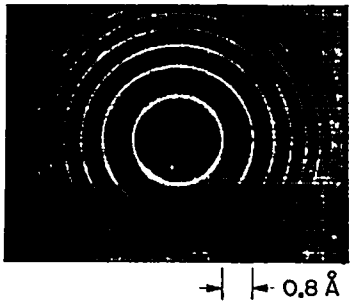

Fig. 28. Oscillogram (above) and Fabry-Perot pattern (below) of exploding wire.

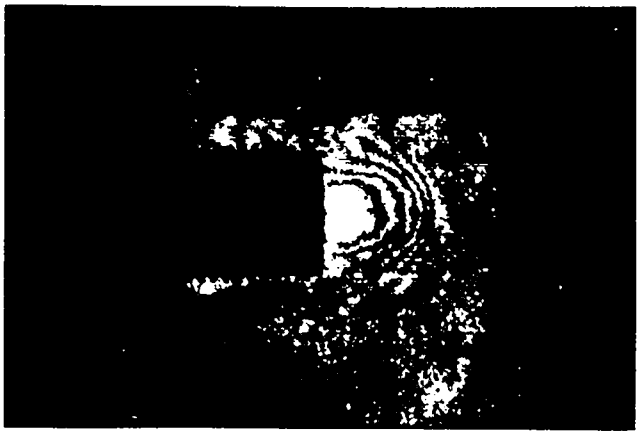

1 cm

Fig. 29. Reconstruction of virtual hologram image of exploding wire.

SCYLLACITA, A SMALL THETA-PINCH MACHINE

(R.S. Dike, E.L. Kemp, R. Kewish, Jr., G.A. Sawyer, D. Thomson, J.L. Tuck)

Scyllacita is a machine to produce a hot compressed plasma in a coil suitable for imploding with a high explosive (HE) system. The HE compression can, in principle, increase the magnetic field by several orders of magnitude and greatly increase the thermonuclear yield.

The Scyllacita bank consists of 24 14-μF, 20 kV, low-inductance capacitors, each with an individual spark gap. The bank circuit connects two capacitors in series when the gaps fire and in normal operation applies 21 kV to the coil terminals.

The system was first installed in Sherwood laboratory space and various modes of operation were investigated using a customary massive coil. A complete parameter study was made to determine optimum values for the D_2 pressure, bias, preionizing, and main fields, and firing times for the three banks. A regime was found that would produce 10^5 neutrons on the first half-cycle of operation.

After the parameter study, a thin-wall, flimsy coil and a glass discharge tube were installed, both suitable for an HE shot. A warm-up procedure which is required for the HE shot was established. Scyllacita reliably produced $> 10^4$ neutrons on the first half-cycle. The capacitor bank switches were completely refurbished and the entire system moved to the firing site for installation and checkout. The performance described above has now been attained at the firing site.

Z-PINCHES: COLUMBA AND FAST DYNAMIC Z-PINCH

Introduction (J. A. Phillips)

The region of interest in the z-pinch experiments is the ultra-high density end of the reactor $n\tau$ diagram[1] where the plasma pressures may greatly exceed the strength of materials. A serious drawback, of course, is the strong hydromagnetic instability of the z-pinch. It is a curious fact, however, that in the early work at LASL and elsewhere with the dynamic pinch culminating in Columbus II (LASL) high plasma temperatures were never obtained. The suggestion was made that the stability of a high temperature z-pinch should be investigated since high conductivity and large Larmor orbit effects may extend the lifetime sufficiently to have reactor possibilities.

Two series of experiments are therefore being made in efforts to produce hot z-pinches: (1) an attempt to produce fast dynamic z-pinches by electric fields considerably higher than have been used heretofore and (2) Columba, the application of a fast dynamic z-pinch to plasma preheated by a Scylla θ-pinch.

In the fast dynamic pinch experiments attempts are being made to apply to a linear discharge those longitudinal electric fields (~ 3 kV/cm) which will give inward radial velocities to the pinch necessary for thermonuclear temperatures. In the past, with Columbus II at LASL, for example, it had been found impossible to apply these fields, primarily because of failure of the discharge tube walls to hold off more than ~ 2 kV/cm. In the present experiments it is hoped to circumvent this limitation by internal magnetic energy storage. Energy from capacitors is fed relatively slowly into the experimental device under those conditions in which an insulator does not fail and is stored as magnetic energy in an inductor

inside the experimental device. At maximum current the z-pinch is switched in series with this inductance and the fast change in current will induce very large voltages and drive a fast dynamic pinch. Since all this takes place inside the system the problem of the insulator is avoided. At present, the role of the switch inside the system is to be performed by the motion of a current sheath.

This concept is perhaps not new to the CTR program as there are a number of examples in which energy is first stored as magnetic energy in the system and then switched into plasma thermal energy or directiod motion of plasma. In the coaxial hydromagnetic gun of J. Marshall and the dense plasma focus of J. W. Mather, capacitor energy is stored as magnetic energy between the electrodes and when the current sheath falls off the end of the center electrode, the magnetic energy drives a fast current pinch radially inward which either accelerates plasma axially outward or focuses plasma in the axis. In these experiments the induced voltage across the ends of the electrodes may be considerably higher than the applied voltage. In the present experiments, it is desired to maximize the stored magnetic energy and utilize this energy to drive a fast linear z-pinch.

Fast Dynamic Z-Pinch Experiments (J. A. Phillips and A. E. Schofield)

It has been necessary first to investigate the characteristics of the current sheath such as its velocity as a function of applied voltage, discharge current, and initial gas pressure. Two geometries have been examined: (1) the axial motion of a current sheath between two coaxial electrodes and (2) the radial inward motion of a current sheath between two end electrodes in a conventional z-pinch.

Axial Motion of Current Sheath

The axial motion of a current sheath was examined in the geometry shown in Fig. 30a. The outer diameter is 26 cm with a length of 92 cm, the inner electrodes have 15 cm diam and are separated by 7.5 cm at

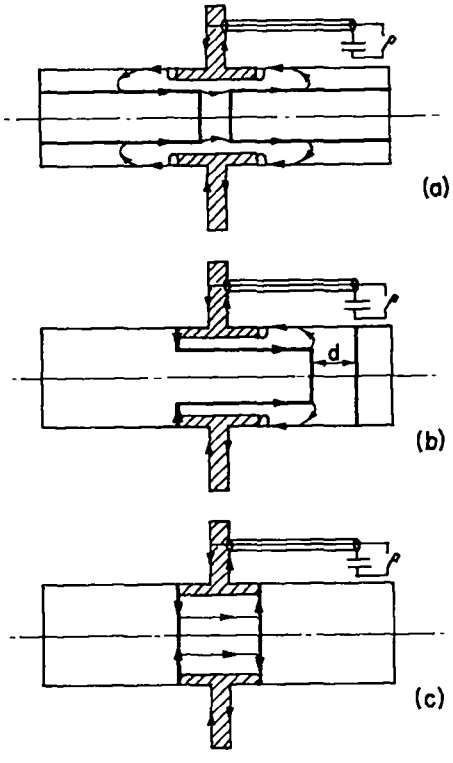

Fig. 30. Three geometries used in fast dynamic z-pinch experiments.

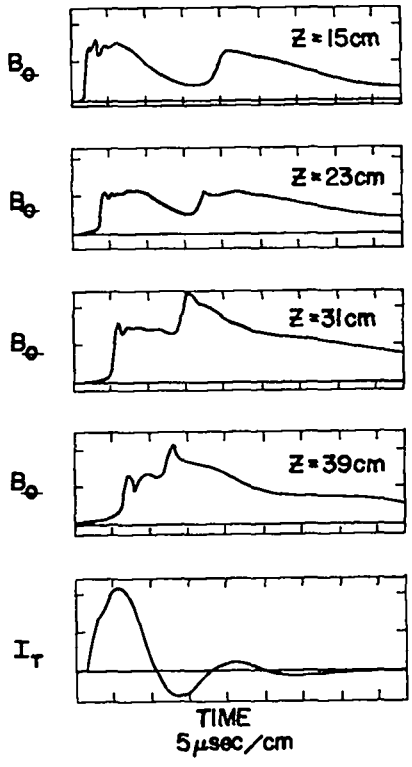

Fig. 31. Magnetic probe traces at four axial positions; the lower trace is the total discharge current.

the midplane. A capacitor bank of 270 μF at 20 kV drives the discharge. This geometry was initially chosen to store magnetic energy in the annular space between the concentric electrodes. During the discharge two current sheaths (one on each sice of the midplane) moved from the midplane and appeared to reflect off the chamber end walls and return to the midplane. Magnetic probe traces taken at four axial positions are shown in Fig. 31, together with the trace of total discharge current (I_T) from the power supply. The first rise of B_θ magnetic field should be noted as the current sheath initially passes over the probes followed by a second rise when the reflected shock returns. A plot of the arrival times of these sheaths as a function of axial position is shown in Fig. 32. These data were taken with a blue glass insulator fused to the outer electrode about the midplane.

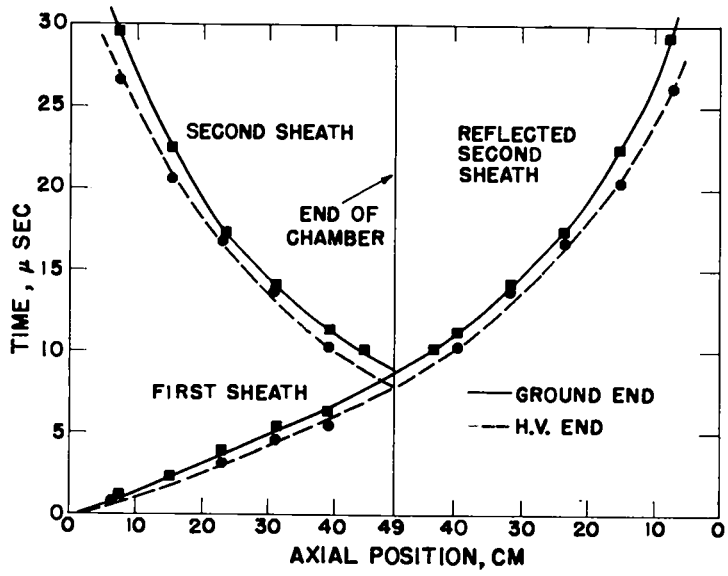

Fig. 32. Arrival time of current sheath vs axial position.

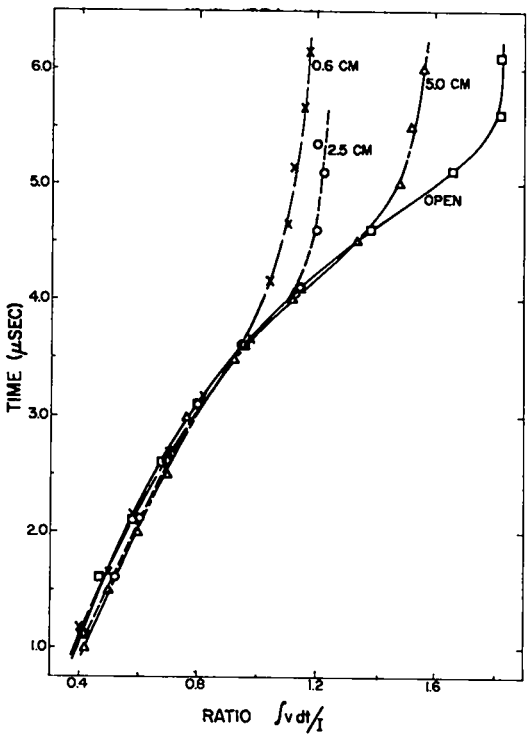

Fig. 33. Contour plot of B_θ as function of axial position and time.

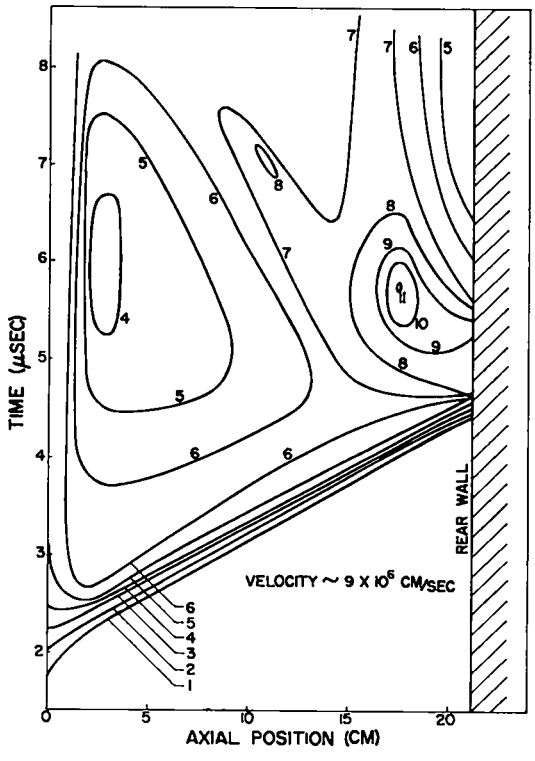

Fig. 34. ∫Vdt/I as function of time for four values of shorting plate-inner electrode separation.

A contour plot of the magnitude of the B_θ field at a constant radius (11.5 cm) as function of axial position and time is shown in Fig. 33. In this case the blue glass insulator was replaced with high-purity alumina. The magnitude of B_θ ("elevations" in the plot) are arbitrary. A current sheath (thickness $\sim$2-3 cm) is seen moving toward the end wall with velocity $\sim 9 \times 10^6$ cm/sec and striking it after $\sim$6.6 μsec. On reflection there is again enhancement of the magnetic field which in this case is most pronounced at the axial position z = 17.5 cm at 5.95 μsec. Here the local B_θ field rises to $\sim$ 11 units whereas the maximum B_θ seen prior to this peak was only 6 units. The magnetic field has almost doubled on reflection of the current sheath by the end plate.

An explanation of this phenomenon is thought to be as follows: An axial current sheath which is perpendicular to the axis does not snowplow up the plasma but is leaky. It has been shown in previous work at LASL that the axial electric field across the sheath in this geometry falls off inversely as the square of the radius. As this electric field accelerates the ions, only those particles close to the center electrode may be swept up by the sheath; those at larger radii are accelerated to lower velocities and fall behind. The net result is that behind the sheath there is a slower moving plasma in which a B_θ field is trapped. When this plasma collides with the end wall the forward momentum of the plasma compresses the contained field which in turn exerts an increasing pressure on the plasma and brings it to rest.

This increase in the magnetic energy density near an end plate, by about a factor of four, has raised the possibility that the enhanced magnetic energy in this region might drive a fast linear pinch. The geometry used is shown in Fig. 30b and is similar to the coaxial gun with the addition of a shorting plate positioned at various distances, d, from the end of the center electrode. The idea was to generate in the region between the end of the inner electrode and end plate the enhanced magnetic field which in turn would drive a linear pinch radially inward between the end of the center electrode and the shorting plate.

The results of a series of experiments at 10 kV and D_2 filling pressure of 0.2 torr are as follows. Between the two concentric electrodes the current sheath moving toward the short was not planar but tipped backward with the leading edge close to the inner electrode. When the leading edge of the sheath arrived at the end of the inner electrode, it "rolled over" the edge of this electrode and contracted radially inward toward the axis. A reflected hydromagnetic shock from the axis then expanded radially outward striking the outer electrode before arrival of the trailing edge of the initial current sheath moving axially between the electrodes. Thus, near the end plate there is a "current vortex" which is due to magnetic energy reflected from the axis. It has not been possible therefore to bring about an enhancement of local magnetic energy density by a reflected shock in the gun geometry.

In these experiments it was of interest to study not only the behavior of the primary current sheath but also to determine whether there were secondary breakdowns during the discharge cycle. This was done by noting that the voltage V across the header is determined by

$$V = \frac{d}{dt}(LI),$$

where L is the inductance of the discharge and I the total discharge current. (It is assumed that the resistance of the discharge is negligible). It follows that

$$L = \frac{\int_0^t V\,dt}{I} + L_o,$$

where L_o is a constant inductance evaluated at $t = 0$.

The behavior of the ratio $\int V\,dt/I$ with time for four values of d, the separation of the shorting plate from the end of the inner electrode, is shown in Fig. 34. Within experimental error, the initial behavior is identical for all four cases. The first divergence between the curves appears for $d = 0.6$ cm at a ratio of 0.96 at 3-6 μsec. It is perhaps safe to assume that the leading edge of the current sheath has at this time

moved over the end of the inner electrode. (The other three curves continue to higher inductances as the discharge is allowed to expand further along the axis). The ratio value of 0.96 corresponds to an inductance which is only 55% of that calculated for the volume between the two electrodes. This result indicates that only part of the axial current returns in the outer electrode,while a considerable fraction passes through the plasma. (This is in agreement with magnetic probe measurements taken as a fraction of radius). From these results it is concluded that at 10-kV charging voltage and 0.2-torr gas pressure the discharge and insulator are well behaved.

As the charging voltage is raised to 14 kV the change in inductance initially increases faster with time, as expected. At 17 kV the rate is still faster but there now appears a sudden break in the curve. At 20 kV this break occurs earlier in the discharge cycle. It is suggested below that these breaks in the curves correspond to secondary breakdowns.

Neutrons were produced for all positions of the shorting plate except with d = 0.6 cm. Peak neutron yields ($\sim 10^7$ n/discharge) were produced at charging voltages of $\sim$ 10 kV falling by a factor of $\sim$ 10 at 15 kV. Neutron generation was relatively insensitive to initial D_2 gas pressure with a broad maximum between 0.1-0.3 torr. There was no increase in yield for filling pressures > 1 torr for all four cases and this indicated that the regime was not that of the dense plasma focus.

The following tentative conclusions have been reached from the "gun geometry" experiments: (1) The region behind the current sheath in these experiments is apparently loaded with conducting plasma. This plasma will slow down the axial flow of magnetic energy in the annular region between the coaxial electrodes and consequently limit the maximum voltage which can be used to drive a dynamic pinch. (2) At the higher charging voltages there is evidence of a secondary breakdown behind the current sheath.

Radial Motion of Current Sheath

The behavior of a current sheath which moves radially inward was examined using the geometry shown in Fig. 30c. Here a 13.2-cm long linear z-pinch was formed between two end electrodes. The alumina insulator used in the preceding experiments was unchanged. Preionization was found necessary to give a uniform breakdown at the insulator and was produced by discharging 0.4 μF at 15 kV about 1-10 μsec before the main capacitor bank was fired. Magnetic probes measured the B_θ magnetic field as a function of time.

The motion of the initial current sheath was again determined from $\int_o^t V\,dt/I$ as a function of time. As the voltage was raised the initial time rate of change of inductance increased. It was seen, however, that as the voltage was increased abrupt changes in this ratio began to occur. There are at least two possible explanations for these breaks: (1) The current sheath is bouncing and changes in radius are reflected in changes of inductance. This explanation is considered to be unlikely since the minimum calculated radius of the discharge is still large, 3 cm at 10 kV, 5 cm at 14 kV, and does not systematically decrease with increasing voltage and discharge current. (2) There is a secondary breakdown of the discharge behind the current sheath which produces an increase in the total current and reduces the ratio $\int V\,dt/I$.

If there is a secondary breakdown, it is of interest to ask whether there might not exist a critical electric field which is the same for all charging voltages at the time of the abrupt break. Such an electric field would be given simply by

$$E_c = \dot{L}\,I + L\,\dot{I}\ ,$$

where in this geometry

$$\dot{L} \propto \dot{R}_p/R_p$$

and R_p is the pinch radius.

From the data E_c can be calculated along the surface of the insulator wall and, with the one exception for a charging voltage of 5 kV, all the experimental values group about an electric field of ~ 640 V/cm. This result suggests that a critical electric field of ~ 600 V/cm exists at which the insulator fails and a secondary breakdown occurs. The relatively low value of 600 V/cm is unexpected since similar discharge tube walls in other linear z-pinch devices, such as Columbus II, hold off ~ 2 kV/cm during the initial stages of the discharge. A possible explanation is that in the present experiments the insulator is being subjected to heavy uv bombardment which reduces the insulating properties of the surface.

From the break in the $\int V\,dt/I$ curves for the gun geometry the same value is obtained (within 10%) for a critical electric field. It is therefore tentatively concluded from the data examined so far that in the two geometries, linear pinch and coaxial gun, there is an apparent failure of the insulator at about the same critical electric field.

The data have not yet been completely analyzed for sheath velocities as a function of voltage and gas pressure. When this is done, it should be possible to match a fast dynamic pinch experiment, using magnetic energy storage, to the available capacitor bank. An expected complication has been found, namely, the possible existence of a critical electric field, considerably below previous estimates above which the insulator fails.

Comparison of Z and θ Geometries

Finally, it is of interest to compare the insulator requirements in the two geometries, θ-pinch and z-pinch. In the θ-pinch the maximum azimuthal electric field occurs near the start of the current cycle and becomes zero at current maximum. In the z-pinch, however, with pre-ionization the electric field is initially a minimum, increases as the

discharge is driven toward the axis, and becomes a maximum near maximum compression at which time the insulator is being bombarded with intense uv radiation and energetic particles. This behavior of the electric field may explain in part the difference in performance between the two geometries. It should be pointed out that the present ideas for magnetic energy storage are designed to reduce the required insulating properties of the discharge tube wall and this observation of a critical electric field during the compression stage supports still further that this is the direction which must be followed.

Columba (J.A. Phillips, A.E. Schofield, J.L. Tuck)

In the Columba experiment plasma is first heated and compressed by a θ-pinch. From work at LASL and elsewhere the density and temperature of this plasma is well known. At peak B_z magnetic field a z-pinch is energized which further compresses the plasma by the much larger magnetic fields that are possible. In the present experiment the θ-pinch is almost an exact duplicate of the Scyllacita experiment (p. 46). The z-pinch is also conventional with an interelectrode spacing twice the length of the θ-pinch coil.

At the outset a possible serious experimental difficulty has been recognized. When the z-pinch is turned on, the electric field is parallel to the B_z field of the θ-pinch. If there is a significant amount of gas or plasma between the discharge tube wall and the θ-pinch plasma, a second discharge will probably be initiated in this region. There is evidence from the Columbus II and Perhapsatron experiments at LASL and the rotating field pinch experiments at Jutphaas (Netherlands) that this secondary discharge may occur. The z-pinch magnetic field must then not only contain the plasma pressure but also the trapped B_z field. The behavior of the system must await the experiment and a number of possible modifications are available which may minimize this difficulty.

In the long run, the Columba experiment is also thought to be the first step in the development of a rotating field pinch at LASL: the continuous application of oscillating B_z and B_θ magnetic fields 90° out of phase. The penetration of these fields into the plasma may lead to a high shear in the plasma-magnetic field interface.

The design specifications of this experiment are as follows:

1. θ-pinch

   Coil: Length 28 cm, inside diameter 8 cm
   C = 44.5 μF at 50 kV, rise time ~ 2 μsec

2. Z-pinch

   Interelectrode spacing 54 cm
   Diameter of outside return ~ 10 cm
   C = 32.4 μF at 50 kV
   Assuming a pinch diameter of 2 cm, the maximum B_θ magnetic field is ~ 140 kG with a rise time ~ 4 μsec

The switches for the θ-pinch are triggertrons designed by R.S. Dike and E.L. Kemp at LASL, and those for the z-pinch the vacuum spark gap follow closely the design of J.W. Mather (cf p.23). To increase the total magnetic pressure, a crowbar switch is available in the θ-pinch at peak B_z magnetic field. Since this switch must close at or near zero voltage a vacuum spark gap is required in this application and we have followed the design of Ornstein, et al.[2] This design lends itself particularly well to applications in which the switch is located between parallel plate transmission lines and differs primarily from the Mather gap in that Teflon is used instead of pyrex glass for the insulator. Inadvertently, it has been found that polyethylene is superior to nylon or Teflon with initial pumpdown times and delays between shots being reduced by about a factor of two.

The experiment is now under construction. The θ-pinch has been run without a discharge tube and the electrical parameters agree with those calculate

References

1. J. L. Tuck in "Review of Controlled Thermonuclear Research at Los Alamos, 1965," LA-3253-MS (Rev.).
2. L. Th. M. Ornstein, et al. J. Sci. Instr., 42, 659 (1965).

CAULKED STUFFED CUSP EXPERIMENT

(L.C. Burkhardt, J.N. DiMarco, H. Karr)

Caulked Stuffed Cusp Interchange Stability (Min. B and Min Av. B)

The caulked stuffed cusp is an axisymmetric device designed to study the stabilizing effects of minimum B or minimum average B and magnetic shear on plasma confinement. The magnetic field has three components: (1) a dc axial field produced by a 180-turn solenoidal winding around the cylindrical vacuum tank (5 ft diam, 10 ft long), (2) a pulsed field (4×10^{-3} sec half-period) from a four turn ring or "caulker" coil at the midplane of the system, and (3) two pulsed stuffer field (8×10^{-3} sec half-period) produced by conductors through the axis of the assembly.

The relative amplitudes of the three field components can be adjusted to alter the location of the minimum B and the shape of the confinement field. Two configurations of particular interest are shown in the field plots in Figs. 35 and 36. To obtain the flux surfaces and surfaces of constant $|B|$ shown in cross section in Fig. 35, the field components are adjusted to form the field minimum near the midplane of the system. By reducing the solenoid current and increasing the stuffer current relative to that of the caulker loop the configuration of Fig. 36 is obtained. Stability theory indicates that the first of these is a minimum-B stable geometry and the second is minimum-average-B stable.

Minimum-B Stable Geometry

Stability Theory

The first field configuration (Fig. 35) forms a magnetic well that satisfies the minimum-B field stability criteria of J. B. Taylor[1]: (a) the magnetic field is nowhere zero so that adiabatic containment is

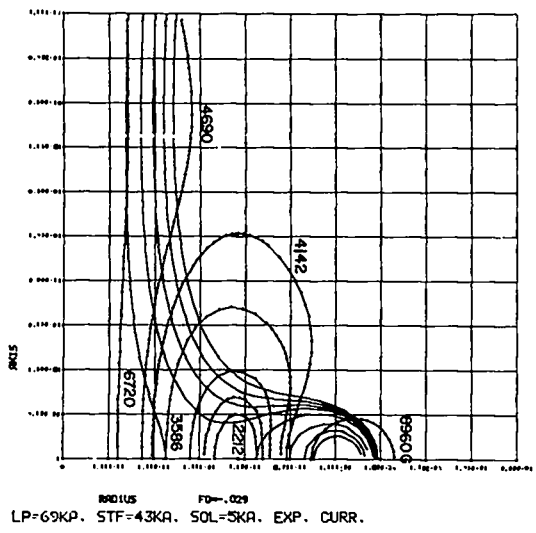

Fig. 35. Magnetic field plot for minimum-B stable geometry.

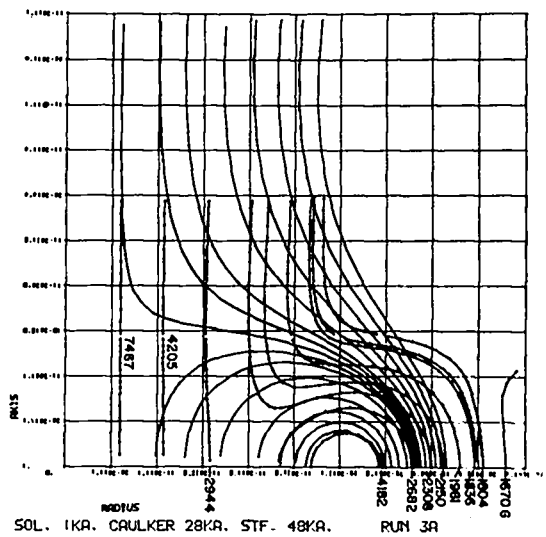

Fig. 36. Magnetic field plot for minimum-average-B stable geometry.

possible, and (b) the field increases outward from the containment region so that the surfaces of constant $|B|$ form a set of closed nested surfaces about the minimum. The magnetic flux surfaces include "closed" field lines that enclose the caulker ring and "open" field lines outside the "closed" system. Particles leaving the minimum region encounter a magnetic mirror ratio of ≤ 3 in the axial direction and a ratio of ≤ 6 along the field lines encircling the caulker. Since the field strength increases radially outward, the mirror or flute instability should not occur. Furthermore, drift instabilities associated with j should be corrected.[1] The loss cone instability, however, may be present in this configuration.

Allowed Regions of Particle Motion

Because of the axial symmetry of the field configuration, the Hamiltonian formalism provides information concerning the general character

of particle motion through the constants of motion $P\varphi$ and H (ignoring collisions and instabilities). The motion of particles of a given $P\varphi$ and H are bounded by an effective potential defined by $\Phi = (P\varphi - qrA\varphi)^2/2mr^2$. Preliminary calculations show effective potential wells capable of confining particles of several keV energy. Additional computer calculations are being made to complete analysis of the allowed region and to determine what part of the $P\varphi$,H phase space occupied by injected particles can be contained within the system.

Minimum-Average-B Stable Geometry

Stability Theory

The field configuration in Fig. 36 is obtained by decreasing the external solenoid field component relative to that of the caulker loop until the stagnation points are moved axially ~ 30 cm from the midplane. The minimum-average-B interchange stability criterion of J. M. Greene and J. L. Johnson[2] is

$$V^{**} = \left(\int \frac{dl}{B_p}\right)' - \left(\int \frac{dl}{r^2 B_p}\right)' \frac{\int \frac{dl}{B_p}}{\int \frac{dl}{r^2 B_p} + \frac{1}{R^2 B_\theta^2(R)} \int B_p dl} < 0 .$$

In this relation, r = the distance from the axis, R = the radius of the caulker loop, B_p = poloidal field in the r-z plane, and the primed quantities are derivatives with respect to the flux surface $\Psi = 2\pi rA\varphi$. If $V^{**} < 0$, the system is stable against interchange for an infinite wavelength perturbation parallel to B. Without stuffer current, the system is unstable. By increasing the axial current the minimum-average-B surface can be made coincident with any chosen magnetic surface within the closed field region. Numerical calculations with the CDC 6600 computer give the critical minimum-average-B surfaces indicated by the dashed lines in Fig. 37 for axial currents of 32 and 48 kA through the seven-turn stuffer toroid. The

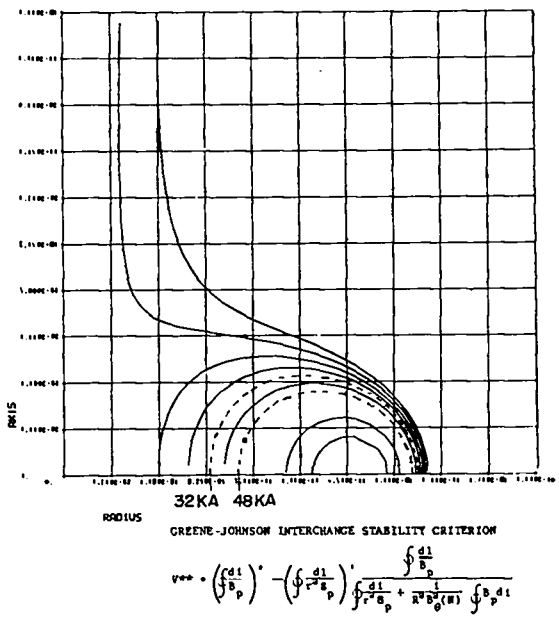

Fig. 37. Greene-Johnson interchange stability criterion.

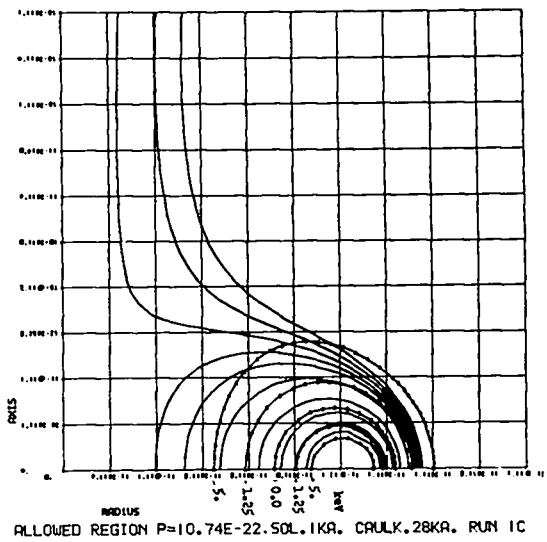

Fig. 38. Effective potential well in minimum-average-B configuration.

resulting closed field containment volume is large ($> 10^5$ cm^3) and combines minimum-average-B and magnetic shear stabilization.

Allowed Regions for the Minimum-Average-B Configuration

Since this configuration also has axial symmetry, the Hamiltonian formalization can be used to determine the allowed regions of particle motion and the confinement limitations of the field geometry through the constants of motion $P\varphi$ and H of the particles (again ignoring collisions and instabilities). The lines with crosses in Fig. 38 outline the effective potential well $\Phi \approx (P\varphi - qrA\varphi)^2/2mr^2$ at the energy level contours of 0, 1.25, and 5 keV for a selected value of $P\varphi$. As in the case of the minimum-B configuration, effective potential well depths capable of containing particles of several keV energy and absolute confinement of particles over a significant region of $P\varphi$, H phase space have been found.

Plasma Generation and Heating in the Caulked Stuffed Cusp

Experimental System

The initial attempts to fill the caulked stuffed cusp device with plasma involved the use of ExB plasma heating using the stuffer and caulker loop as electrodes in the crossed field discharge. This method has the potential advantages of generating the plasma in situ and of control of the plasma energy and density. A major obstacle is electrical breakdown to the mechanical supports and electric feed line of the caulker loop. The magnetic field lines near the separatrix charge up rapidly during the pre-ionization phase of the breakdown and "short circuit" the discharge from stuffer to caulker, thus precluding ExB plasma generation and heating in the enclosed region. Attempts to eliminate this problem by use of insulators and magnetic shielding with double leads at the support points were not successful (LA-3434-MS, p. 12).

Changes in the electrode design and positioning that might avoid the breakdown to the caulker supports were considered, e.g., using ExB at the ends of the system and injecting the plasma into the confinement volume by means of a radial E field and the azimuthal stuffer field component. As an interim experiment, however, for study of the potentialities of the ExB method of heating the device was operated with reduced caulker field. In this configuration, the magnetic field lines terminate on the surface of the caulker loops forming two ring cusps and the localized discharges to the supports are avoided.

Voltage Hold-off Mode

The device exhibits widely different characteristics depending on the applied voltage (between caulker and stuffer for ExB heating), injected gas pressure, relative magnitudes of caulker, stuffer, solenoidal field, and the series current limiting resistors. Over a limited range of these

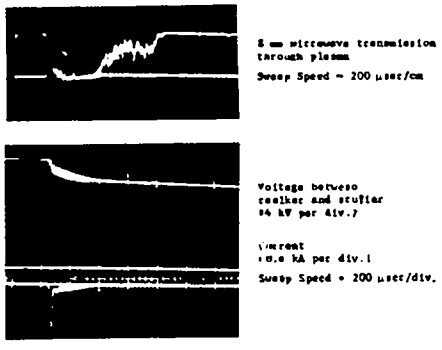

Fig. 39. Voltage, current, 8 mm microwave transmission signals for the hold off mode.

Operating conditions: 6 kA solenoid current (~ 4800 gauss at center of machine), 1 kV caulker voltage (~ 2100 gauss at center of machine), 17.5 kV between caulker and stuffer, no stuffer field, no series resistor. D_2 gas injection (~ 5 x 10^{16} atoms).

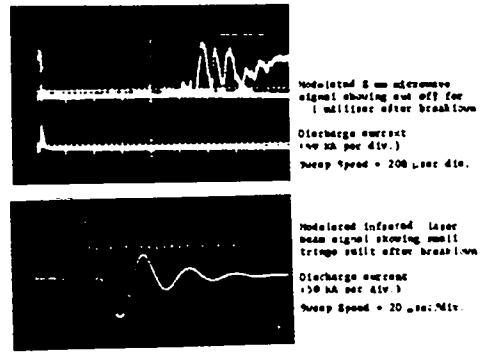

Fig. 40. Plasma density measurements by caulked cusp device using 8 mm microwave absorption and reflected laser beam interferometer

Operating conditions: 5 kA solenoid current (~ 4000 gauss at center of machine), 1.6 kV caulker voltage (~ 3000 gauss at center of machine), 17.5 kV between caulker and stuffer, No gas injection (~ 10^{16} atoms), No stuffer field. 0.25 series resistor for upper trace, no resistor for lower trace (current signal polarity inversion due to change of Rogowski current loop in upper current trace)

parameters, a voltage hold-off mode as shown in Fig. 39 is obtained. Gas breakdown occurs ~300 μsec after gas injection (approximate time for gas to flow from the injection ports in the stuffer to the caulker electrode) with a current pulse of ~ 1 kA and ~20-μsec duration. The bank voltage falls to ~ 80 or 95% of its initial value and remains there with a decay time of ~ 0.1 sec. This mode was initially regarded with interest because of its classical behavior. Typical current and voltage traces are shown in Fig. 39. Plasma densities of > 10^{13} cm^{-3} are obtained, for ~500 μsec as indicated by cut off of the 8 mm microwaves. The transmitted microwave signal is also shown in Fig. 39. Measurements of plasma temperature and confinement time, however, determined from spectroscopic Doppler shifts and line broadening, plasma diamagnetism, and reverse current from the rotating plasma after crowbarring the device show that the plasma was of low energy ($T_i \leq 10$ eV). Electric field measurements with electrostatic double probes reveal that a large fraction of the applied voltage occurs across a narrow

sheath near the stuffer electrode limiting the rotational energy that can be obtained over most of the plasma volume. It is found that the plasma energy remains small until the power input exceeds a critical level of ~ 30 kA at 17.5 kV. This threshold effect is in agreement with the observations reported by Lehnert[3] who concluded that the energy of the plasma is limited until the transition to the fully ionized state is complete.

Higher Current Modes

By varying the injected gas pressure, caulker field component, and axial magnetic field, the ExB discharge in the high-current modes is obtained. This results in higher plasma densities and higher temperatures. Density determinations were made using microwave transmission and the infrared laser beam interferometer; typical results are shown in Fig. 40 where in the upper pair of traces the 8-mm microwaves are cut off for ~ 1 m indicating electron densities in excess of 1.5×10^{12} cm^{-3} for this time period. A resistor of 0.25 Ω was used in series with the discharge to limit the current to a single unidirectional pulse as shown. In the lower pair of traces the phase shift of the infrared interferometer is shown for the high oscillating current case with the series resistor omitted. The small fractional fringe shift indicates a plasma density of $\leq 2 \times 10^{14}$ cm^{-3} at the time of peak current with a slow fall off in time as also indicated by the microwave transmission results.

Plasma temperature and confinement times were investigated through measurements of plasma diamagnetism, spectral line broadening and Doppler shifts, and reverse currents from the plasma after crowbar. Doppler shifts and line widths corresponding to plasma temperatures of ~ 250 eV have been observed at the time of approximately peak plasma current. Figures 41 and 42 show typical time behavior of line emission and total spectra, respectively. The He II line radiation used for the spectral temperature determinations has only short time duration probably because of the rapid cooling of the plasma electrons by excitation of impurities to energies below the high

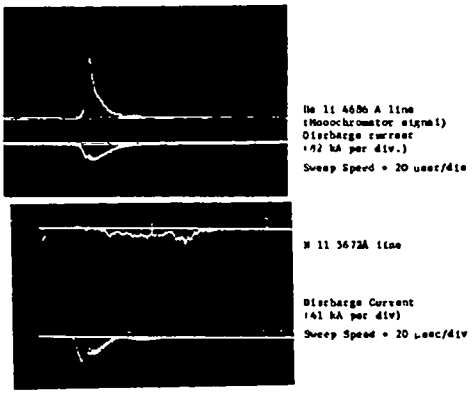

Fig.41. Line emission from cusped cusp device observed with McPherson 1.0 meter monochromator showing short duration of Be II emission and longer duration of N II emission

Operating conditions: 5 kA solenoid current, 7.4 kV cusher voltage, 17.5 kV between cusher and stuffer in upper traces and 12.5 kV in lower. He II gas injection (~ 10^{18} atoms), 0.25 Ω series resistor.

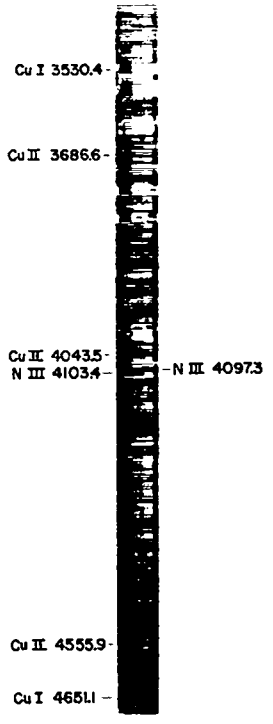

Fig. 42. Plasma spectrum.

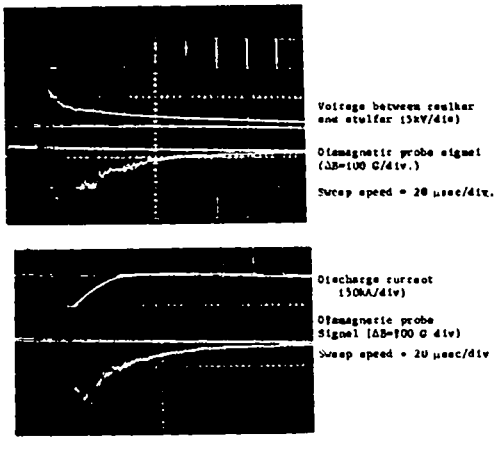

Fig.43. Diamagnetic field signal obtained with probe positioned in plasma 25 cm from midplane and 14 cm from axis of machine.

Operating conditions: 5kA solenoid current (~4000 G at center of machine), 1kV cusher voltage (~2000 G at rotor of machine), 0.2 kV stuffer (~700 G at stuffer surface), 0.25 Ω series resistor, He gas injection (~ 10^{18} atoms).

excitation levels of He II. Other line emissions such as N II 5672Å shown in Fig. 41 last much longer. Cu II radiation has been observed for ~ 500 μsec. Diamagnetic probe measurements (Fig. 43) also indicate plasma temperatures of ~ 200 eV but the probe disturbs the plasma sufficiently to affect the current and voltage wave forms when it is inserted into the discharge. Since the present diagnostics do not give conclusive lifetime results, a neutral particle detector has been designed and assembled to give more reliable information on temperature and lifetimes. Testing and calibration of this device is being carried out.

Coaxial Gun Plasma Injection Method

The ExB plasma heating technique, as applied in the caulked stuffed cusp system, had three apparent limitations: (1) considerable amounts of impurities were released from electrodes during the crossed field discharge, (2) experimental observations suggest energy losses due to thermal contact of the plasma with electrodes through the neutral gas and ionized impurities released during the discharge, and (3) breakdown occurs to the supports of the caulker loop despite efforts to shield them. In view of these limitations, a different approach to filling the system with plasma is being tested, namely, plasma injection from a coaxial gun. With the gun plasma injected through the closed field region in the confinement volume, it is expected that the plasma can be stopped by the self-depolarization process that has been tested successfully by Hammel, Kerst, and Ohkawa. The magnetic shielding of the caulker loop supports against plasma bombardment has been demonstrated by Hammel and Henson to be effective against plasma injected from a coaxial gun. Further work by J. E. Hammel and R. M. Henson (see p. 94) has shown that the slow plasma component from the coaxial gun, which is

believed to contain the undesirable impurities, can be reduced considerably by a transverse magnetic field barrier between the gun and the confinement volume. In view of the encouraging results, a coaxial gun and transverse field trap have been designed and are being assembled and tested preparatory to their use as an injection device for the caulked stuffed cusp confinement studies.

References

1. J. B. Taylor, Plasma Physics (Trieste Conference) pp. 449, 462 (1964).

2. The authors are indebted to S. Yoshikawa for information concerning the stability of this field configuration. They also wish to express their appreciation for discussions with D. Kerst and D. Rose.

3. B. Lehnert, Arkiv Fysik, 28, 205 (1964).

HYDROMAGNETIC PLASMA GUN PROGRAM

Introduction (J. Marshall)

Coaxial guns in the stage of development reported previously (LA-3434-MS, p. 48) provide a simple, efficient source of plasma for certain thermonuclear experiments. If they are to serve as a means of charging a pulsed reactor they must produce plasmas with much larger energies. The present aim of the gun program is such a development, both in actual attainment of larger energies and in the discovery of any fundamental limit preventing energies in the multimegajoule region.

An attack might be made on the problem simply by increasing the energy stored in the capacitor bank driving a gun, e.g., by raising the bank voltage, the bank capacitance, or both. If this is done, the first effect is for the plasma to leave the gun before an appreciable fraction of the bank energy has been transferred through the gun terminals. The difficulty might be described as one of poor impedance matching. With higher voltage the plasma is driven to higher speeds, and reaches the end of the gun sooner. This would require a higher ringing frequency of the electrical system for efficient energy transfer. With higher capacitance and no change in voltage the speeds would be the same but the time to discharge the bank would be longer. The situation can be remedied in both cases by increase in the gun dimensions and in the mass of gas to be converted to plasma and accelerated. The latter must be increased by a large factor in any case, since the speeds already available are nearly as high as is desirable. Bank voltage can be raised, but not by a very large factor with any certainty. Difficulties are to be expected with feed-through insulators at very high voltage. A large

increase in gun dimensions is undesirable, if it can be avoided, in that it implies an increase in the volume of the plasma produced.

An important fact to be kept in mind is that in these devices, and in many others depending on hydromagnetic effects, a significant fraction of the energy transferred through the terminals from the capacitor bank is stored magnetically for a time, and is then delivered to the plasma. This occurs whenever plasma is driven by a magnetic field in such a way that the field can expand by a substantial amount as the plasma moves. The total energy of a field is reduced when it is allowed to expand, and the decrement of energy appears as work on the moving boundary. The effect is particularly marked when, as in a gun, the plasma is driven into a vacuum so that the field can expand by a large factor. A convenient way of looking at the effect is to consider the circuit equations of the system with time-dependent inductance in the regions with moving current sheaths. The magnetic forces on an inductor are such as to deform it into a shape having larger inductance. The back emfs caused by the varying currents and moving boundaries are expressed by the equation

$$E = \frac{d}{dt}\varphi = \frac{d}{dt}(LI) = L\frac{dI}{dt} + I\frac{dL}{dt}.$$

If the inductance of the circuit suddenly increases, as when a z-pinch occurs, the back emf due to the increasing inductance is balanced by a current reduction emf. The reduction of current decreases the energy stored in the fixed inductance parts of the circuit, and the energy appears as work done on the moving boundaries.

The foregoing effects complicate the problems of plasma guns, but introduce behavior which might be quite beneficial. In particular, if the energy is transferred to the plasma from internal magnetic fields, the high voltages involved need not appear across feed-through insulators.

This may make it possible to develop dynamic pinch devices or guns with enormous voltages, but without the usual technical limitations. Effects of this sort have been observed before occurring spontaneously in gun and in dense plasma focus studies, and in addition are being consciously applied by J. A. Phillips (p. 47 et seq.).

Experimental Facilities for Gun Program (I. Henins, J. Marshall, R. Dike)

As mentioned above, the main objective of the gun program at present is toward a large increase in plasma production. First plans were to go from 20 to 50 kV with considerably larger bank energy. For this purpose the high-voltage system had to be provided as well as a vacuum chamber capable of handling the much larger plasma energies expected. A x4 Marx voltage multiplying bank was designed and installed in the capacitor room in place of two of the 20-kV banks then in use. Eighteen 20-kV capacitors are in each of four modules with a single size-A ignitron in each bank to switch them in series. The system is used with as many of the capacitors connected in each module as are considered desirable. The result is a very flexible pulsed charging supply for high-voltage banks up to 80 kV.

A stainless steel sectional vacuum chamber was designed and procured with the idea of providing flexibility for the high-energy gun experiments. It consists of three sections, each 48-in. i.d. and 40-in. long. The length was chosen to allow the sections to be brought through the laboratory door. They are mounted on flanged wheels on a track system so that they can be moved apart for access to the interior. The system (two sections at present, Fig. 44) is pumped by a 12-in. Orbitron, a 500-liter/sec VacIon, and a 700-liter/sec diffusion pump which is normally valved off for oil contamination safety, but used with a noncreep LN_2 trap for roughing to Orbitron starting pressure ($\sim 2 \times 10^{-5}$ torr). Base vacuum is slightly less than 10^{-7} torr, the residual gas being mostly H_2O adsorbed on the ~ 20 m of viton gasket used for sealing.

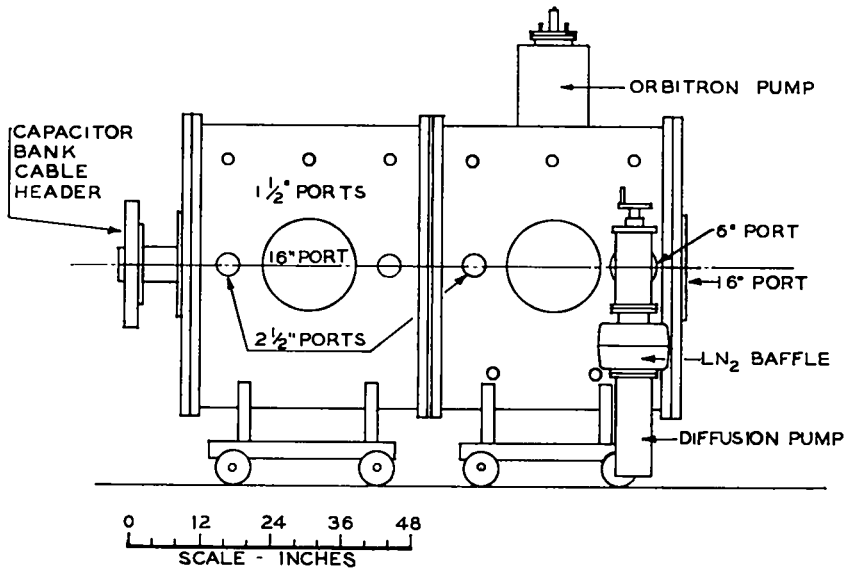

Fig. 44. Section of vacuum tank with two sections of three shown assembled; cable header for Mushroom I, II, and III in place (see p. 74).

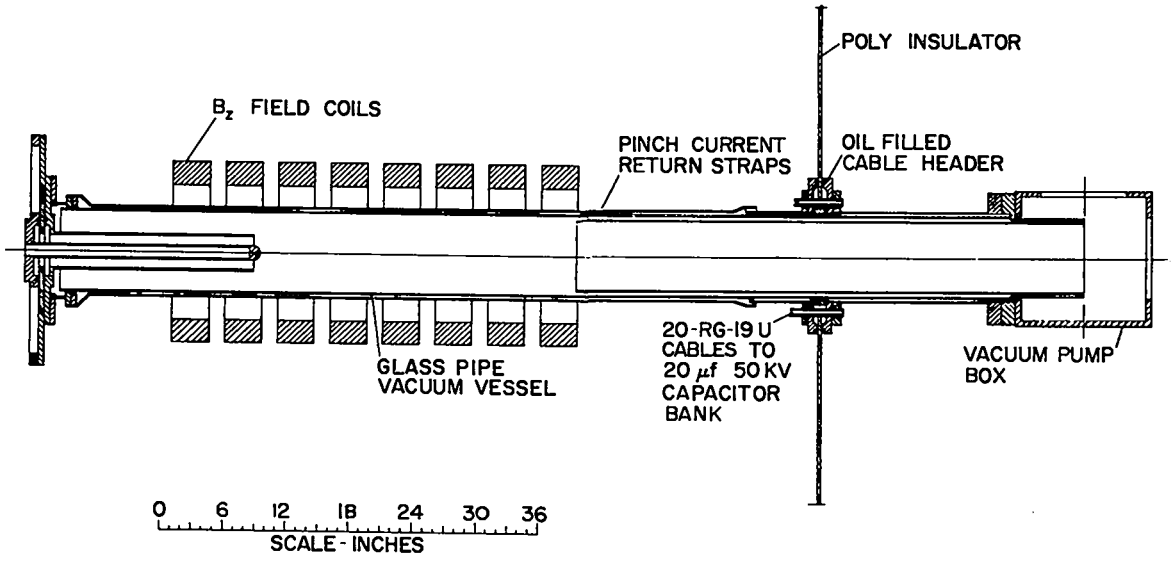

Fig. 45. Gun injected pinch.

The Orbitron handles heavy gas loads very easily, returning the system to $\sim 5 \times 10^{-7}$ torr between 20 kJ, 15 cm^3 STP D_2 gas injection shots 5 min apart. For larger gas loads, expected in the future, additional Ti sublimation will be supplied.

A vacuum-insulated pulsed field solenoid was designed and procured so that a guide field could be provided inside the sectional tank. It is intended to provide up to 20 kG of guide field over a 40-cm diam and up to 1.5-m length. It is planned for use with the permanent closure solid dielectric switch (LA-3434-MS) as a crowbar. It has not been installed as yet since the present experiments do not require a guide field.

Gun-Injected Pinch (I. Henins, J. Marshall, J. L. Tuck)

After the Marx high-voltage pulse charge system was installed, and before the sectional vacuum tank was delivered, an experiment was tried for a time involving the z-pinching of a gun plasma. It was felt that a truly hot z-pinch obtained from the pinching of a hot plasma might show interesting new effects. In addition some of the experience was expected to be applicable to high-voltage gun experiments which were thought to be imminent.

The layout of the apparatus is shown in Fig. 45. The existing coaxial gun was inserted at one end of a glass tube whereas the entire other end was at 50 kV supplied from a pulse-charged bank of 22 μF. Switching was by the gun plasma itself, but it was expected that it would be replaced by solid dielectric switching in later versions. Low-inductance connection to the capacitor bank was provided by a set of cables terminating in an oil-filled header on the apparatus. Vacuum pumping was by an Orbitron isolated from ground by chokes and a high-voltage insulated filament transformer. In this way the pump could be hung on the high-voltage end of the equipment.

Operation of the equipment showed interesting behavior, with indications from terminal current and voltage oscillograms that pinching was taking place, with its characteristic electrical reactions. Neutrons were produced at the presumed pinch times, under some conditions in sharp bursts, but under others apparently in a well-behaved manner such as might be expected from containment for μsec times. The behavior depended strongly on polarity of the pinch, which is not surprising, considering that the gun has a polarity associated with it, and that magnetic fields from the gun are carried well out into the pinch region. The presence or absence of a B_z field in the pinch region also affected the results strongly, reliable operation requiring the presence of some magnetic field. The situation was made difficult experimentally by the fact that self-switching on the gun plasma initiated the pinch. This made it impossible to control breakdown time, and meant that it occurred as soon as it was possible, i.e., when the first tenuous plasma reached the high-voltage electrode, and thus when conditions were strongly nonuniform along the length of the discharge.

At this point two events interrupted the work: an insulation failure in the oil-filled cable header destroyed the apparatus, and the sectional vacuum tank was delivered. It was decided to install the new vacuum system and perform all subsequent experiments in the improved conditions hopefully to be provided thereby. It might well be desirable to return to this experiment in the future in which case controllable switching of the pinch capacitor bank will certainly be provided.

"Mushroom", A Dynamic Pinch Gun with Inverse Pinch Internal Energy Storage

(I. Henins, J. Lohr, J. Marshall)

Introduction

This series of experiments represents an attempt to enhance the storage of magnetic energy beyond the terminals of a gun or pinch-type device by the use of an inverse pinch.

The essential geometry can be seen in Fig. 46 which represents Mushroom I, the first experiment in the series. It was set up, as were Mushroom II, III, and IV, in the new sectional vacuum tank which was acquired with high-energy gun experiments in mind. Gas is injected with a fast valve into the region behind a mushroom hat electrode. After an appropriate delay a high-voltage capacitor bank is switched across the gap between the hat and the tank wall. An insulating sleeve prevents breakdown between the stem of the mushroom and the tank. A more or less cylindrical current sheet, depending on gas distribution, would then be expected to move outward, snowplowing plasma ahead of it, and forming the boundary between a $B_\theta = 0.2i/r$ vacuum field region and the snowplowed plasma and gas. The inverse pinch would be expected to be hydromagnetically stable and to move outward in a well-behaved manner to the edge of the hat. At this point it would suffer a catastrophic loss of equilibrium. The current sheet would burst like a bubble inward and forward over the edge of the hat. High speeds would be expected because of the relative vacuum in front of the hat and the 1/r increase of the field inward.

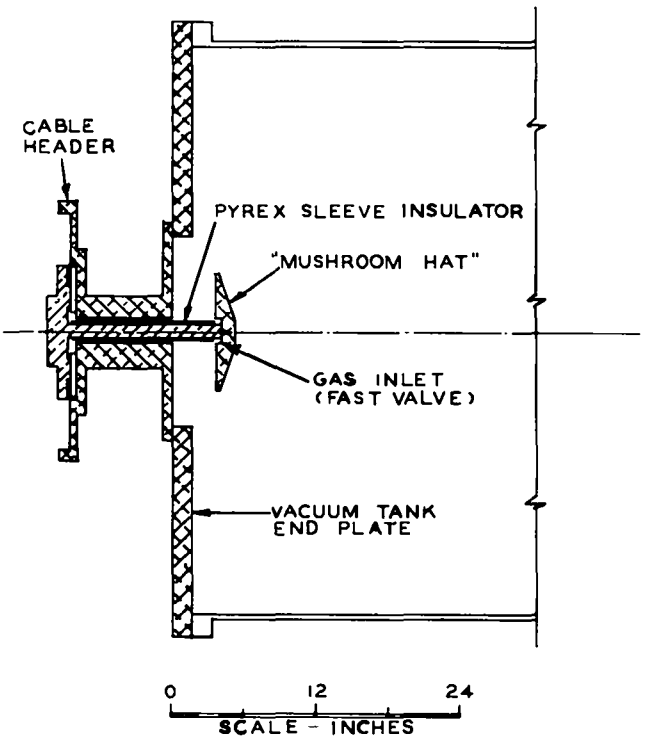

Fig. 46. Mushroom I

The inverse pinch was chosen because of its hydromagnetic stability and because it is one of the poorest possible methods for transferring magnetic energy to a plasma. The 1/r field dependence inside the current sheet ensures that a small field pressure drives the

plasma and that a large amount of field energy will be built up close to the mushroom stem. As a consequence, most of the energy transferred from the bank past the terminals is stored magnetically in a vacuum, and is available for rapid transfer when the current sheet spills over.

Another reason for choosing the inverse pinch was the suspicion, since confirmed, that the insulator arrangement would lead to increased voltage and pressure tolerance in the initial breakdown. It had long been apparent that J. W. Mather's dense plasma focus experiment was tolerating much higher gas pressures at the insulator than were possible in the coaxial gun arrangement with its pierced glass disk insulator. Pressures at the insulator in the coaxial gun coming anywhere near the 5 torr reported by Mather invariably led to a discharge crowbarred on the insulator and therefore hydromagnetically useless. The dense plasma focus is arranged to have the initial discharge in the form of an inverse pinch, driving outward away from a tubular section of the insulator. Incidentally, the current sheet in the dense plasma focus was reported to be in the form of a snowplow, whereas this was not the case in the coaxial gun. A snowplow should be better, a priori, for energy storage.

The various experiments of this series have followed each other at short intervals, changes in design being made rapidly in order to optimize parameters and to understand the influence of the variety of phenomena involved. None of the experiments has been really thoroughly diagnosed, but from the total has emerged a reasonably consistent picture of the device and its way of working. The experiments will be mentioned first, and then the results which apply more or less to all of them will be described.

Mushroom I

The first attempt at the concept (Mushroom I, Fig. 44) had dimensions and design based on guesses and expediency. To make the work fast and easy, most of the parts were adapted from the coaxial gun then

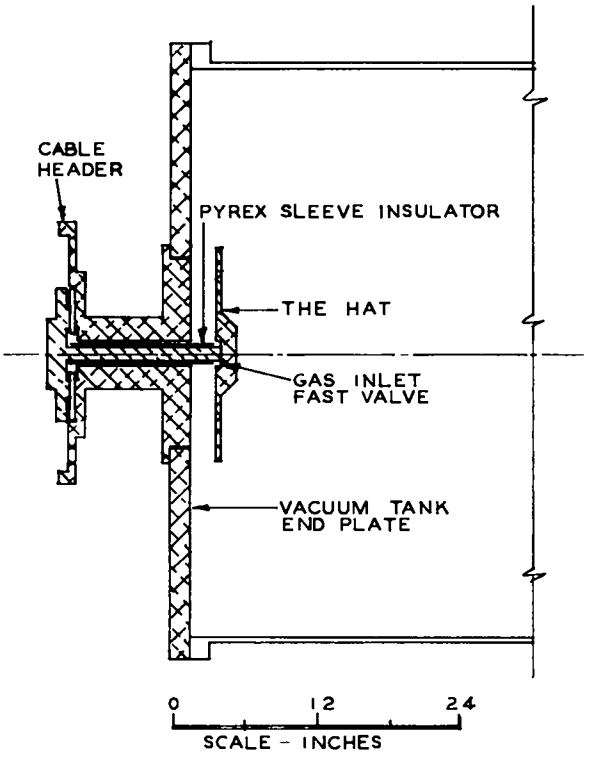

Fig. 47. Mushroom II.

in service. These included the capacitor bank, switching cable header with feed-through insulator, part of the center gun electrode, and the fast valve system. The center electrode was truncated just beyond the gas inlet slot and a mushroom hat electrode was attached. A glass sleeve insulated the stem from the tank wall, and the problem of joining the pierced glass disk gun insulator to the sleeve was met by a vacuum gap. It was expected that gas diffusion along the narrow channel occupied by the glass sleeve would be slow enough so that the bank energy would be dissipated before the vacuum at the gap was seriously affected.

Mushroom I behaved superficially very much as expected as far as could be determined directly from simple measurements. These included terminal voltage and current, image converter photography, neutron yield measurements, both time resolved and by silver activation, and a probe measurement of voltage between the edge of the hat and the tank wall. Enough of an understanding of the system was acquired to design a second version intended to behave better in the inverse pinch energy storage phase.

Mushroom II

In the second experiment of the series a hat of larger diameter was used closer to the wall as shown in Fig. 47. Mushroom I had shown a tipped current sheath, explainable qualitatively as being due to uneven gas distribution. The gas density near the valve port appeared to be higher than elsewhere, a situation which could be improved presumably by a longer

delay after gas injection. Best performance was achieved with the maximum possible delay after gas admission, longer delays being impossible because the gas would not break down. The narrower gap and larger radial distance in Mushroom II led to improved energy storage in the inverse pinch and good current break characteristics. The size of the bank was increased from 30 to 107 μF by substituting a different type of capacitor. It was found impossible to transfer all the energy of the larger bank to internal magnetic storage because the high speed of the current front made it spill over the edge of the hat before the voltage on the capacitor bank came to zero. Admission of a larger amount of gas would have been desirable, but the valve could not withstand sufficient gas pressure without leaking.

Mushroom II performed in a poorer way than Mushroom I as a gun, but better as a pinch machine. These judgments are somewhat qualitative, being based on visual observation of the flash of light produced by the plasma striking the far end of the tank and on neutrons detected by a silver activation counter with no collimation to determine place of their origin.

Mushroom III

The name Mushroom III is used to designate a rapid series of changes of geometry in which attempts were made to modify the gas and field distribution so as to raise the amount of energy stored before the current sheet spilled over. The hardware borrowed from the coaxial gun was still used although the glass insulating sleeve had been replaced with high-alumina ceramic midway through the Mushroom II experiment. The geometries tried are indicated in Fig. 48. In all cases the idea was to raise the inductance of the system while slowing down the escape of gas from behind the hat. These changes were successful in storing more energy but did not in general improve performance as a gun or dynamic pinch. In some cases it appeared that secondary plasma evolved from the electrodes interfered with clean bursting of the current sheet bubble.

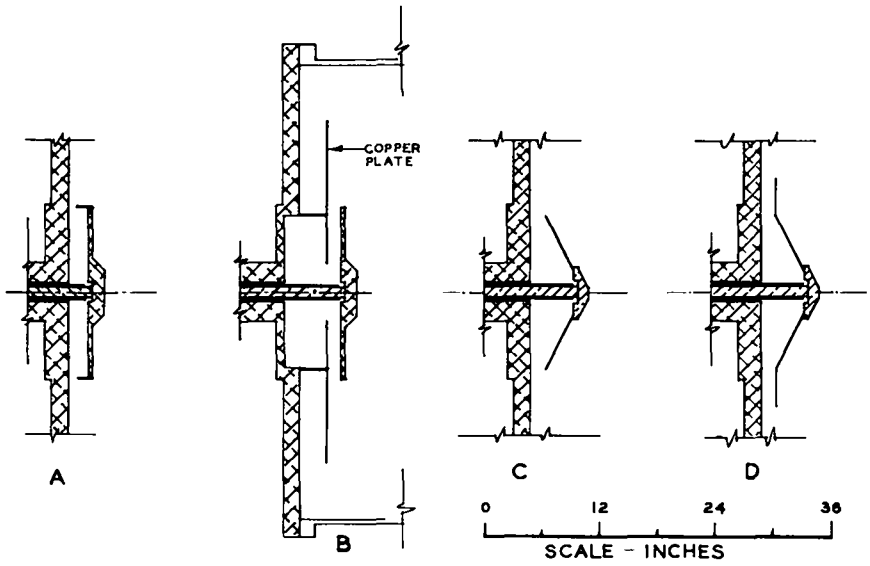

Fig. 48. Variations of Mushroom III.

The series of experiments was terminated by a catastrophic failure of the electrical insulation at the terminals which required redesign and rebuilding of the system. The failure occurred in the vacuum gap between disk and sleeve insulators. The condition leading to ultimate failure was a tendency for the system to crowbar in this gap, usually on some half-cycle subsequent to the first one. The explanation for the crowbarring appears to be associated with the larger energy storage achieved. For complete energy transfer from the bank, energy has ceased to flow from the bank to the inverse pinch just as the current sheet is about to spill over. If spillover does not occur for some reason, e.g., if the bank was fired at slightly reduced voltage, energy will start flowing back toward the bank. Even if spillover does occur, some energy may flow back, since there is none stored in the bank. Energy flow implies a Poynting vector ($\vec{E} \times \vec{B}$) flux in the direction of the flow. The crossed field particle or plasma drift ($v = \frac{\vec{E} \times \vec{B}}{B^2}$) will then carry plasma along with the energy. Plasma in a vacuum gap intended to provide electrical insulation is highly detrimental. Apparently a crack developed in the ceramic sleeve insulator during one of these crowbars. The next shot

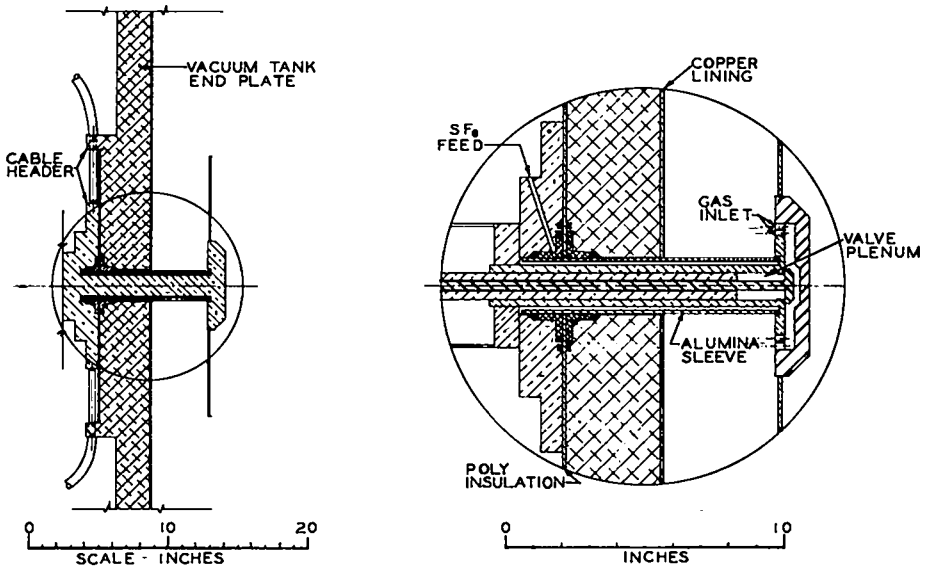

Fig. 49. Design of Mushroom IV.

dumped the entire bank energy into the crack, and all the surrounding parts were ruined by the explosion. The necessity for reconstruction was taken as an opportunity to redesign the entire system.

Mushroom IV

It was decided in the Mushroom IV design to eliminate the vacuum gap in the terminal insulation, and to increase the volume of the valve plenum, so that much larger charges of D_2 gas could be introduced. The insulator problem has been solved very satisfactorily by an SF_6 insulated joint between a pierced sheet of polyethylene and a high-alumina ceramic tube. The design is indicated in Fig. 49. Some trouble was encountered in leaks through the greaseless viton seal to the ceramic tube. This was overcome by a thin coat of epoxy resin in the regions under the O-rings. To save time, the cable header used previously was adapted to this system together with the same ignitron-switched capacitor bank.

The fast gas valve used previously, which was ruined by the explosion, had been operated by thermal expansion. A valve of this sort capable of a wide range of plenum volumes would have been difficult and time consuming to build, so it was decided to go back to one operated by a mechanical hammer. There was no problem of synchronization of the valve with other machine functions, all necessary start times occurring after hammer contact. An electrical contact from the hammer was brought through a coaxial bifilar choke capable of holding off the 20-kV bank voltage to trigger the time delay system. An electrolytic resistor across the choke protects it from the necessity of handling the energy of the bank in the event of a prefire. The valve hammer is operated by tank N_2 pressure through a reducing valve, and a storage plenum with a solenoid valve near the hammer. The size of the valve plenum is adjustable from about 3 to 35 cm^3 so that, with variable D_2 pressure also possible, a wide range of gas charges is available. The width of the gap behind the hat is adjustable from small values up to about 11 cm, the initial width being 10.6 cm. The hat brim is made of copper, as is the wall lining behind it, and is replaceable so that different diameters and perhaps shapes can be substituted for the initial flat, 48-cm diam disk.

Mushroom IV has performed entirely satisfactorily in a technical sense. There appears to be need for adjustment of size and shape of the inverse pinch region behind the hat in order to increase the amount of stored energy before spillover. The temptation to make these adjustments has been resisted so far and hopefully will continue to be for some time yet in the interest of performing a reasonably complete set of diagnostics on one unchanged system. As a hot dynamic pinch machine it has performed better than any of its predecessors, producing a reliable volume yield of $\sim 10^8$ neutrons per shot.

Diagnostics and Interpretation of Mushroom Experiments

The various embodiments of the Mushroom series have much in common in their behavior. Initial breakdown is along the insulator

surrounding the stem, and is followed by an inverse pinch phase where a current sheet drives outward snowplowing gas ahead of it until it reaches the edge of the hat brim. Field strength along the insulator can be considerably higher than what appears to be practical in an ordinary pinch. A 20-kV bank can be applied to a 5-cm gap with no trouble. This is not to say that 4 kV/cm field strength actually appears on the insulator, but 3 kV/cm certainly does. The initial breakdown along the insulator is established by time-resolved, image-converter photography in Mushroom I, where a direct view of the inverse pinch region was available through a tank port. In addition, analysis of terminal voltage and current in Mushroom II shows an early inductance which is compatible only with a current sheath very close to the insulator.

The existence of a snowplow, i.e., of a virtual vacuum behind the current front, is established less directly but nonetheless quite definitely by a variety of evidence. One is the quantitative calculation performed by J. L. Shohet, of the motion of the current front in Mushroom II, which is covered later in this report (p. 87). It is based on measured gas density distribution and circuit parameters. The calculation requires an assumption as to the exact model for the snowplow. A very good fit to the experimental data is obtained by adopting a model half way between a Rosenbluth sheath and a simple snowplow. As a matter of fact, each model is unrealistic in this case and it would be reasonable for the actual behavior to lie between them.

Another measurement is a series of probe observations of B_θ in the inverse pinch phase. These show an outward moving current sheet followed by a magnetic field which is indistinguishable from the terminal current in shape, once it has risen. The field in these measurements (Mushroom II) rose in a time implying approximately a sheath 3-cm thick in the outer regions of the inverse pinch. When the sheet spills over, B_θ and terminal current behave similarly again. Any appreciable plasma density behind the sheet would be expected to interfere with the

spillover process because of its inertia and to cause differences between terminal current and B_θ as measured by a probe.

The voltage between hat and wall was measured on Mushroom I by inserting an electrical probe through the outside wall and making contact with the edge of the hat. Before breakdown this probe shows full bank voltage. Breakdown is followed by a period during which the voltage is indistinguishable from zero on the scale used. Arrival of the current front brings a voltage pulse similar to the one observed on the terminals at spillover but larger by a factor agreeing with the best estimate of the source inductance from this point divided by the source inductance at the terminals. The voltage pulse measured with the probe was as large as 45 kV on some shots compared with a bank voltage of 21 kV.

The voltage pulse discussed above accompanies, and is caused by, a sudden increase in inductance when the current front spills over the edge of the hat. Expectations were that a strong pinch would result from the spillover, but observations show that the current never pinches down to a small diameter. Analysis of terminal current and voltage in Mushroom II shows occasional shots in which the total inductance increases by a factor as large as 3, i.e., an inductance for the part of the discharge in front of the hat of up to ~ 60 nH. Neutron collimation measurements on Mushroom IV indicate that a source of volume neutrons extends a distance of at least 70 cm in front of the hat. The ratio of radii of a coaxial current system 70-cm long having this inductance is calculated to be ~ 1.5. The first attempts to measure the current system in front of the hat were made with a Rogowsky loop in a glass tube encircling the axis of the tank with an 18-cm diam. No reasonable signals were seen. Next a B_θ probe was inserted just in front of the hat in Mushroom II and a current system was found having a rather diffuse edge and a diameter not too different from that of the hat (46 cm in this case). These measurements imply a pinch of quite large diameter and the only reasonable explanation for not having pinched down to a small diameter appears to be that plasma pressure is resisting the inward pressure of the magnetic field.

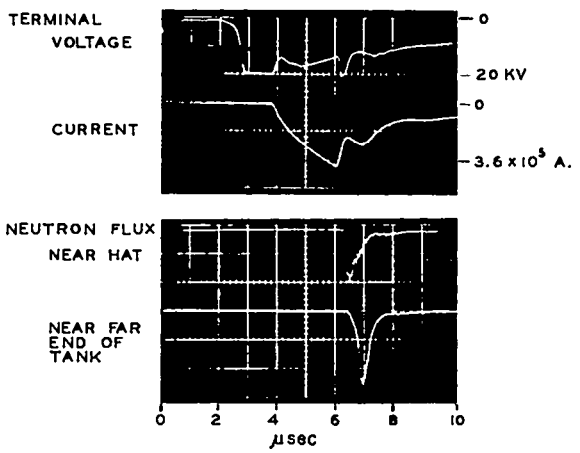

Fig. 50. Mushroom IV oscillograms.

Time-resolved neutron measurements, performed with scintillation detectors shielded with lead to eliminate possible confusion by x rays, indicate an early and a late source of fast neutrons (Fig. 50). Collimation measurements on Mushroom IV show the early neutrons to be produced in a region along the axis extending at least 70 cm in front of the hat and having a radial extent about the same as the hat. The hat itself does not contribute more than about 10% of the early yield. The late source is produced mostly at the far end of the tank. A scintillator placed some distance from the tank and as nearly as possible equidistant from the two sources shows them to be approximately equal in size. A calibrated silver activation counter shows the strength of each source to be $\sim 10^8$ neutrons per shot.

The time between the early and late neutron sources is presumably the time of flight of D's from the pinch region in front of the hat to the far end of the tank. The pinch region centers at perhaps 1.5 m from the far end, and the time between neutron peaks is about 0.5 μsec. From this, an average axial velocity of 3×10^8 cm/sec or a D energy of 100 keV is obtained. The energy of the average D from the pinch region bombarding the end of the tank is probably smaller than this since the neutron yield from the faster D's is enhanced, both by their larger range in the target surface and the larger D-D reaction cross section.

Attempts to correct for this effect lower the apparent velocity by up to 50%, so the average D energy in the axial direction might be as low as 25 keV. There is no direct way of knowing the energy of the D's in the transverse direction, but for a first guess it may be set equal to the axial energy, 25 keV.

In principle, it should now be possible to estimate the plasma density from pressure balance against the containing pinch field. Unfortunately field distribution is not known accurately enough to do this very well. The rather poor measurement of field was made on Mushroom II, and the best neutron measurements are from Mushroom IV. By doing as well as possible, i.e., by taking the radius to be 24 cm, current = 2×10^5 A, length = 70 cm, kT = 25 keV, containment time = 0.4 μsec, it is found that $n = 2.9 \times 10^{12}$ cm^{-3} and neutron yield = 2×10^6. This does not agree with the observed neutron yield of $\sim 10^8$. The discrepancy would be removed if the D density were as high as 1.4×10^{13} cm^{-3}. It is difficult, although not completely impossible, to rule this out from the present measured quantities.

It appears that a higher density might be derived if plasma inertia as well as magnetic field pressure could be included in the pressure balance equation. It may be, however, that something else is required in addition; a highly non-Maxwellian ion energy distribution for instance, with an exaggerated high-energy tail, might allow pressure balance and still give the observed neutron yield.

The existence and extent of the neutron-producing plasma was established by collimated plastic scintillation detectors. These measurements were laborious because of the large extent of the neutron sources, which made background leakage through the sides of the collimators serious. They were accomplished by mounting massive shields on railroad tracks, one beyond the end of the tank and one along side as indicated in Fig. 51. Backgrounds were determined for subtraction by plugging the collimator holes with wood.

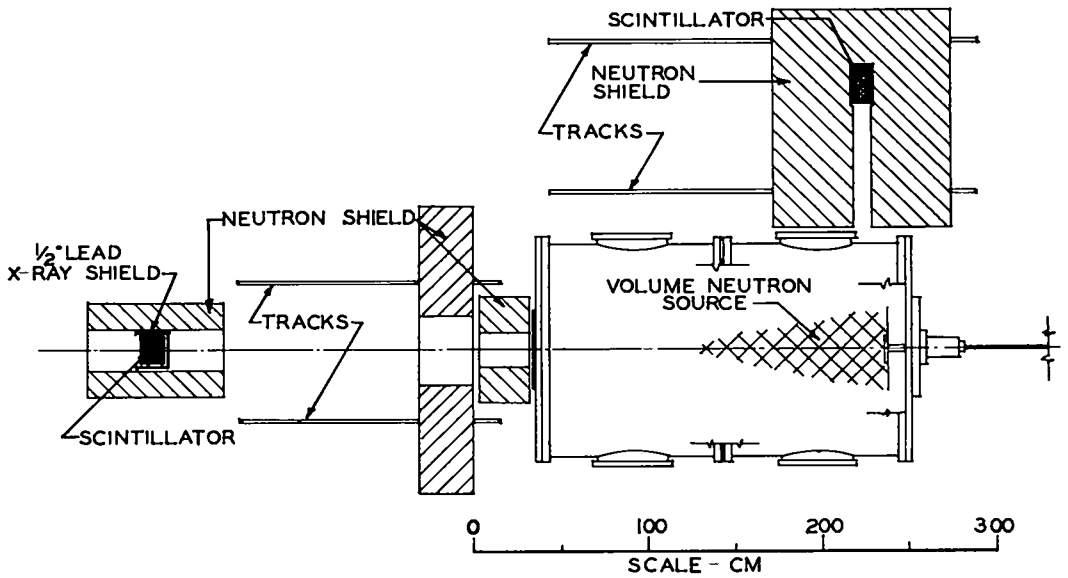

Fig. 51. Neutron collimation arrangement

The problem of measuring volume neutrons through the background of target neutrons caused by plasma striking the end of the tank was overcome by time separation. The target neutrons peak ~ 0.5 μsec after the volume neutrons because of the time of flight for plasma to reach the end of the tank. When the collimator is open, i.e., when it is in a position close to the detector so that the entire tank can be seen, the target neutron pulse interferes with the volume neutrons, since it appears larger, being closer to the detector. When the collimator is moved toward the tank, however, so as just not to obscure the volume neutrons, most of the target neutrons are screened off and the sources are easily separable. By measuring the height of the first neutron peak compared with that of a monitor observing neutrons produced near the hat, and by doing this at a number of end-wall collimator positions, it was determined that practically all of the first peak intensity originates within the 48-cm diam of the hat, and that 50% of the neutrons come from within a diameter of ~ 27 cm. Measurements with the collimated side detector in a number of positions showed that none of the second peak originated within 70 cm of the hat and that the first peak extends out at least to 70 cm, although

at this distance the yield is on the average somewhat smaller and is more erratic than close to the hat. An estimate of the region in which the volume neutrons originate is given in Fig. 51 by the cross-hatched area in front of the hat. Measurements more than 70 cm from the hat were not made because of limited maneuvering room in the laboratory for the collimator-detector system.

Infinite Conductivity Snowplow Model of the Inverse Pinch (J.L. Shohet, revised by J. Marshall)

The Rosenbluth model of the pinch has been applied to an inverse (hard core) pinch device. The experimental configuration has been described elsewhere. The configuration and external circuits used in this model are shown in Fig. 52.

It will be assumed that the current I flows only through the pinch, and not back through the charging circuit. Two equations are needed to determine the properties of the device. They are (1) a circuit

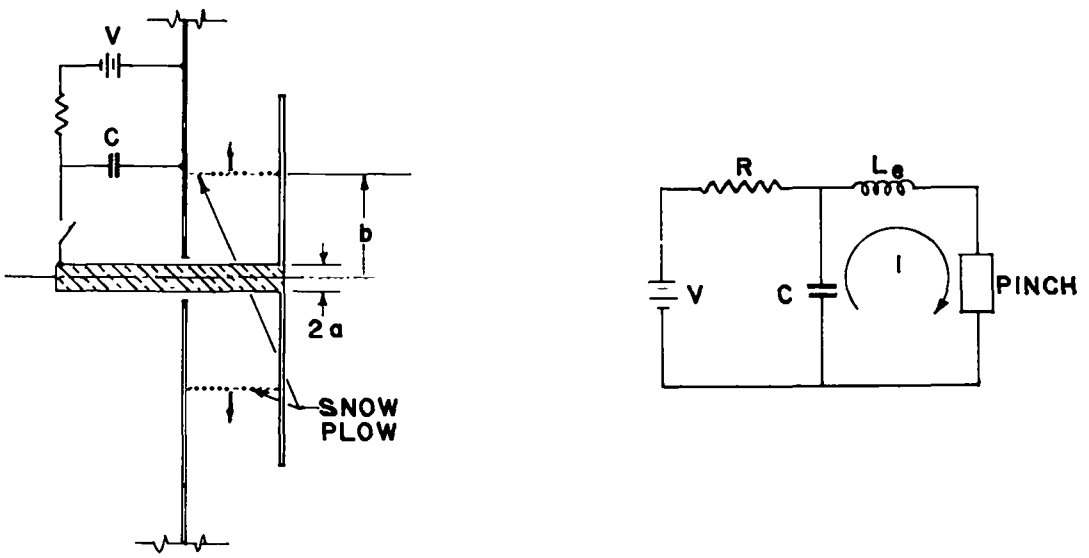

Fig. 52. Infinite conductivity snowplow model of inverse pinch.

equation, and (2) a force equation. The problem can be solved assuming either constant ambient gas density or a variable density, the actual situation. The two equations for constant density are

$$0 = (L_e + L_p)\frac{d^2I}{dt^2} + 2\frac{dL_p}{dt}\frac{dI}{dt} + I\frac{d^2L_p}{dt^2} + \frac{I}{C} \tag{1}$$

and

$$\pi\rho_o(b^2 - a^2)\frac{d^2b}{dt^2} + 2b\pi\rho_o\left(\frac{db}{dt}\right)^2 = \frac{\mu_o I^2}{4\pi b}. \tag{2}$$

where L_e = external inductance, L_p = inductance of the pinch $\left(\frac{\mu_o \ell}{2\pi}\ln\frac{b}{a}\right)$, C = the capacitance of the energy storage device, and ρ_o = ambient neutral gas density in kg/m^3. The plasma pressure per unit length is $B_\theta^2 \times 2\pi b/2\mu_o$ and $B_\theta = \mu_o I/2\pi r$, which results in the second equation. The equations are nonlinear and have been solved numerically for b and I on the IBM-7094 computer with the following conditions set:

$V = 20 \times 10^3$ V $a = 1.59$ cm

$C = 30 \times 10^{-6}$ F $\rho_o = 10^{-5}$ kg/m^3

$\ell = 5$ cm $L_e = 10^{-8}$ H

In addition, at time = 0, $dI/dt = V/L_e$

$b/a = 1.0001$, $I = 0$

and $db/dt = 0$.

The results of the numerical calculations were qualitatively similar to the experimental data and agreed reasonably well quantitatively with an appropriate gas density.

A nonuniform gas density profile was then used to match as nearly as possible the actual experimental conditions. The density as measured with a fast ionization gauge on a probe in Mushroom II is well approximated by the exponential decrease with radius. At r = 6.2 cm it is 10^{-1} torr and at 22.1 cm it is 10^{-3} torr, these applying at normal

firing time, about 250 μsec after the fast valve opens. Eq. (2) was revised to include this as shown in Eq. (2A).

$$\frac{2\pi\rho_o'}{\alpha^2}\left[e^{-\alpha a}(1+\alpha a) - e^{-\alpha b}(1+\alpha b)\right]\frac{d^2b}{dt^2} + \alpha e^{-\alpha b}\left((1+\alpha b) - 1\right)\left(\frac{db}{dt}\right)^2 = \frac{\mu_o I^2}{4\pi b}, \quad (2A)$$

where α is the exponential decay factor obtained from the experimental data and ρ_o' is the appropriate density coefficient of the exponential. The equations were integrated with

$$\alpha = 0.115 \text{ cm}^{-1} \text{ and } \rho_o' = 5.5 \times 10^{-5} \text{ kg/m}^3.$$

The force equation as written here assumes a simple snowplow, with all of the gas swept up to form a thin sheet in the current front. This is unrealistic since the snowplowed gas is hot, and would certainly expand ahead of the current sheet. Another well known model is the Rosenbluth sheath, in which the gas is assumed to be preionized, at low temperature and collisionless. In this model the ions acquire twice the momentum which they do under the snowplow model. More thermal energy is left in the swept-up gas as well. The Rosenbluth sheath model is also unrealistic and the actual case might be expected to behave like a mixture of the two. To achieve quantitative agreement with the experiment a model approximately half-way between the snowplow and the Rosenbluth sheath was required.

INCREASED SENSITIVITY LASER DENSITY MEASUREMENTS ON GUN PLASMAS

(J.E. Hammel, R.M. Henson, D.L. Rode)

Introduction

The Ashby-Jephcott laser interferometer technique was extended to a 1/10 fringe sensitivity by Jahoda[1] with a constant velocity motion on the external mirror. The 1/10 fringe sensitivity is just sufficient to show the 0.4 to 0.5 fringe shift produced by the fast component of the coaxial gun.

A scheme for increasing the sensitivity was tried in early 1965 using a ferroelectric transducer (PZT-5a) for moving the external mirror in a known linear motion for a distance equivalent to a few tenths of a fringe. The amplitude change in the infrared signal given by the transducer motion was calibrated by the injection of a known amount of gas from a fast Williams valve into a cell in the laser beam path. Calibration of the mirror motion was not complete because of the difficulties in producing the linear motion with a kilovolt ramp and clamp.

A similar laser interferometer used in density measurements on a small repetitively pulsed plasma has been described.[2] The method uses acoustic modulation of a gas in the laser beam path with the modulation frequency equal to the repetition rate of the plasma. A continuous small sinusoidal modulation of this type is less difficult to achieve than the kilovolt ramp and clamp, but the resistance losses in the PZT transducer prove to give excessive heating of the ceramic when continuous drive is used. A simple solution to the problem has been found by mounting the external mirror on the coil of a 6-in., 5-W loudspeaker. A sinusoidal modulation for frequencies to several kHz is obtainable with displacements up to a wavelength or so.

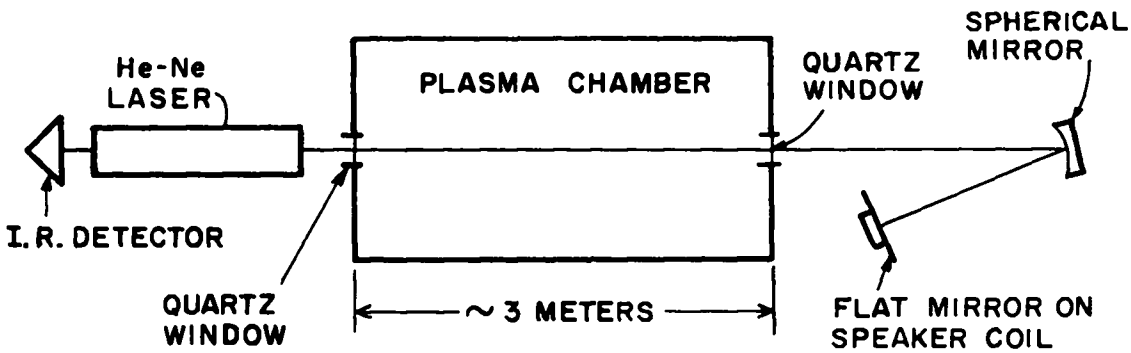

Fig. 53. Schematic of laser interferometer for density measurement across 3-m plasma chamber.

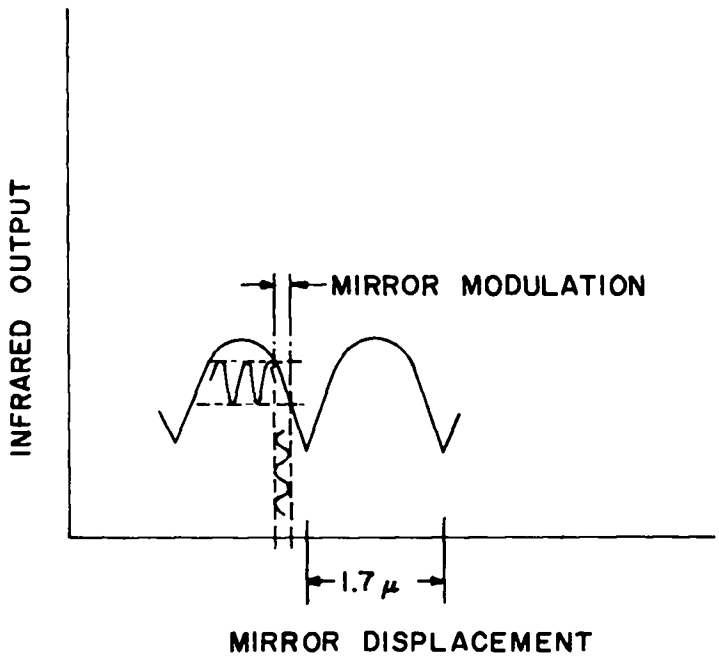

Fig. 54. Illustration of laser infrared output with small-amplitude modulation.

Schematic for Interferometer

Figure 53 is a diagram of the fractional fringe shift interferometer arrangement. The mirror is given a 1000-Hz sinusoidal displacement with an amplitude of 1/20 wavelength. In the ordinary Ashby-Jephcott arrangement with two passes, this is given an infrared modulation corresponding to the 1/10 fringe. The modulation is nearly sinusoidal since the response is essentially linear for this small motion as shown in Fig. 54. The 1000-Hz frequency is chosen since it is considerably higher than the ambient vibration of the system when set up across the 3-m length of the Transverse Injection tank. The period of the modulation must also be long compared with the plasma event. A frequency of 1000 Hz is about optimum for these two requirements.

Mirror Amplitude Calibration

The coil-driving voltage corresponding to a fractional fringe displacement is found by multiplying the effective displacement by multiple reflections off the mirror. A 1/20 wavelength mirror displacement gives one fringe with 10 reflections. More than 10 reflections are easily realized and 1/10 fringe calibrations are readily made.

Applications

Gas Density

As a first test, a density measurement was made on a fast injection of gas into a cell placed in the laser beam path. A comparison of density thus measured and that given by an equilibrium pressure measurement is shown in Fig. 55. The agreement is very satisfactory and eliminates most doubts about such things as refractive effects.

Plasma Density

The density range covered by this method is of great interest for the "filtered" gun plasma stream. The result found with the Jahoda-

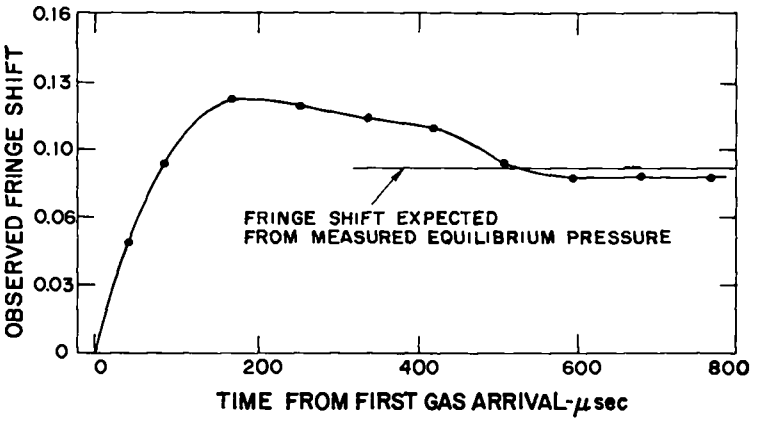

Fig. 55. Observed fractional fringe shift for injected gas density.

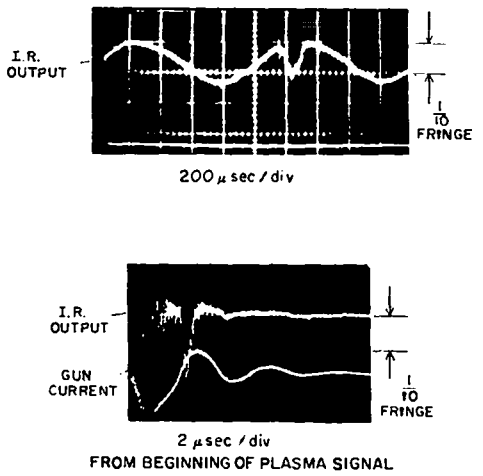

Fig. 56. Interferometer measured density of gun plasma in transverse field B = 5 kG.

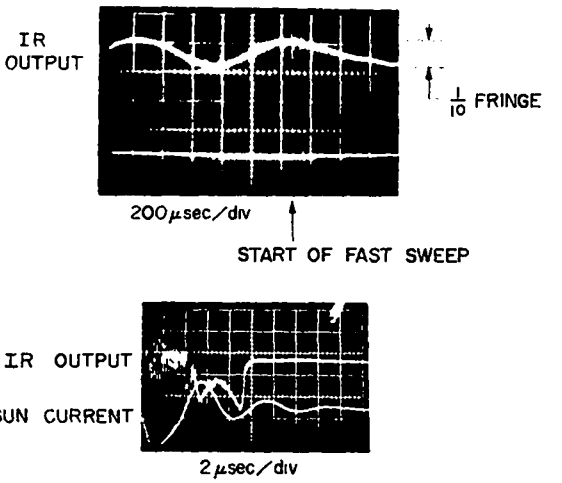

Fig. 57. Interferometer measured gun plasma density at high transverse field B = 7.5 kG

Baker-Hammel technique was a fast component from the stream of 0.3 to 0.5 fringe and slow component below the 0.1 fringe threshold. The "filter" in this case was a transverse-B field of 5 kG.

Examination of the "filtered" stream with this new increased sensitivity is shown in Fig. 56 with B-transverse = 5 kG. The fast component as seen on the fast 2-μsec/cm scope trace has a density in excess of 0.3 fringe, whereas the slow component seen in the 200-μsec/div trace for more than 100 μsec has a peak density of about 0.1 fringe. The new sensitivity has revealed slow plasma to be present at an unacceptable level.

Further experiments were then initiated to see if the slow component could be reduced to an acceptable level without losing the fast component. Fortunately, the simple act of increasing the transverse field to 7.5 kG reduced the slow component almost one order of magnitude. Figure 57 represents the same measurement as in Fig. 56 but is taken with B-transverse = 7.5 kG. The slow-plasma density is reduced to about 0.01 fringe which is probably an acceptable level.

The increased sensitivity has provided more confidence in the quality of the plasma from the coaxial gun. Moreover, if trapping of the injected plasmas is reasonably efficient, the laser interferometer will be an invaluable device for density measurements in the confinement region.

References

1. F.C. Jahoda, Rev. Sci. Inst., 36, 395 (1965).

2. E.B. Hooper, J. Bekefi, Appl. Phys. Letters, 7, 133 (1965).

DIPOLE GUARD AND THE FEASIBILITY OF A TOROIDAL QUADRUPOLE INJECTION EXPERIMENT

(J.E. Hammel and R.M. Henson)

The serious problems inherent in an inductively-fed levitated multipole containment geometry were discussed in detail in LA-3320-MS. The resistance of the interior conductors presents a fundamental difficulty because of the electric field which produces an $\vec{E} \times \vec{B}$ drift toward the conductor. A directly-driven interior conductor does not have this difficulty, but does substitute the prohibitive feature of a current feed which must cross the plasma confinement region.

Lehnert in 1959 proposed a linear dipole guard for the current lead to an inner conductor in a rotating plasma machine. As far as is known, however, the first experiment in which a dipole guard for a current was used with some success was in a rotating plasma experiment by L. Burkhardt, J. N. DiMarco, and H. Karr at LASL. These results were sufficiently successful so that an experiment was designed to test the possible effectiveness of a linear dipole arrangement as a guard for a lead-in or support crossing a containment region. The approximate field configuration around the guard is shown in Fig. 58 with the currents at a value which makes the leads force-free.

The guard currents produce two null lines which extend the full length of the currents. Plasma will certainly enter the region of these nulls and move along the null line. It is important, therefore, to consider where the null line goes after it crosses the containment region. It is proposed that the guard would end before it reaches the interior conductor so that the null does not reach its surface. Thus the only leak along

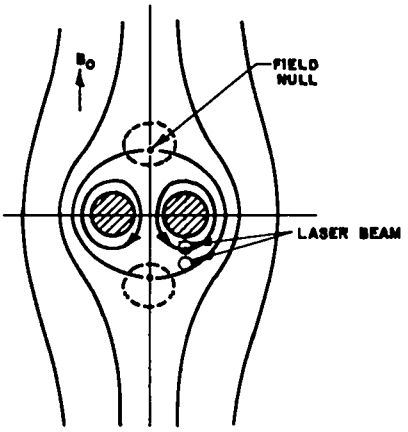

Fig. 58. Field configuration at the dipole guard for the force-free case.

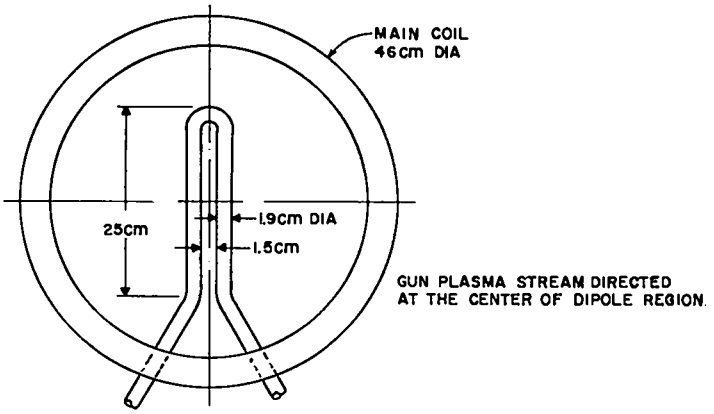

Fig. 59. Schematic of test of dipole shielding.

the field null will be at the outer boundary where the plasma can be dumped outside the machine. This direct leak toward the outside should guarantee a low density in the null. The guard is thus a hairpin which terminates slightly before it reaches the inner conductor. A preliminary test of such a dipole guard has been made by placing it in a gun plasma stream.

The physical arrangement is indicated in Fig. 59. The plasma stream from a coaxial gun is directed generally along field lines toward the dipole. The coaxial gun produces a short pulse of fast D plasma with a velocity of from 60 to 70 cm/μsec and a density of $\approx 4 \times 10^{14}$ ions/cm^3. The fast plasma is followed by a very dense slow plasma. Two simple measurements are made in the experiment. First, image converter pictures are taken of the light emitted at the dipole when the energetic

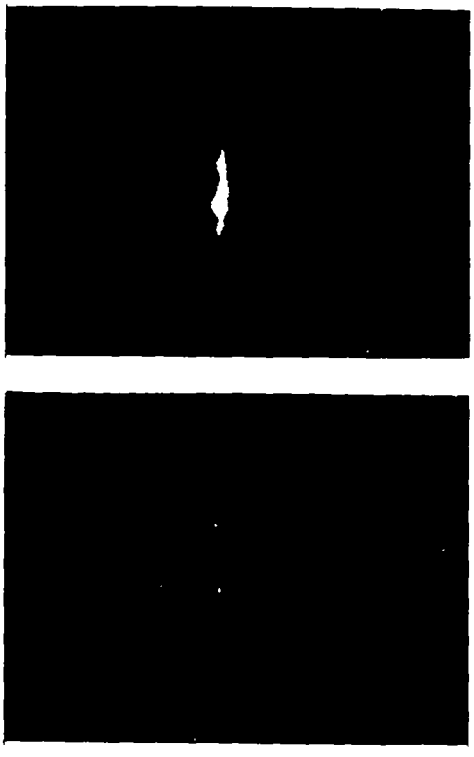

Fig. 60. Image converter picture of the light from fast plasma bombardment of dipole; (a) no dipole current, (b) dipole current equals force-free condition.

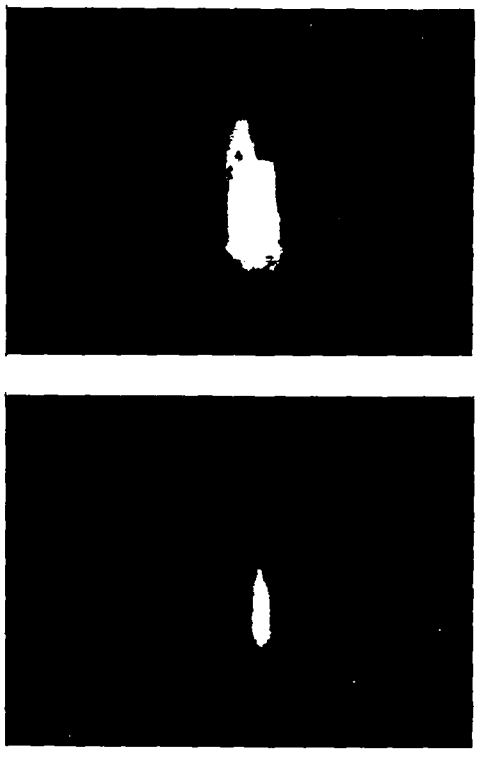

Fig. 61. Image converter photographs of dipole guard under plasma bombardment with small Pyrex rod between dipole legs; (a) no dipole current, (b) current equal to force-free case.

plasma strikes the aluminum surface. The region is photographed without current flowing in the guard, and this is compared with photographs with current flowing in the guard. Such a comparison of the light emitted under these two conditions is given in Fig. 60. The pictures were taken during the time of passage of the fast plasma. The background field in the plane of the guard is about 5 kG and the field at the surface of the $\frac{3}{4}$-in. lead in the force-free condition is near 20 kG. It is evident that the guard current very effectively prevents the energetic plasma from bombarding the structure sufficiently to give off light.

A second measurement was made to get some quantitative idea on the reduction of density at the guard. A He-Ne laser beam was directed

along one leg of the guard and within 2 mm on the upstream edge. The phase shift was measured interferometrically with and without the guard energized. During the fast plasma pulse the guard reduced the density by a factor of at least 5 which is the limit of sensitivity of the laser method at these densities.

It was found that plasma flows between the legs of the guard, as detected by a small cylinder of pyrex placed between the conductor legs. Figure 61a shows the bombardment of the dipole guard and pyrex cylinder with no current in the dipole leads; in Fig. 61b the dipole is protected when energized but the pyrex target is well bombarded and indicates that a large amount of energetic plasma is moving along the special line which crosses the field nulls (cf. Fig. 58). It appears that the fast plasma stream is "tied" to lines and thus avoids the guard because of currents along field lines back to the very dense slow plasma. An experiment (described later) in which the plasma stream is directed across field lines to the guard supports this view.

At a background field of 5 kG, when the fast plasma pulse is deflected from the dipole guard, the slow plasma arriving later does strike the dipole. The slow plasma is more dense than the fast component and is thus less tightly tied to the following plasma. Since communication velocity to the following plasma is proportional to the Alfvén speed, $B^2/\mu_o\rho$, the plasma drift across lines toward the dipole guard should decrease with increasing B. Experiments performed at higher B-fields show the slow plasma is held off for longer times, up to 8 μsec with B at 9 kG, which is the maximum field obtainable.

The guard leads were then set up at the center of a magnetic mirror geometry. The plasma stream was directed transverse to the field direction and again image converter photographs were taken with and without guard current. It was found that the fast plasma struck the legs with 5 kG in the main field whereas it was deflected from the guard in the first experiment when the plasma stream was directed along field lines.

At about 8 kG in the main field and about 26 kG at the surface of the guard lead, the plasma stream no longer struck the guard surface. With the plasma stream directed along the field lines a dense plasma was present to "tie" the low-density fast component to the field lines. With transverse injection the slow high-density plasma is not connected to the fast plasma along field lines, and the plasma flow toward the guard is stopped at high fields for unknown reasons. The stopping of a plasma stream at high fields has been observed before in transverse injection experiments.

With the encouraging results from the experiments with dipole guards, the feasibility of a larger injection experiment was investigated. Such an experiment would be designed to obtain data on three important features pertaining to gun plasmas injected into multipolar geometries. The first test would be on the efficiency of trapping of the fast, dense component of the coaxial gun by self-depolarization. Qualitative experiments have shown that the stream is self-depolarized in the region of a quadrupole null. It is clear, however, that quantitative data on such a mechanism are needed. A small quadrupole would be ideal for this test.

If a large portion of the gun plasma is captured and becomes quiescent in the quadrupole, the effectiveness of the dipole guards in protecting the feedthrough supports will be tested. The 2.5- to 5-keV plasma will make it very apparent (light and contamination) if the supports are being struck. If these two tests are successful, the quadrupole experiment will then allow assessment of the effect on confinement of the disturbance caused by the dipole guard.

A leak at the dipole guard is unavoidable as demonstrated by the result shown in Fig. 61. A fair estimate of this leak would be given by the diffusion through a hole two gyro-radii in diameter. This estimate is in agreement with experiments of T.K. Allen of Culham (private communication). For a quadrupole of the size to be described this leak would give a containment time of ~ 500 μsec. The loss rate from charge

exchange and Bohm diffusion would be lower than the rate estimated for the guard null; thus, it is probable that the injection process and dipole guards are the controlling features of such an experiment.

To determine the feasibility of a small injected quadrupole experiment, calculations were made on a geometry that could fit into the present Transverse Injection vacuum tank (1.5-m diam x 3.0-m long). Two possible configurations are considered: (a) with the conducting rings coplanar and (b) with the conducting rings coaxial and the same size. The results of these calculations are reported on p. 127 et seq. The coaxial geometry will give a minimum of 10 gyro-radii across the stable region with the field at the injection point no higher than 10 kG, which is the maximum field which the present gun plasma will penetrate. The energy required is ~ 1 MJ and is obtainable with the present facility. Preliminary engineering studies have been made on a configuration shown schematically in Fig. 62. These preliminary studies show that no serious mechanical difficulties should be encountered in the construction of such a configuration for 2.5-keV deuterons. A similar study is now under way for the coplanar geometry.

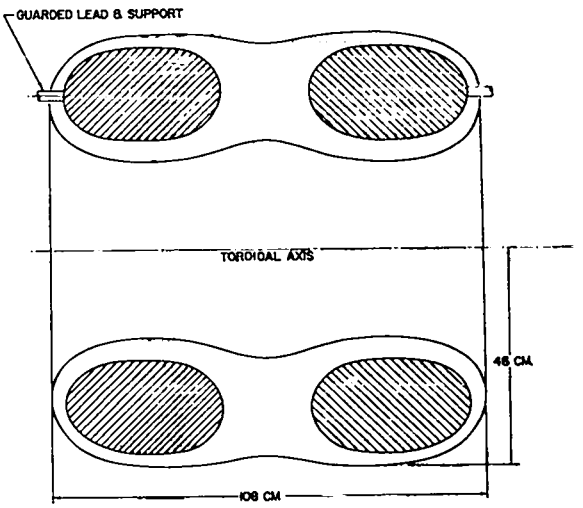

Fig. 62. Preliminary configuration of injected quadrupole experiment.

SUMMARY OF PLASMA THEORY GROUP ACTIVITIES

(W. B. Riesenfeld)

During its first year of existence the mathematical physics group of the LASL Sherwood project pursued a program of investigations which in most of its phases was closely related to the experimental program. It also included, however, relatively modest efforts directed toward fundamental topics in plasma theory, such as the coherent scattering of radiation, single-particle dynamics, and plasma diffusion studies. The work done is described in the six following sections of this report (pp. 103-129).

A major objective was to gain a better understanding of the existence, nature, and stability properties of cylindrical and toroidal plasma column equilibria, with growing emphasis on the high-β aspects of the problem. This program is closely tied to the planning and design studies for the Scyllac proposal (p. 16). The methods of attack are both analytical and numerical, with attention given to a judicious overlap of approaches for flexibility and to deepen understanding of the results obtained. Toroidal equilibria displaying very reasonable properties have been found, and studies of the hydrodynamic and kinetic stability of such equilibria have been fruitful in providing a high-β, thin-skin stability theory. A characteristic feature of the solutions is the unavoidable presence of localized instabilities (high-β ballooning) whose growth rates, however, are much less than the corresponding growth rates predicted by low-β, hydromagnetic ballooning theory. It is found that, under ideal circumstances, a system of dynamic (time dependent) stabilization might provide a cure for these residual gross instabilities. The efficacy of

these dynamic stabilization fields in practice depends upon such factors as the excitation of microturbulence in the tenuous plasma surrounding the dense main plasma column; these problems are under both experimental and analytical attack.

Work has proceeded toward understanding the detailed kinetic structure of linear θ-pinches, and toward constructing a quantitative theory describing the particle end loss rates.

In a major numerical computer program, pulsed magnetic field calculations have been carried out for systems with generalized toroidal symmetry; the results have relevance to the design and analysis of experiments in cusped and multipole confinement devices, in the low-β limit. Similar programs are being planned for transverse injection devices, and an exact numerical treatment of the structure of plasma flow transverse to a magnetic field is also being considered as a natural extension of present activities.

The study of single-particle dynamics in externally imposed magnetic and electric fields is a classic one, with elegant theories providing prescriptions for constructing asymptotic expansions for the adiabatic invariants of motion. Nevertheless, this field of investigation is still capable of yielding some surprises, as exemplified by the discovery that, for certain field configurations, it is possible to construct a rigorous, exact invariant in closed form, which constitutes a generalization of a well-known adiabatic invariant. Work is in progress to extend this result to more general electromagnetic fields.

NUMERICAL STUDIES OF THE PLASMA EQUILIBRIUM CONFIGURATION IN THE PROPOSED SCYLLAC DEVICE

(T. A. Oliphant and W. B. Riesenfeld)

The θ-pinches (like Scylla IV) now operating produce a hot (ion energies > 3 keV), dense (particle density of order $5 \times 10^{16} cm^{-3}$) plasma having a lifetime of the order of a few μsec. Such devices are open-ended, with the plasma free to stream out along the magnetic lines of force at the ends of the confining region. Detailed experimental analyses of the behavior of such devices suggest that this leakage is in fact the dominant loss mechanism limiting the plasma lifetime. Gross hydromagnetic instabilities can be suppressed by proper choice of the operating mode, but in theory it is possible that microinstabilities may lead to anomalously rapid diffusion of the plasma across the magnetic field. Such a process, occurring simultaneously with the streaming of plasma along the field lines, may also be responsible for the observed decay of plasma density with time. A resolution of the foregoing questions, together with a potentially significant extension of the lifetime, appears possible in the Scyllac proposal, described earlier in this report.

The toroidal confinement of a plasma is well known to pose serious problems with respect to achieving plasma equilibrium and ensuring that the equilibrium is a stable one. As an aid in the solution of the first of these problems, a numerical calculation has been made of a hydromagnetic equilibrium shape of the plasma ring resulting from both the externally imposed magnetic fields and the self-generated fields due to the electric currents flowing in the plasma. The plasma is assumed to be perfectly diamagnetic, the interface between the plasma and the magnetic field is

taken to be infinitely sharp; the solution satisfies the demands of hydromagnetic pressure equilibrium of the interface, and the geometry used in the calculation represents a reasonably realistic description of the apparatus which will be used to confine the plasma. The calculation, which involves an iteration scheme successively adjusting the field distribution and the interface shape, turns out to be quite complicated; The crudest problem which still illustrates all the essential features consumes approximately 5 h of CDC 6600 computer time.

The most accurate solution found to date bears a striking qualitative resemblance to the so-called Meyer-Schmidt "bumpy torus" configuration.[1] The correspondence is not quantitative because of restrictions on the planes of current flow which are imposed in the Meyer and Schmidt solution. A convenient test of the pressure equilibrium condition is the constancy of the lengths of magnetic lines of force on the plasma surface. These lengths agree with each other to within 0.10% whereas the corresponding deviations from the smooth torus peripheries average to 0.44%.

Further improvements of the calculation in the direction of iteration convergence and mesh refinement, which are needed to achieve the desired accuracy, will proceed during the coming year.

1. F. Meyer and H. U. Schmidt, Z. Naturforsch. 13a, 1005 (1958).

THEORY OF θ-PINCH EQUILIBRIA AND STABILITY

(R. L. Morse)

Introduction

Roughly half of the present work was concerned with linear θ-pinches such as Scylla IV and was done to help understand experimental results which have already been obtained. Calculations have been made in this area on end losses, thick plasma sheath development, and instabilities induced by plasma rotation. The remainder of the θ-pinch work concerns problems which are expected to appear in the proposed toroidal Scyllac. In this area conditions have been obtained for a type of dynamic toroidal equilibrium, and calculations have been made on the form and growth rates of ballooning modes which may be induced by a "bumpy torus"[1] equilibrium configuration.

End Losses

A significant amount of plasma escapes from the ends of existing θ-pinches during the time of the experiment. This end loss, which is caused by thermal motions of the plasma particles in directions approximately parallel to magnetic field lines, can be reduced by mirroring, i.e., increasing the magnitude of the magnetic field at both ends of the pinch. A method has been developed for estimating the effect of mirroring on loss rates. The configuration of plasma and magnetic field is obtained self-consistently for the center and end regions of the pinch from given values of the vacuum magnetic field in both regions and from a given particle distribution for the plasma. The rate of plasma flow through the increased field regions and out of the ends of the pinch

can be obtained directly from such a description. This method has been applied to the rigid rotor model of the plasma (see below). If the resulting loss rates are compared to free thermal effusion through a hole then, in general, the equivalent hole radius is greater than the gyro-radius of an ion of average energy moving in the magnetic field of the end region.

Adiabatic Development of θ-Pinch Sheaths

In practice it is found that the thickness of the sheath or transition region between a θ-pinch plasma and its confining magnetic field is of the order of the ion collisionless skin depth, $\lambda_i = c/\omega_{pi}$, which is usually in the range of 0.1 to 1 cm. On the other hand, it is expected that the sheath which is formed during the initial compression of the plasma is much thinner than this. The result of the relaxation of a relatively very thin sheath to a sheath with a thickness of the order λ_i has been obtained self-consistently under the assumption that the canonical angular momentum and radial adiabatic invariant, $I_r = \oint dr P_r$, are conserved for all ions during the relaxation. This relaxation is associated physically with the decay of strong radial electrostatic fields which must exist in any sheath whose thickness is much less than λ_i. Such a decay might be caused by electrical shorting of field lines in the sheath through their contact with material walls at the ends of a linear θ-pinch. The method used replaces ion energy, which is not conserved during the relaxation, by I_r, which is conserved. The resulting time-independent distribution function is used to obtain currents for any given field configuration which is self-consistent with these currents under the condition that there is no electrostatic field present.

The results predict that the sheath of a pinch whose line density is less than about $5 \times 10^{16} cm^{-1}$ will be too thick relative to the plasma radius to give the impression of a sheath region which is distinct from the main body of the plasma. In this case the diamagnetic shielding of the center of the plasma will be incomplete and β there will not be unity.

This prediction is in reasonable agreement with experimental results. The solutions for line density $< 5 \times 10^{16} cm^{-1}$ were found to have the interesting property that they are very nearly rigid rotor solutions of the Vlasov equations, i.e., their mean angular velocity is nearly independent of radius. Values were also obtained for the angular momentum which the plasma acquires during the relaxation and for the decrease in plasma energy which occurs because the plasma effectively expands into the confining magnetic field during the relaxation.

Rotational Instabilities (with J. Palsedge)

Plasmas in linear θ-pinches have been observed to have a net angular momentum of sufficient magnitude to cause significant destabilizing centrifugal forces. One class of modes which could be driven by such centrifugal forces are those of the cylindrically $m = 0$ or "sausage" type in which all perturbed quantities have the form $\delta(r)e^{ikz}$. A systematic method has been found for determining the existence and structure of marginally stable modes of this form. The method starts from a self-consistent, z-independent, equilibrium configuration of plasma and field and relies on the fact that the canonical angular momenta of all particles are conserved because of the cylindrical symmetry of the $m = 0$ modes and that the energies of almost all of the particles are unchanged by the development of an $m = 0$ mode with vanishingly small growth rate. Consequently, the unperturbed distribution function, which is a function of particle energy and angular momentum, can be used in a perturbation treatment of marginally stable modes. The perturbation calculation determines if a real eigenvalue of k exists for a given plasma. If so, then the radial dependence of the perturbed magnetic field and plasma density can be obtained.

The significance of the eigenvalue of k for a given plasma configuration is that for all smaller values of k unstable modes of the system exist. The method has been applied to rigid rotor solutions of the Vlasov equations for values of plasma parameters in the range of experimental interest. The results to date suggest that this class of rotational

instabilities may only be dangerous for θ-pinch plasmas containing reversed magnetic field, and it is not clear that such a plasma can acquire a significant angular momentum without first losing its reversed field.

Dynamic Toroidal Equilibrium

If a linear θ-pinch containing a high-β plasma is bent into a torus, the resulting toroidal magnetic field has a spatial gradient which works to push the plasma outward away from the major axis of the torus and into the wall of the confinement region. This toroidal drift is essentially an $m = 1$ motion of the plasma column and may be suppressed by inducing a current to flow lengthwise around the toroidal plasma as has been done in numerous toroidal devices in the past. This current produces a poloidal field encircling the plasma, the effect of which is to compress the plasma on the side nearest an exterior conducting wall and to resist the motion of the plasma toward that wall. In this way a confined plasma equilibrium can be obtained.

The addition of such a poloidal field to a high-β plasma, however, is known to induce unstable helical flutes at the surface of the plasma. It is believed that these flutes can be suppressed by causing the auxiliary poloidal field to oscillate sufficiently rapidly but at the expense of causing a forced oscillation of the equilibrium position of the plasma. An equation of motion for these forced oscillations has been verifed; it has the form of an harmonically driven Mathieu equation. The conditions for boundedness are of experimental interest.[2] According to these solutions, oscillating dynamic equilibria of acceptably small amplitude can be obtained for the plasma anticipated in the proposed toroidal Scyllac, by using an oscillating poloidal magnetic field with amplitude and frequency which are technically feasible.

Ion Trajectories in High-β Toroidal Plasma (with R. Lewis)

In low-β toroidal confinement systems particles of all species are adiabatically tied to magnetic field lines because their gyro-radii are

small compared to the characteristic dimensions of the field configuration. Consequently collisionless equilibria can be constructed on the basis of drift surfaces. Important classes of ions in hot, high-β, linear θ-pinch plasmas do not satisfy the drift approximation but can contribute to a stationary solution of the Vlasov equations because cylindrical symmetry allows the conservation of their canonical angular momenta. On the other hand, some proposed toroidal θ-pinch field geometries possess no symmetries which could have a similar effect. In order to study the effect of this difference on toroidal high-β equilibria, single-particle trajectories have been computed for ions of large gyro-radius moving in a deep toroidal magnetic well. No effort has been made to obtain self-consistency. The results to date, although far from complete or conclusive, show a tendency of the trajectories to remain localized to the region of the well.

Ballooning of $\beta = 1$ Plasmas with Sharp Boundaries

The Meyer-Schmidt high-β, bumpy torus geometry has been suggested for obtaining equilibrium in the proposed toroidal θ-pinch, Scyllac. In order to estimate the growth rates of any instabilities which might be induced by the regions of convex curvature on the bumps, a study has been made of the stability of a bumpy cylinder of $\beta = 1$ plasma with a sharp boundary of radius $a(z) = \bar{a}(1 + \delta \cos 2\pi z/\lambda)$.

It was assumed that the interior of the bumpy cylinder is field free and that the plasma is collisionless. Surface perturbations of the form $\epsilon = \epsilon_o(z)\, e^{\gamma t} \cos m\theta$ were considered. It was found that all $m = 1$ modes are stable and that if $\delta \ll 1$, the growth rates of the unstable modes with small $m > 1$ are approximately $\gamma = \delta^2 \pi^{5/2}(m - 1)\,(\bar{a}/\lambda)^2(v_o/\bar{a})$. For large m, the growth rates are bounded by $\gamma < 2\delta\pi^{5/2}(\bar{a}/\lambda)^2(v_o/\bar{a})$. These

growth rates are considerably smaller than those predicted from a fluid model of the plasma. Numerical calculations verify that no qualitative changes are found for δ of the order of unity. The ballooning character of these modes is seen from the fact that $\epsilon_o(z)$ for the unstable modes is largest in the regions of convex curvature of the unperturbed boundary.

References

1. For a discussion of "bumpy torus" equilibria see p. 103 et seq.

2. LA-3487-MS, Appendix VI.

INVARIANTS AND ADIABATIC INVARIANTS

(H. R. Lewis)

Introduction

In an attempt to understand the nature of adiabatic invariants of charged particle motion better, extensive work has been done during the past year on the application of Kruskal's asymptotic theory of nearly periodic Hamiltonian systems[1] to study the magnetic moment series for a charged particle in a general electromagnetic field. One reason for studying adiabatic invariants is to investigate the possibility of applying them, or generalizations of them, to a wider range of interesting cases. For example, if it were possible to generalize them to be valid in weak magnetic fields and in fields with rapid temporal and spatial variations, then it might be possible to apply them fruitfully to study the stability of highly diamagnetic plasmas or the injection of plasma transverse to a magnetic field starting in a region of low field strength.

Applying Kruskal's theory with a general electromagnetic field is very tedious. It has been possible, however, to formulate the problem in a sufficiently systematic way to permit use of a computer for performing the required manipulations. This work, which is described below under the title "Magnetic Moment Series," has progressed nearly to the point of actually calculating the expressions in Kruskal's theory order by order.

If a charged particle moves in a uniform, but time-dependent, magnetic field and the associated induced electric field, then the equations of motion can be reduced to the equation of an oscillator with a time-dependent frequency exactly. For such an oscillator it has been possible to work

out Kruskal's theory in closed form. As a consequence, some exact results have been obtained from the asymptotic theory, one of which is the form of an exact invariant which contains the usual adiabatic invariant, energy/frequency, as a limiting case. There are indications that an analogous treatment is possible for the case of a particle in a general electromagnetic field. It is expected that this can be determined when the calculations mentioned in the preceding paragraph are completed.

Theory of an Oscillator with a Time-Dependent Frequency

The equation considered is

$$\epsilon^2 \frac{d^2x_1}{dt^2} + \Omega^2(t)x_1 = 0, \tag{1}$$

and the Hamiltonian for this equation is

$$H = \frac{1}{2\epsilon}(x_2^2 + \Omega^2 x_1^2), \tag{2}$$

in which x_1 is considered as the canonical coordinate and x_2 as its conjugate momentum. The corresponding canonical equations of motion are

$$\epsilon \frac{dx_1}{dt} = x_2 \qquad \text{and} \qquad \epsilon \frac{dx_2}{dt} = -\Omega^2(t)x_1 . \tag{3}$$

In order to apply Kruskal's theory it is necessary to replace Eqs. (3) by an equivalent autonomous system, i.e., by a system in which the derivatives are not functions of the independent variable. The new system must also be such that, in terms of the independent variable, all of the solutions are periodic with the same period in the limit $\epsilon = 0$. These two conditions can be realized by introducing a new independent variable s, defined by $s = t/\epsilon$, and treating t as an additional dependent variable. The new system of equations is then

$$\frac{dx_1}{ds} = x_2 , \qquad \frac{dx_2}{ds} = -\Omega^2(t)x_1 , \text{ and } \frac{dt}{ds} = \epsilon. \tag{4}$$

Since t is now a dependent variable, this system is autonomous. In the limit $\epsilon = 0$, the solution of the last equation is t = constant and, therefore, the other two equations are just the equations of a harmonic oscillator. Thus, the dependent variables are all periodic with period $2\pi/\Omega(t)$ in the limit $\epsilon = 0$.

The Kruskal theory defines a one-parameter family of closed curves in (x_1, x_2, t) space such that a point in that space moving according to Eqs. (4) stays on the same curve for ever; these closed curves are called rings. In the general theory, the transformation from (x_1, x_2, t) to the rings and the variable which parameterizes the rings is defined as an asymptotic series in positive powers of ϵ, and a prescription is given for calculating the series order by order. In this case of an oscillator with a time-dependent frequency, however, it is possible to obtain the transformation in closed form, a possibility that was previously unknown. Once the rings have been found, it is possible to evaluate the quantity

$$I = \oint_{\text{ring}} x_2 dx_1 \tag{5}$$

explicity; I is an exact invariant of the system.

The result for the invariant I is

$$I = \frac{1}{2}\left[\rho^{-2} x_1^2 + (\rho x_2 - \epsilon\rho' x_1)^2\right], \tag{6}$$

where ρ is a function of t satisfying

$$\epsilon^2\rho'' + \Omega^2\rho - \rho^{-3} = 0, \tag{7}$$

and a prime denotes differentiation with respect to time. The function ρ can be taken as any particular solution of Eq. (7). It is easy to verify that $dI/dt = 0$ by differentiating Eq. (6) using Eqs. (3) to eliminate dx_1/dt and dx_2/dt, and Eq. (7) to eliminate ρ''.

There are two possibilities known at present for solving Eq. (7) for ρ. One of these is to integrate the equation numerically. Because any particular solution suffices, it is necessary to perform the numerical integration only once for each Ω. Thus, for numerical work, the expression for I is practically explicit. The other possibility is to obtain ρ as a power series in ϵ^2. By virtue of the fact that ϵ^2 multiplies ρ'' in Eq. (7), this is easy to do using the equation directly. To lowest order the result is $\rho = \Omega^{-\frac{1}{2}}$. Therefore, to lowest order, I is proportional to (energy/frequency) the usual adiabatic invariant. It is thus possible to obtain corrections to the lowest-order adiabatic invariant by using a truncated power series in ϵ for ρ when calculating I. It is of interest to speculate whether I so calculated is more nearly invariant than the corresponding truncated power series for I.

Now that the invariant I has been obtained, it is possible to find a canonical transformation such that I is a canonical momentum. For this purpose it is convenient to expand the original Hamiltonian system as follows. Take the Hamiltonian to be

$$K = \frac{1}{2}\left(x_2^2 + \Omega^2 x_1^2\right) + \epsilon P, \tag{8}$$

in which t is a new canonical coordinate and P is its conjugate momentum. The value of P which solves the canonical equations is minus the Hamiltonian given in Eq. (2). The canonical equations are

$$\frac{dx_1}{ds} = x_2, \quad \frac{dx_2}{ds} = -\Omega^2 x_1, \quad \frac{dt}{ds} = \epsilon \text{ , and } \frac{dP}{ds} = -\Omega \frac{d\Omega}{dt} x_1^2 .$$

Kruskal has shown that it is possible to take a new set of canonical variables in which one coordinate is the variable that parameterizes the rings and the conjugate momentum is I. The Poisson bracket relations

for the other pair can then be solved. Denoting the new coordinates by Q_1 and Q_2, and the new momenta by P_1 and P_2, the results can be written as

$$\left.\begin{aligned} Q_1 &= -\tan^{-1}\left[\rho^2\frac{x_2}{x_1} - \epsilon\,\rho\,\rho'\right] \\ P_1 &= \frac{1}{2}\left[\rho^{-2}x_1^2 + (\rho x_2 - \epsilon\rho' x_1)^2\right] \\ Q_2 &= t \\ P_2 &= P + \frac{1}{2\rho^2}\left[2\rho\rho' x_1 x_2 - \epsilon(\rho'^2 + \rho\,\rho'')x_1^2\right] \\ K &= \epsilon P_2 + \rho^{-2} P_1 \quad . \end{aligned}\right\} \tag{9}$$

Thus, Q_1 is indeed cyclic, as it must be if $P_1 = I$ is an invariant.

An interpretation of the function of ρ is provided for by the equation for Q_1, which may be written as

$$\epsilon\rho^2\,\frac{dQ_1}{dt} = 1. \tag{10}$$

Multiplying through by I, the result is

$$\epsilon(I^{\frac{1}{2}}\rho)^2\,\frac{dQ_1}{dt} = I. \tag{11}$$

This is of the same form as the equation for conservation of angular momentum for a particle of mass ϵ moving in an axially symmetric force-field if $I^{\frac{1}{2}}\rho$ is interpreted as a generalized radius, Q_1 as a generalized angle, and I as a generalized angular momentum.

Magnetic Moment Series

In order to apply Kruskal's theory to the problem of a charged particle moving in a general time-and-space dependent electromagnetic

d, it is necessary to perform very tedious manipulations. Once this
one it may be possible to see how to treat the problem in a way analogous
he treatment for an oscillator with a time-dependent frequency. It
been possible so far to formulate the calculation in a way that it can
lone on a computer using the IBM FORMAC system. This system is capable
performing literal algebra and,also, implicit and explicit differentiation.
the Kruskal theory it is necessary to work with complicated polyadic
ressions, and a procedure has been invented for applying the FORMAC
tem to such expressions. Even the required integrals can now be obtained
h the computer. It is expected that the computer program will be finished
on.

ference

M. Kruskal, J. Math. Phys., 3, 806 (1962).

GENERAL PURPOSE COMPUTER CODE FOR PARTICLE TRAJECTORIES AND OTHER PROBLEMS

(H. R. Lewis and K.R. Crandall)

The computer code which was used previously for computing and graphing trajectories of a charged particle in a stuffed-cusp field has been rewritten so that it is easily applicable to a general particle trajectory problem or, indeed, to the problem of solving a general system of not more than six first order differential equations of the form

$$\frac{dy_i}{dt} = f_i(t, y_1, \ldots, y_n),\ i = 1, \ldots, n (n \leq 6).$$

The heart of the code is the subroutine DEQ described in a LASL Report.[1]

The name of the trajectory code is ORB, and it is written for use on the IBM 7030 (STRETCH) computer. The user is allowed very flexible control of the type and format of graphical output (made by the SC-4020 which produces graphs on 35-mm film). In addition to t and y_i, up to three other quantities, completely determined by the user, may be calculated, printed, and graphed. Both two-dimensional and three-dimensional (stereoscopic) graphs can be obtained. The f_i, the initial conditions, and the type and format of the display of results may be altered with a minimum of effort.

Reference

1. H. R. Lewis, Jr. and E. J. Stovall, Jr., "A FORTRAN Version of Nordsieck's Scheme for the Numerical Integration of Differential Equations," LA-3292.

PARTICLE TRAJECTORIES IN THETA-PINCH TYPE PLASMAS

(H. R. Lewis)

In order to obtain some information about particle orbits in θ-pinch plasmas, particularly of the toroidal type, the computer code described in the preceding section has been applied to the following problem. Suppose that a torus contains a plasma with coordinates shown below. Further, suppose that there is a magnetic field in the φ direction given by the vector potential

$$A_r = A_\varphi = 0, \quad A_\theta = \frac{A_o(r)}{1 + \frac{r}{\rho_o}\cos\theta} \quad .$$

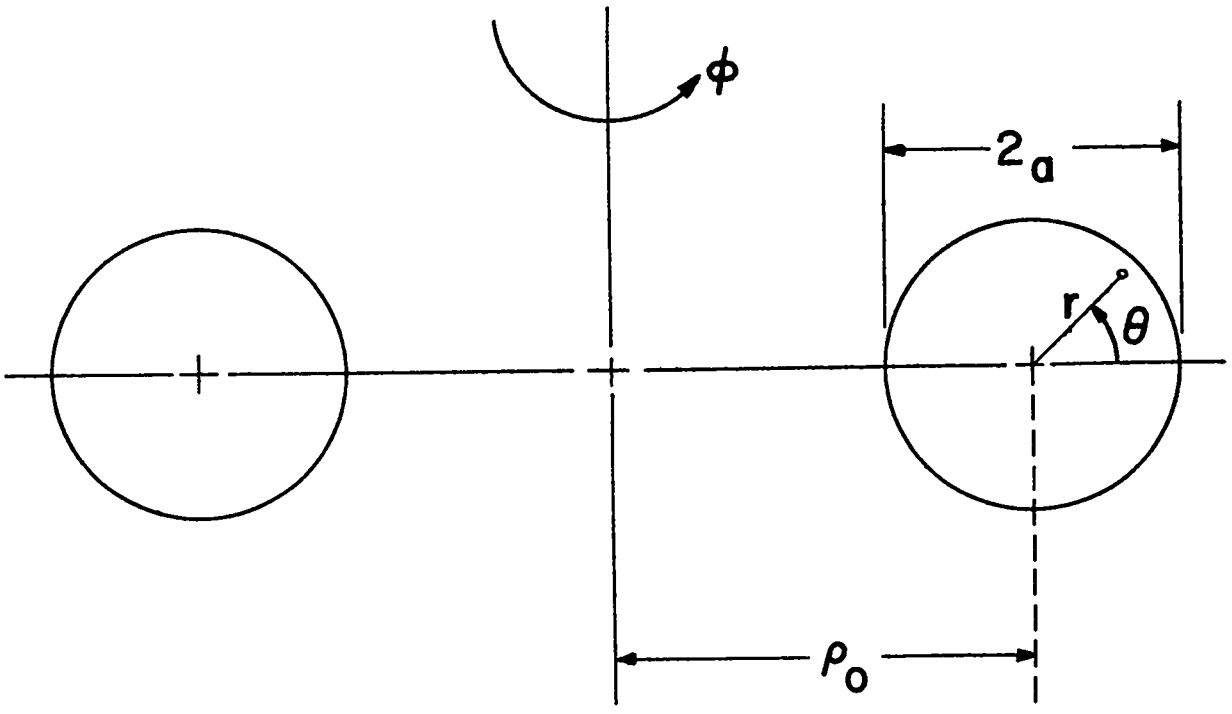

$A_o(r)$ is arbitrary and so it can be specified by its values at a discrete number of values of r, in which case it is automatically represented by a spline function which is continuous and has continuous first and second derivatives.

Preliminary results, based on a few cases, suggest that particles moving in a field of this type may remain within the torus and exhibit considerable regularity in their motion for long times even when the magnetic field at $r = 0$ is very small. The gyroradius near the edge of the torus is not small compared to the minor radius, a/ρ_o is rather large ($\lesssim 0.2$), and the magnetic moment is far from constant ($w_\perp/B$ far from constant and the series beginning to diverge with the next term). Further study is required to confirm and define this behavior better.

PULSED FIELD SKIN EFFECT CALCULATIONS FOR CYLINDRICAL CONDUCTORS

(D.A. Baker, M.D.J. MacRoberts, and L.W. Mann)

Introduction

The design of pulsed magnetic field systems often requires an estimation of (1) the rate at which the pulsed magnetic fields penetrate conductors, (2) the electric field at the surface of the conductors, and (3) the field loss due to resistive damping of a pulsed RLC circuit. In the past year a method has been developed which allows the designer to make a more accurate estimate of these factors than is possible by the rather crude methods previously employed. A computer program has been developed which solves numerically the differential equations involved for the three factors given above, including the effects of time-varying skin depth. Although the code is designed to solve equations for a cylinder only, a suitable modification of the input will allow it to make good approximations for flat-plate conductors and series connections of conductors with different cross sections. The computer output has been displayed, for the most part, in dimensionless curve form which permits the user to make quick calculations for his particular geometry. The work has been reported in detail elsewhere,[1,2] and so the discussion here will give only an outline of the results.

Magnetic Field Distribution in a Hollow-Cylindrical Conductor

A set of curves has been obtained showing the time dependence of magnetic field penetration into a conductor carrying a prescribed current.[1] Only a few examples are given because too many graphs are needed to cover the range of all interesting parameters. If a specific case not covered in the report is to be studied, the computer code for the IBM-7030 (STRETCH) can be used.

Surface Electric Field

The electric field at the surface of the conductor can be employed to estimate the $\vec{E} \times \vec{B}$ drift of charged particles toward current carrying conductors and to compute the flux in a conductor. A group of dimensionless curves has been derived which show the electric field at the surface of the hollow cylinder as a function of time for various ratios of inside to outside radii.[1] There is a set of curves for several current waveforms presently being used in Sherwood applications.

The Current which Flows During the Discharge of a Capacitor Through a Solid Cylinder

A dimensionless curve makes it possible to predict the peak current in inductive loads formed by a solid conductor with a circular cross section.[1,2] The results of these calculations have been compared with the predictions of an approximate rule, based on the ac skin depth, that is often used.[2]

Extension to Circuits Formed from Wide Conductors

In pulsed field applications circuits are frequently encountered which are constructed by deforming flat plate conductors, e.g., a parallel plate transmission line feeding a single turn coil (θ-pinch). Cases where the conductors are wide (in the direction normal to current and parallel to the conductor surface) compared to their separation can be treated by writing a corresponding set of field equations in rectangular coordinates. If fringing field effects are ignored, the fields reduce to single components depending on one space variable. The calculation will be valid provided all radii of curvature of the conductors are large compared to the current penetration depth. Under these conditions the same code can be

used because the Maxwell equations for cylindrical coordinates reduce to their form in rectangular coordinates when the radius of the conductor is large, i.e., the 1/r terms in the field equations become negligible.

A calculation has been made showing how the field penetration into conductors can sustain the field of a "crowbarred" circuit appreciably longer than that predicted by commonly used steady-state skin depth approximations.[1]

References

1. D. A. Baker, M.D.J. MacRoberts, L. W. Mann, LA-3500, 1966.

2. D. A. Baker, M.D.J. MacRoberts, L. W. Mann, J. Appl. Phys., 37, 2792 (1966).

INVESTIGATION OF $\int d\ell/B$ CLOSED SYSTEMS

(D.A. Baker)

Introduction

Investigations have been made into the possibility of producing a practical, $\int d\ell/B$ stable, magnetic bottle having no rotational transform or floating conductors for use with a toroidal Scylla . The results are summarized below.

Alternating Quadrupoles

The magnetic field first proposed[1] as a $\int d\ell/B$ stable, closed system having no floating conductors consisted of a periodic alternating quadrupole field superposed on a longitudinal field. The latter field in turn periodically increases to produce mirrors in the regions of the quadrupole reversals. Optimization studies[2] of such systems, as well as of higher multipoles, showed that, even with very large excursions of the field lines in the radial direction, the attainable well depths in $-\int d\ell/B$ were only a few tenths of a percent. Such systems also require impractically large mirror fields.

An attempt to produce an alternating quadrupole not requiring the large mirror field energy was discussed in a previous report.[3] There it was stated that by placing crossfeed currents on a set of alternating quadrupole conductors, in such a fashion that the bad curvature regions were strengthened and the good ones weakened, a stable configuration of field was produced if the current feeds to the system were neglected. It was subsequently found, however, that the current feeds are all important and when they are included in the calculation, the $\int d\ell/B$ stable field then becomes an unstable one.

Investigation of $\ell = 0, 1, 2, 3$, Systems

In view of the unsuitability of the alternating single multipole approach, investigations were then made on $\ell = 0, 1, 2, 3$ systems following the invention of such systems by J. L. Johnson for the rotational transform case. H. P. Furth suggested an investigation of $\ell = 0, 1, 3$ sections joined by quadrupole sections to shape the flux surfaces to exploit the stabilizing regions. The early arguments were based on a scalar magnetic potential of the form

$$U_F = fz + g_1(z) \cos\theta + (r^3/3)\, g_3(z) \cos 3\theta, \qquad (1)$$

where f is a constant and g_1 and g_3 are periodic functions of z. Cylindrical geometry is used with the argument that it should be applicable to toroidal regions with large aspect ratios. It can be shown that for a small r expansion and up to terms of order $(1/f)^3$

$$W_F \equiv \int dz/B_z = (L/f) + f^{-3} \int_0^L \{g_1^2 + g_1'^2\, r^2 \cos^2\theta + 2g_1 g_3 r^2 \cos 2\theta\}dz, \qquad (2)$$

where L is the periodicity length and the prime denotes differentiation with respect to z.

For a given sign of $g_1 g_3$ and a sufficiently small g_1' this integral implies stability in the x-direction (i.e., it decreases away from the the axis in the x direction) and instability in the y-direction ($g_1 g_3 < 0$) or vice versa ($g_1 g_3 > 0$). It was then argued that overall stability would result from a periodic array of such systems, alternating the sign of $g_1 g_3$. These are combined with $\ell = 2$ quadrupole sections (guide fields) of alternating signs to transform y-excursions to x-excursions of field lines. By making the outward excursions in a given $g_1 g_3$ section in its stable direction, it was hoped that a good well depth could be achieved without the use of mirrors and with acceptable field line excursions.

The foregoing argument has two defects which have been remedied. (1) The potential does not give fields which satisfy Maxwell's equations

to lowest order in r. (2) the $\ell = 2$ contribution for the shaping field is not included. The first defect is remedied by adding another term, $-\frac{1}{8} g_1'' r^3 \cos\theta$ and the second by adding on the $\ell = 2$ term. The new potential is then

$$U = U_F + \tfrac{1}{2} g_2 r^2 \cos 2\theta - \tfrac{1}{8} g_1'' r^3 \cos\theta. \tag{3}$$

The corresponding formula for $\int d\ell/B$ is

$$W = L/f + (1/f)^3 \int_0^L dz \{g_1^2 + g_2^2 r^2 + 2 g_1 g_2 \, r \cos\theta + g_1'^2 r^2 \cos^2\theta - (1/8) g_1 g_1'' r^2 (1 + 2\cos^2\theta) + 2 g_1 g_3 r^2 \cos 2\theta\}. \tag{4}$$

This form includes several terms that were omitted in the previous calculation. The quadrupole introduces a destabilizing term $g_2^2 r^2$ and the $\ell = 1$ field introduces a destabilizing term $g_1'^2 r^2 \cos^2\theta$. For a periodic system, $g_1 g_1''$ of necessity will have regions where $g_1 g_1'' < 0$ which gives a destabilizing contribution in those regions. The term $2 g_1 g_2 r \cos\theta$ contributes instability or stability according to whether $g_1 g_2 \cos\theta$ is greater or less than zero. Since this term has half the θ period of the $g_1 g_3 \cos 2\theta$ term, it appears that the quadrupole helps only by shaping the field lines to weight the stable part of $g_1 g_3$ term by giving it larger values of r. To be of value this stabilizing effect has to outweigh the destabilizing effect of the new quadrupole terms that are introduced as well as those produced by the g_1 field.

Systems of $\ell = 1, 3$ coils[4] and alternating quadrupole currents were studied by numerically integrating field lines with the IBM-7030 (STRETCH) computer. No stable system was found.

Johnson and Mosher computed a nonrotational transform $\ell = 0, 1, 2, 3$ system using expansions and concluded that a well is obtainable.[5] The well depth of their system was examined by coding the expanded field for the computer and calculating the field lines. It was found that, for

the parameters where the expansions were valid, $W = \int d\ell/B$ did not change except in the fourth or fifth figure, a position where the value of W is in doubt due to the numerical integration of the equation for the field line. Larger parameters were tried and no stable field was found. From private communications it was learned that Wakefield and Christensen at Princeton had obtained a similar result when the expansion parameters were small for an $\ell = 0, 1, 2, 3$ system having rotational transform. They found a well depth of $\sim 1\%$ after a thorough systematic parameter search using large amounts of computer time. Their best configuration was for a set of parameters in which the expansions which led to a study of the system were not valid.

A large amount of computer time would be required for a complete parametric study. From the calculations done to date it is evident that, at least for the types of configurations studied, well depths of $\geq 3\%$ required to compensate the toroidal curvature of a toroidal θ-pinch with a major diameter of 5 m are highly unlikely. Moreover, it appears that nonrotational transform systems have considerably smaller well depths than those found by the Princeton group.

References

1. H. P. Furth and M. N. Rosenbluth, Phys. Fluids 7, 764 (1964).
2. J. M. Greene, Princeton Plasma Physics Laboratory, (unpublished manuscript).
3. Semiannual Status Report of LASL Controlled Thermonuclear Research Program for Period Ending October 31, 1965. Los Alamos Scientific Laboratory Report LA-3434-MS, p. 84 (1965).
4. Details of the derivation of Eq. (4) and the $\ell = 1, 3$ coil arrangements are given in Reference 3, p. 157 and 22, respectively.
5. J. L. Johnson and D. Mosher, Princeton Plasma Physics Laboratory Report MATT-435 (1966).

CAULKED CUSP CALCULATIONS

(D.A. Baker, M.D.J. MacRoberts, L. W. Mann)

The earlier Los Alamos efforts in the direction of a free-fall quadrupole device were discontinued when it was found that long-time containment (50 msec) and strength of materials constraints required either cryogenic cooling of the conducting rings or unsuitably high field energies and large machine dimensions.

A feasibility study of a much less ambitious experiment is now under way in collaboration with J. Hammel and R. Henson (see p. 95 et seq.) The construction of the device is greatly simplified because: (1) free-fall rings will be abandoned in favor of mechanical supports which it is hoped can be shielded magnetically, (2) the confinement will be studied for a much shorter time $\sim$ 1 msec, and (3) the previous stringent requirement of 10 gyro-radii of stable field (10-keV D's) has been replaced. Instead, the machine is limited to a maximum outside diameter of 140 cm to be compatible with an existing vacuum chamber. Effort will then be made to maximize the number of gyro-radii of stable field with the additional constraints of single mirror bridges, 10-kG injection field, and allowable mechanical forces.

Two double-ring, caulked-cusp configurations have been investigated: Case I, concentric, coplanar rings and Case II, coaxial, non-coplanar rings with equal radii. In both cases the systems have mirror symmetry about a plane normal to the rotational symmetry axis.

Various geometries have been examined by trial and error using a field iteration code (PAVAL). The best geometry found to date for each of the configurations is shown in Figs. 63 and 64. The parameters for each case are tabulated on page 129.

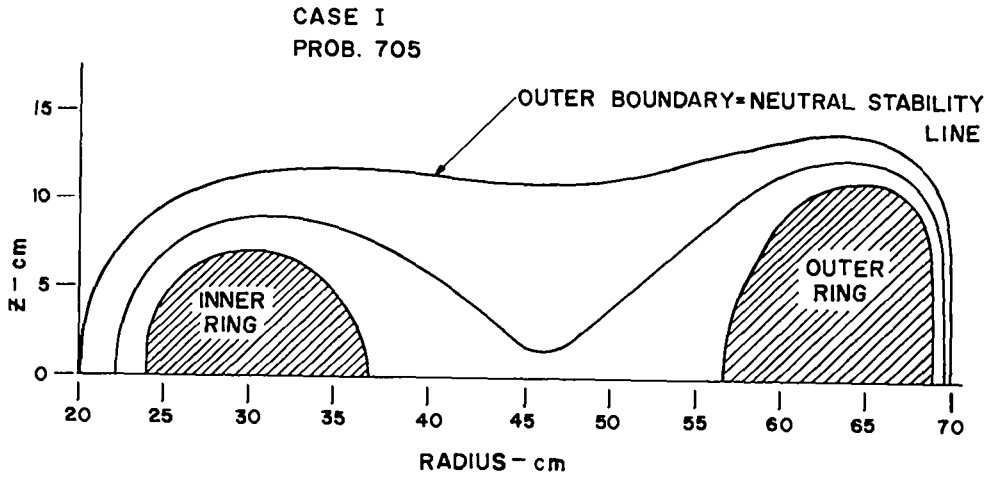

Fig. 63. Boundary configuration for the concentric, coplanar ring case. (Rotational symmetry about r = 0 and mirror symmetry about the plane z = 0.)

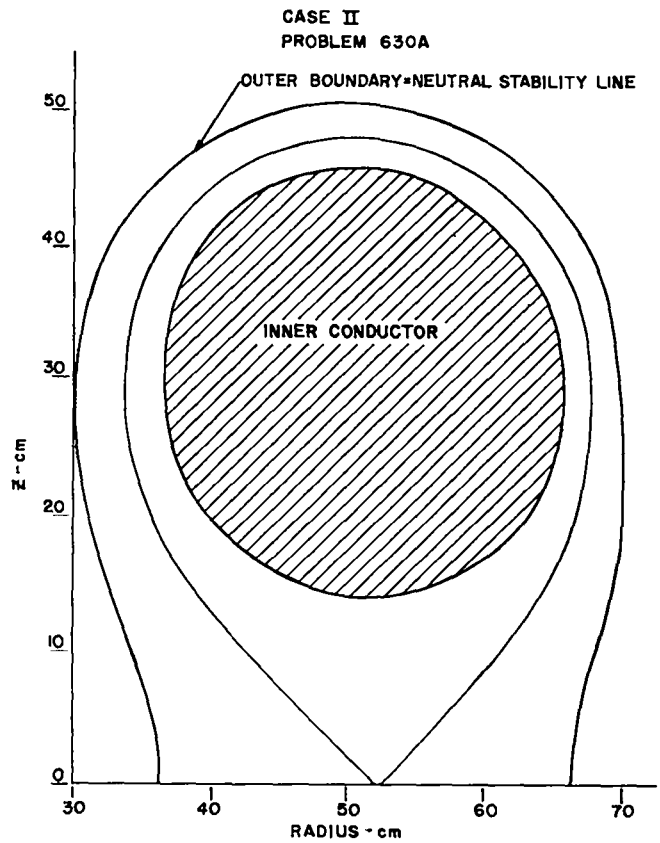

Fig. 64. Boundary configuration for the coaxial equal radii ring case. (Symmetry conditions same as in Fig. 63.)

	Case I Concentric rings (Prob. 705)	Case II Equal Radii rings (Prob. 630A)
No. of gyro-radii of stable field (5-keV D)	6.1	10.2
Energy of stable field, MJ	0.70*	1.7
Injection field, kG	10	10
Sum of ring currents, MA	3.8	5.8
Maximum field inner conductor, kG	86	57
Maximum field outer conductor, kG	67	41
Total force between rings, lb	-	1.3×10^6
Torus hole diameter, cm	41	60
Torus o.d., cm	140	140
Torus thickness (in z direction), cm	29	100

*This energy is required for inductive drive; for direct feed the energy can be reduced because the region around the innermost ring has excess gyro-radii and can be made larger.

The energy in the stable field is very nearly that amount which must be supplied to the device for either direct or iron-core inductive current feed to the rings. Approximate calculations indicate that an air-core inductive feed for the geometry of Case II above would require an order of magnitude more energy.

A comparison of the two cases shows that Case II has more gyro-radii of stable field at the expense of field energy. It has the additional complication of having to support the rings against their large attractive force.

NEW FUNDAMENTAL PLASMA PHYSICS GROUP

(H. Dreicer)

A group was established on April 1, 1966 for the purpose of strengthening LASL Sherwood's research into the fundamental properties of plasmas. Its membership presently consists of four physicists, D. Henderson, J. McLeod, D. Michael (graduate student), H. Dreicer (group leader), N. Gardner (technician), A. Mondragon (technician), and F. Wittman (engineer). Henderson and Mondragon joined this group during the past two months.

EFFECT OF INTENSE LASER LIGHT UPON THE DENSITY OF EXCITED ATOMS IN A PLASMA

(D. Michael)

An investigation is under way to study the rate at which excited atoms reappear in a plasma after they are suddenly destroyed by photoionization with an intense laser light beam. The purpose of the work is to extend the understanding of the atomic processes which determine the population of excited atoms in a Cs plasma partially ionized (1-5%) by thermal means. Such a source[1] has been constructed and tested. The experiment is to be performed by perturbing the plasma with a giant (30 MW) pulse of 6943Å light emitted by a ruby laser. Fast electronic circuitry has been assembled to aid in the search for the disappearance and reappearance of certain Cs atomic lines as the upper atomic state is photoionized and then repopulated.

A block diagram of the experimental arrangement is shown in Fig. 65. By utilizing an "advance warning" sync pulse provided by

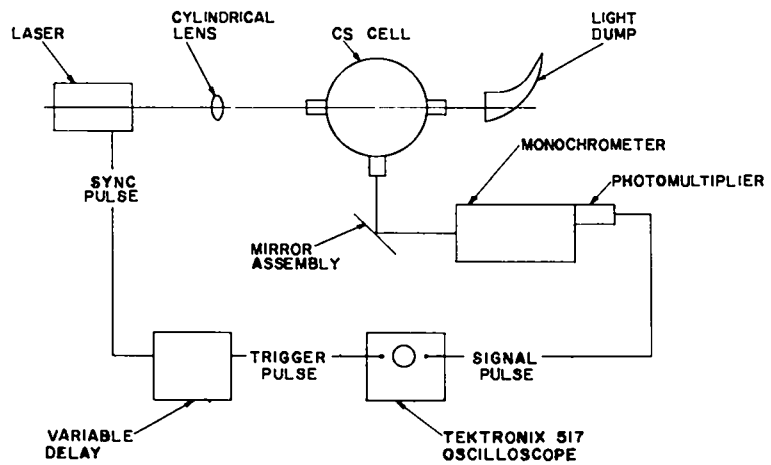

Fig. 65. Experimental arrangement for study of excited atoms in a plasma.

the laser the scope can be triggered before the laser pulse passes through the Cs cell, and the photomultiplier output can be sampled while the plasma is still in an equilibrium condition. The photomultiplier is fastened directly to the exit slits of a Jarrell-Ash scanning monochromator which is tuned to pass light emitted in a particular electronic transition between two excited states of a Cs atom. Various adjustments and improvements are still being carried out on the system.

Reference

1. P. M. Stone and L. Agnew, Phys. Rev., 127, 1157 (1962).

RADIATIVE RECOMBINATION INDUCED BY INTENSE LASER LIGHT

(H. Dreicer)

The experiment on the photoionization of Cs by a high-power laser pulse, described in the preceding section, has spurred a calculation of the induced inverse process, namely,

$$Cs^+ + e^- + h\nu \rightarrow Cs_n^* + 2h\nu,$$

which represents the stimulation of radiative recombination to the nth excited state by an intense laser beam. The end result of the calculation gives the time rate of change of the neutral particle density in the excited state n, denoted by $N_g^{(n)}$. It takes the form of a balance between the induced recombination and photoionization as follows

$$\frac{dN_g^{(n)}}{dt} = 2\,\frac{E_n}{kT}\,\lambda\left[I(\nu,\Omega)\,\frac{c^2}{h\nu^3}\,\Delta\nu\Delta\Omega\right] \cdot\iint F(E_n,\theta,\Phi)\,d(\cos\theta)d\Phi \cdot\left\{N^2\, e^{-E_n/kT} - \frac{2S_i}{S_n}\, N_g^{(n)}\,\frac{1}{\lambda^3}\right\}, \quad (1)$$

where $E_n = h\nu - x_n$ = electron energy prior to recombination, x_n = energy required to ionize the atom from the given excited state n, $\lambda = h/(2\pi mkT)^{\frac{1}{2}}$, ν = frequency of laser light, $\frac{3}{2}$ kT = average electron energy, N = electron or ion density, $I(\nu,\Omega)$ = specific intensity of the laser light, h = Planck's constant, $\Delta\nu$ = frequency band width of the laser light, $\Delta\Omega$ = solid angle within which laser light is confined, S_i and S_n = statistical weights of ion and excited neutral, respectively, and $\iint F(E,\theta,\Phi)\,d(\cos\theta)d\Phi$ = appropriate total cross section for spontaneous radiative recombination.

In the calculation leading to Eq. (1) the electrons were assumed to be Maxwellian, and spontaneous radiative recombination was assumed negligible compared to the induced recombination. The last assumption follows from the fact that the average number of photons per mode in the laser light is much greater than unity, i.e.,

$$I(\nu,\Omega)\,\frac{c^2}{h\nu^3} \gg 1.$$

Equation (1) predicts that a completely ionized gas will be slightly de-ionized by the passage of an intense laser beam until the density of excited states is given by

$$\frac{N_g}{N} = \lambda^3 N \sum_n \frac{S_n}{2S} e^{-E_n/kT}.$$

Since $S_n/2S_i$ and the exponential are of the order of unity for most laboratory plasmas of interest, and since $N\lambda^3$ is generally much less than unity, the amount of de-ionization is found to be small for the Cs experiment and incidentally also for highly ionized Scylla plasmas. Moreover, since highly ionized plasmas are only slightly de-ionized or additionally ionized by this process, it is not likely that laser light used in incoherent scattering experiments will excite strong plasma oscillations unless the laser pulse rise time becomes comparable to the oscillation period.

INFLUENCE OF PLASMA UPON CYCLOTRON EMISSION*

(H. Dreicer, F. Wittman)

The emission spectrum at the electron cyclotron frequency and its harmonics have been studied with the help of microwave radiometers operating at $\omega/2\pi = 18$ and 36 kMHz. A P.I.G. plasma of radius large compared to the microwave free space wavelength served as the source of the radiation. Three major areas were studied: (1) The line shape of the extra-ordinary wave fundamental emission in the neighborhood of $\omega = \omega_B = (e/m)\,B$ was measured. (2) The conditions were investigated under which the profuse emission of the higher harmonics takes place.[1] (3) The line shape of these harmonics was studied. The results of the last of these studies have already been published[2] and will not be described here.

Experiments of the first category are typified by the spectra in the neighborhood of $\omega_B/\omega = 1$ shown in Fig. 66a-66d. It is believed that the asymmetric doublet line near $\omega = \omega_B$ is due to the effect which the plasma dielectric coefficient has upon the cyclotron emission. Since the radiation rate depends upon the index of refraction, the amount of energy radiated will vary from point to point on the plasma profile. In fact regions on the plasma profile between cutoff and hybrid resonance layers where

$$1 - \frac{\omega_B}{\omega} < \left(\frac{\omega_p}{\omega}\right)^2 < 1 - \left(\frac{\omega_B}{\omega}\right)^2$$

contribute no radiation at all. They may also effectively block the emission from all interior electrons for which $(\omega_p/\omega)^2 > 1 - (\omega_B/\omega)^2$, if

---

* This work was carried out in 1964 prior to the departure of one of the authors (H.D.) on an 18-month leave.

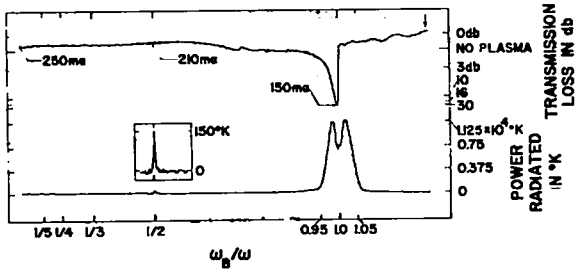

Fig. 66a

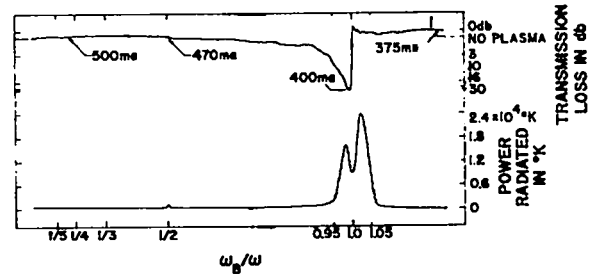

Fig. 66b

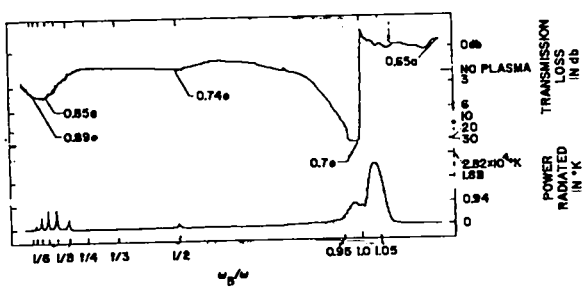

Fig. 66c

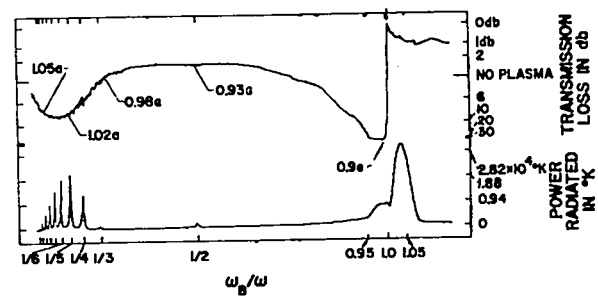

Fig. 66d

Fig. 66a-66d. Extraordinary cyclotron emission and transmission loss vs ω_B/ω; $\omega/2\pi$ = 18 kMHz. He gas pressure = 3 mtorr. P.I.G. voltage = 1.0-1.2 kV. P.I.G. current vs ω_B/ω is indicated on each spectrum. The electron densities for $\omega_B/\omega \approx 1$ are as follows:

Fig. 66a	$n = 1.3 \times 10^{11}$ cm^{-3}
Fig. 66b	$n = 3.9 \times 10^{11}$
Fig. 66c	$n = 7.8 \times 10^{11}$
Fig. 66d	$n = 1.2 \times 10^{12}$

the cutoff and resonance layers are sufficiently far apart in space to reduce the Budden tunneling to a negligible amount. When this is the case, a Doppler broadened fundamental emission line, which is detected even by a fairly directional microwave horn, will split into an asymmetric doublet since the number of electrons and their radiation rate is generally greater for $\omega_B/\omega > 1$ than for $\omega_B/\omega < 1$. The effect is not very pronounced for $(\omega_p/\omega)^2 \ll 1$ (Fig. 66a), since here the cutoff-hybrid layers exist only in the immediate neighborhood of $\omega_B/\omega = 1$; hence the doublet will be very nearly symmetric.

For larger densities, however (Figs. 66b, c, d) these layers may persist on the profile over a considerable (or even the entire) range of $\omega_B/\omega < 1$, and prevent much of the radiation emitted by electrons in the plasma interior from reaching the detector. It appears that a small fraction of fast electrons orbiting in the dielectric medium provided by the remaining majority of slow electrons in the P.I.G. plasma can account for this emission. A theory proceeding from this point of view is in preparation. Further experimentation is planned with a quiescent alkali plasma source which is now under construction.

Figures 66a-66d also indicate the conditions under which the profuse emission at the higher harmonics occurs. By making simultaneous emission and transmission measurements through the plasma volume (transmission data are also shown in the figures), a correlation between such harmonic emission and poor transmission was established. Further experiments indicated that such poor transmission could be attributed to the existence of the cutoff and hybrid resonance layers on the profile. This conjecture was established by detecting the harmonic emission simultaneously at the two frequencies, 18 and 36 kMHz, under conditions which predicted the cutoff and hybrid layers on the profile at the low but not the high frequency. The result is given in Fig. 67. High harmonic emission occurs at the low frequency ω_1, but not at the high

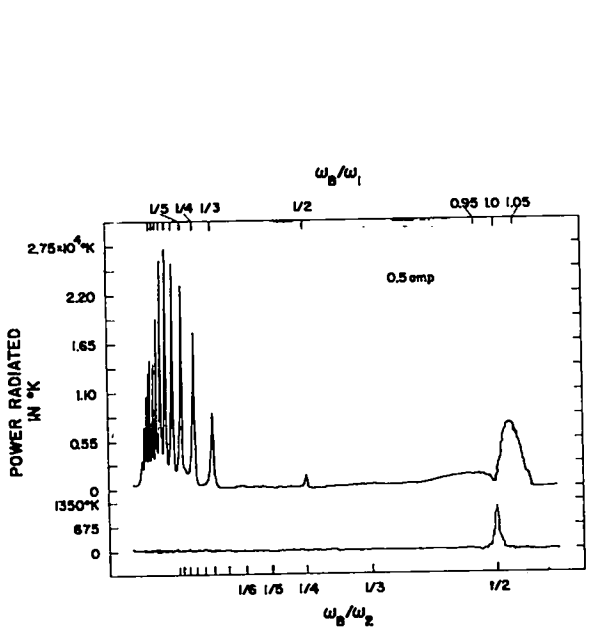

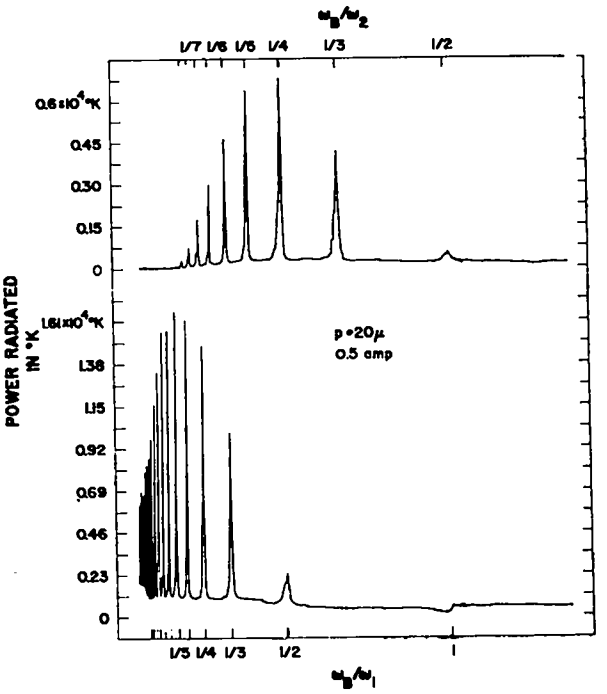

Fig. 67. Extra-ordinary cyclotron emission vs ω_B/ω for two values of ω; $\omega_1/2\pi$ = 18 kMHz, $\omega_2/2\pi$ = 36 kMHz. He gas pressure = 3 mtorr.

Fig. 68. Extra-ordinary cyclotron emission vs ω_B/ω for two values of ω; $\omega_1/2\pi$ = 18 kMHz, $\omega_2/2\pi$ = 36 kMHz. He gas pressure = 20 mtorr.

frequency ω_2. Figure 68 shows the effect of increasing $(\omega_p/\omega)^2$ so that the double layers exist also at ω_2. Although these experimental studies indicate a correlation between harmonic emission and the cutoff-hybrid layers on the profile they are unable to distinguish between several interesting theories that have been proposed, all of which incorporate energy conversion in the neighborhood of these double layers.

References

1. G. Landauer, Proc. Inter. Conf. on Ionization Phenomena in Gases, Munich 1, 389 (1961).
2. H. Dreicer, Proc. of Inter. Conf. on Ionization Phenomena in Gases, Belgrade (1965).

ELECTRON CYCLOTRON ABSORPTION BY ELECTRONS TRAPPED IN THE ELECTROSTATIC FIELD OF A HIGH VACUUM P.I.G.

(H. Dreicer, F. Wittman)

Measurements have been made on the microwave absorption by electrons at cyclotron resonance and the quantity of light emitted simultaneously by the residual background gas (10^{-5} - 10^{-6} torr) in a P.I.G. cold-cathode system operating at approximately 1 kV. Relatively strong light emission was observed with a photomultiplier when the microwave frequency was held fixed (18 kMHz) and the magnetic field approached the value necessary for cyclotron absorption. Under these circumstances the microwaves were propagated in the extra-ordinary mode between two horns which were fed by a klystron emitting several mW. Apparently the microwave energy absorbed by a very small number of electrons which are electrostatically trapped in the P.I.G. is utilized to excite and ionize the residual neutral molecules, i.e., to cause electrical breakdown. When cyclotron resonance is approached from the high magnetic field side of $\omega_B/\omega = 1$, there is a residual photomultiplier light signal which remains on the low-field side of resonance, i.e., a discharge is sustained. The opposite is true when resonance is approached from the low-field side. This effect is shown in Figs. 69a and b.

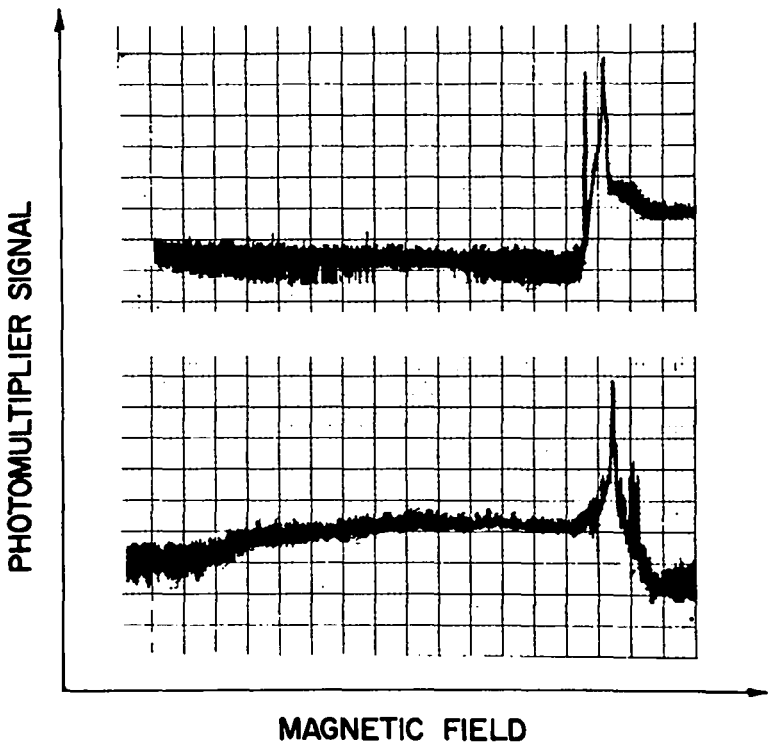

Fig. 69a (upper) and b (lower). Photomultiplier light signal vs magnetic field; at cyclotron resonance the light signal maximizes. On the upper trace cyclotron resonance was approached from small magnetic fields; on the lower trace the approach was reversed.

DEVELOPMENT OF ALKALI PLASMA MACHINE COMPONENTS

(H. Dreicer, D. Henderson, F. Wittman)

An alkali plasma machine is being designed for cyclotron radiation studies and other experiments. Various hot-plate structures, ovens, and associated electron-beam bombardment structures are presently being designed and others have been tested.

To avoid the serious lifetime problems caused by distortion of filaments in strong magnetic fields, a heater structure has been designed and tested with filament wires positioned very nearly parallel to the applied magnetic field (Fig. 70). A perveance of 2×10^{-6} $A/(V)^{3/2}$ was achieved by use of a conical accelerating grid inserted between filaments and hot plate (not shown in Fig. 70). Such a structure, consisting of six filament wires of 13-mil diam tungsten doped with 3% rhenium, has given 350 h of trouble-free operation at 2300°-2500°K. During this time the magnetic field was cycled between 0 and 8-9 kG a total of 300 times. Although this system was adequate for heating a 1-in. diam, $\frac{1}{8}$-in. thick tantalum hot plate to 2700 $\pm$ 50°K, it suffered

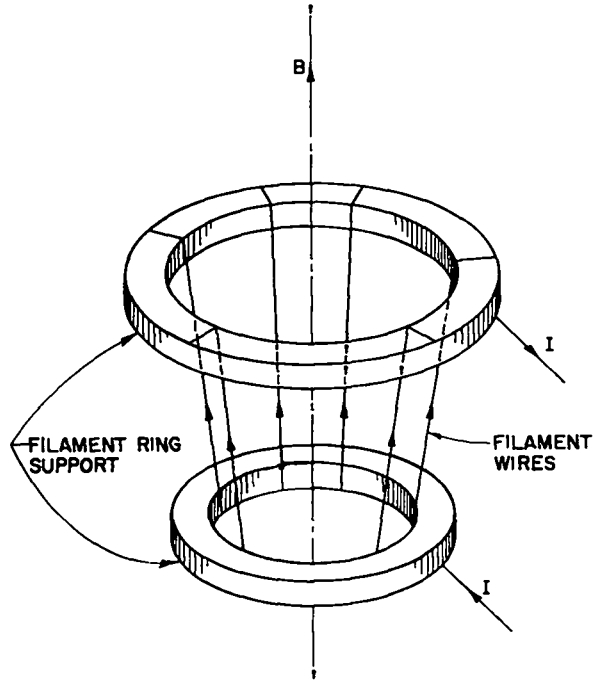

Fig. 70. Simplified representation of heater structure.

from the fact that the plate received its power in six concentrated spots, and thus possessed a limited life due to erosion by the electron beams. This difficulty can be avoided by increasing the number of filament wires or using wire mesh to spread the power carried by the electrons from the filaments over a larger area of the hot plate.

A tungsten cross wire mesh filament with its plane parallel to the hot plate has also been tested. Such a structure has an intrinsically large perveance without the necessity for auxiliary accelerating grids, possesses sufficient structural strength to overcome failure due to magnetic forces, but has not yet resulted in as uniform a hot-plate temperature distribution as the former.

In an additional attempt to achieve uniform hot-plate temperature distribution, hot plates have been designed of extremely large thermal conductance similar to the"heat pipes" pioneered at LASL by Grover et al.[1] In these, heat flows in hollow conductors filled with a fluid which is continuously evaporating and condensing. Mandrels for these pipes are now being machined.

Reference

1. G. M. Grover, T. P. Cotter, and G. F. Erickson, J. Appl. Phys., 35, 1900 (1964).

DEVELOPMENT OF A HIGH-CURRENT, LOW-VOLTAGE ELECTRON BEAM

(J. McLeod, N. Gardner)

The purpose of this work is to develop electron beams suitable for the study of beam-plasma interaction of the type reported by Nezlin.[1] A conventional electron gun technique will not produce the required parameters of 10 A at 2 kV, and it is necessary to resort to space charge neutralization. This process generally involves the introduction of gas into the accelerating region of the electron gun followed by several stages of differential pumping to reduce the gas pressure by one to two orders of magnitude in the beam-plasma interaction region. An attempt has been made to avoid this pumping problem by utilizing a pulsed electron beam suitably delayed with respect to a pulsed gas valve located in the electron gun section. In this way the delays inherent in the expansion of the gas into the vacuum were expected to provide the required pressure differences. This expectation has proved to be oversimplified. Extensive measurements with a fast-acting denuded ionization gauge have been made of the spatial distribution of neutral gas as a function of time following gas injection. The principal feature emerging from these measurements is the long-term persistence of large pressure differences in the relatively unrestricted volume of the beam-plasma interaction chamber which has a minimum inside diameter of $10\frac{1}{2}$ in. and is 90 in. long. Pressure ratios as high as 10 persist between the two ends of the tanks for as long as 15 msec. Molecular gas flow calculations are in adequate agreement with these results.

A beam current of 10 A at 2 kV has been obtained but only sporadically. Attempts at controlling the gas pressure distribution by modifying the gas conductance between the electron gun chamber and the beam-plasma chamber can not yet be interpreted unambiguously, because of the possibility that the dispenser cathode used was not functioning properly. It appears, however, that beam-plasma interaction or breakdown across magnetic field lines occurs in the gun chamber, as indicated by noise on the cathode current, while simultaneously the electron beam current outside of the gun chamber is much smaller than the cathode current.

Reference

1. M. V. Nezlin, JETP (Engl. Transl.), 19, 26 (1964).

REGULATION OF 500-KW GENERATOR AND 2.5-MW RECTIFIER SUPPLY

(H. Dreicer, J. McLeod)

A substantial improvement has been made in the stability of the output current of the 500-kW dc generator which is the largest regulated magnet supply at LASL, and is to be used in future studies involving cyclotron radiation. This improvement was accomplished primarily by rebuilding the compensation network, which now includes three Philbrick UPA-2 operational amplifiers, so that it compensates for the measured properties of the high-power equipment. The previous compensation network was based on grossly oversimplified assumptions concerning the properties of the higher power equipment, so that the system was unstable unless the loop gain was reduced to a very low value. As a result of the small loop gain, the regulation was unsatisfactory. The new loop has a loop gain in excess of 100 at zero frequency, and closed loop bandwidth of 2 cps. The stability of the output current should now be 0.01% or better. This has been verified at low magnet currents with the help of a nuclear magnetometer.

Initial steps have been taken in collaboration with E. Kemp to provide current regulation for the 2.5-MW rectifier supply. This system, together with the water cooling system, is presently under study to determine the best way to provide such regulation.

PUBLICATIONS

Sprague, "Capacitor Bank Charging System," Symp. on Engineering Problems of Controlled Thermonuclear Research, LRL, Livermore, Calif., May 1965. CONF-650512, p. 52 (1966).

Boicourt, "Electrical Characteristics of Coaxial Cables," ibid., CONF-650512, p. 72 (1966); LA-3318.

Dike, Kemp, and Marshall, "Development of an Interleaved, Fractional-Turn Coil," ibid., CONF-650512, p. 162 (1966).

Quinn, Little, Ribe, and Sawyer, "Stability, Heating, and End Loss of a 3.5-MJ Theta Pinch (Scylla IV)," Proc. Conf. on Plasma Physics and Controlled Nuclear Fusion Research, Culham Lab., Eng., Sept. 1965. IAEA, 1966, Vol. 1, p. 237.

Mather, "High Density Deuterium Plasma," ibid., IAEA, 1966, Vol. 2, p. 389.

Marshall and Henins,"Fast Plasma from a Coaxial Gun," ibid., IAEA, 1966, Vol. 2, p. 449.

Hammel and Baker, "Transverse Injection Experiment," ibid., IAEA, 1966, Vol. 2, p. 499.

Mace, "Investigation of Stimulated Emission in Multiply Ionized Plasmas Produced by Scylla I Theta Pinch Machines," Quantum Electronic Conf., Phoenix, Ariz., April 1966. IEEE, 1966. Digest of Papers, p. xlii.

Kemp, Dolnick, Dike, Sawyer and Tuck, "Scyllacita-Compact High Voltage Theta Pinch Machine," Rev. Sci. Instr., 37, 1065 (1966).

Dreicer, "Gaps in the Spectrum of Electrostatic Plasma Waves," Phys. Fluids, 8, 1568 (1965).

Karr and Osher, "High-Velocity Plasma Injection into a Cusped Magnetic Field," ibid., 9, 750 (1966).

Baker, MacRoberts and Mann, "Calculations for Capacitor-Driven RLC Circuits Including the Penetration of Fields into Conductors," J. Appl. Phys., 37, 2792 (1966).

Stratton, "X-Ray Spectroscopy," in Plasma Diagnostic Techniques, R. L. Huddlestone and S. L. Leonard, eds., Academic Press, New York, 1965, p. 359.

Atkinson and Phillips, "Some Observations on the Flow of a Tenuous Plasma in a Uniform Magnetic Field," Bull. Am. Phys. Soc., Ser. 2, 11, 452 (1966) (Abstract).

Marshall, Baker, and Henins, "Design Study for a Toroidal-Quadrupole Closed-Field Containment Experiment," ibid., Ser. 2, 11, 550 (1966)(Abstract).

Baker and Mann, "Study of the Optimization of a $\int d\ell/B$ Stable Caulked Cusp Field," ibid., Ser. 2, 11, 550 (1966)(Abstract).

Lewis, "Computation of Electrostatic and Rapidly Pulsed Magnetic Fields," ibid., Ser. 2, 11, 558 (1966)(Abstract).

Ribe, Oliphant, and Quinn, "Feasibility Study of a Theta-Pinch-Type, Pulsed, Thermonuclear Reactor," ibid., Ser. 2, 11, 558 (1966)(Abstract).

Mather, "Dense Deuterium-Tritium Plasma Focus Discharge," ibid., Ser. 2, 11, 573 (1966)(Abstract).

Morse, "Bounce-Model Pinch Stability," ibid., Ser. 2, 11, 579 (1966) (Abstract).

Quinn, Little, Ribe and Sawyer, "Stability, Heating, and End Loss of a 3.5 MJ Theta Pinch (Scylla IV)," ibid., Ser. 2, 11, 580 (1966)(Abstract).

Kemp, Dolnick, Dike, Sawyer and Tuck, "Compact High-Voltage Theta Pinch," ibid., Ser. 2, 11, 581 (1966)(Abstract).

Boicourt, "Electrical Characteristics of Coaxial Cable," LA-3318.

Morse, "Stability of a Bumpy Linear, $\beta = 1$, θ-Pinch," LA-3442-MS.

"Proposal for a Toroidal Theta-Pinch (Scyllac)," LA-3487-MS.

Dike, Kemp, and Quinn, "Proposed Straight θ-Pinch Devices Energized by the Energy Storage Supply of the Toroidal θ-Pinch (SCYLLAC)," LA-3553-MS.

Ribe and Quinn, "Anticipated Scylla IV Experiments Pertaining to Scyllac," LA-3596-MS.